COMPRESSED AIR ENERGY STORAGE: MODELLING & APPLICATIONS FOR SUSTAINABLE ELECTRIC POWER SYSTEMS

A Thesis Submitted to the College of

Graduate and Postdoctoral Studies

In Partial Fulfillment of the Requirements

For the Degree of Master of Science

In the Department of Electrical and Computer Engineering

University of Saskatchewan

Saskatoon, SK, Canada

By

Osama Aslam Ansari

Permission to Use

In presenting this thesis in partial fulfillment of the requirements for a Postgraduate degree from the University of Saskatchewan, I agree that the Libraries of this University may make it freely available for inspection. I further agree that permission for copying of this thesis in any manner, in whole or in part, for scholarly purposes may be granted by the professor or professors who supervised my thesis/dissertation work or, in their absence, by the Head of the Department or the Dean of the College in which my thesis work was done. It is understood that any copying or publication or use of this thesis or parts thereof for financial gain shall not be allowed without my written permission. It is also understood that due recognition shall be given to me and to the University of Saskatchewan in any scholarly use which may be made of any material in my thesis.

Requests for permission to copy or to make other uses of materials in this thesis in whole or part should be addressed to:

Head of the Department of Electrical and Computer Engineering
57 Campus Drive
University of Saskatchewan
Saskatoon, Saskatchewan, S7N 5A9
Canada

OR

Dean
College of Graduate and Postdoctoral Studies
University of Saskatchewan
116 Thorvaldson Building, 110 Science Place
Saskatoon, Saskatchewan S7N 5C9
Canada

Abstract

With the increasing concerns about the climate change and depletion of non-renewable energy sources, there has been a growing emphasis on the deployment of renewable energy sources in electric power systems. However, due to inherent stochasticity of renewable energy sources, this transition toward sustainable electric power systems creates serious challenges for the reliable and safe operation of such systems. Large-scale energy storage systems are considered to be key enablers for integrating increasing penetration of renewable energy sources by adding flexibility to the electric power systems.

This thesis investigates compressed air energy storage (CAES) as a cost-effective large-scale energy storage technology that can support the development and realization of sustainable electric power systems.

Firstly, this thesis develops a novel planning framework of CAES to consider its benefits from an electric utility's perspective. The proposed framework is used to investigate different applications of CAES which depend upon the location and size of CAES in an electric power system. The proposed framework also considers the option of installing a dynamic thermal line rating (DTLR) system which measures real-time, maximum power ratings of transmission lines.

Next, this thesis examines the existing models of CAES employed in electric power system studies and proposes a novel thermodynamic-based model of CAES which is more accurate yet suitable for electric power system studies. The importance and significance of the proposed model is established through its application in the problem of optimal scheduling of CAES in electricity markets. It is demonstrated that through the proposed model, the operator of a CAES can submit bids in electricity markets without violating any of the technical constraints of CAES.

Lastly, this thesis inspects the reliability benefits of CAES to an electric power system. In this part of the thesis, a four-state reliability model of CAES is developed. The reliability model of CAES is then applied to evaluate the reliability of a wind-integrated electric power system. It is revealed that CAES can significantly improve the reliability indices of an electric power system. Moreover, it is shown that this improvement depends on the location and size of CAES.

Acknowledgments

Firstly, I am highly grateful to God Almighty, who in His immeasurable capacity of knowledge and kindness granted me patience and strength to work on this thesis.

I owe my deepest gratitude to my supervisor, Prof. C. Y. Chung. Without his invaluable guidance, encouragement and continuous support, this thesis would not have been completed. His breadth of knowledge and vast experience was crucial toward the completion of my research work. I could not have hoped for a better supervisor for my MSc. degree.

I would like to pay my sincere gratitude to members of my advisory committee, Prof. Rajesh Karki and Prof. Anh V. Dinh, as well as external examiner, Prof. Reza Fotouhi, for their valuable and useful suggestions which served to improve the quality of my thesis. I would also like to thank my graduate study professors, Prof. Rajesh Karki and Prof. Nurul Chowdhury, for broadening my knowledge on the topics of power systems reliability and power systems operation.

A very special thanks goes out to all students and staff at the Smart Grid and Renewable Energy Technology Lab, for creating a pleasant working environment. In particular, I would like to thank Dr. Junpeng Zhan, Dr. Yuzhong Gong, Mr. Nima Safari and Mr. Alireza Zare, for several insightful technical discussions and many hours of brainstorming.

I would also like to gratefully acknowledge the financial support for my MSc. degree from the NSERC/SaskPower Senior Industrial Research Chair Program, the University of Saskatchewan and the Government of Saskatchewan.

Last but not the least, I would like to pay special heartiest thanks to my family: my parents, my brothers and my sister, for rendering unfailing support, endless encouragement and unconditional love during my time as a MSc. student. I would not have accomplished this achievement without them.

Thank you all for your support!

Table of Contents

List of Tables

List of Figures

List of Abbreviations

BESS	Battery Energy Storage System
BPECI	Bulk Power Energy Curtailment Index
CAES	Compressed Air Energy Storage
CCL	Convex Combination Linearization
DFIG	Doubly-Fed Induction Generator
DRER	Distributed Renewable Energy Resource (DRER)
DSM	Demand Side Management
DR	Demand Response
DTLR	Dynamic Thermal Line Rating
EENS	Expected Energy Not Supplied
EDNS	Expected Demand Not Supplied
ESS	Energy Storage System
EV	Electric Vehicle
EWC	Expected Wind Curtailment
FSA	Forward Selection Algorithm
Log-CCL	Logarithmic Convex Combination Linearization
LHS	Latin Hypercube Sampling
MILP	Mixed Integer Linear Programming
MINLP	Mixed Integer Nonlinear Programming
OPF	Optimal Power Flow
PHS	Pumped Hydro Storage
PH	Pre-Heater
PLC	Probability of Load Curtailment
RES	Renewable Energy Sources
RPS	Renewable Portfolio Standards
RBTS	Roy Billinton Test Sytem
RTS	Reliability Test System

SI	Severity Index
SMCS	Sequential Monte-Carlo Simulation
SOC	State-Of-Charge
STLR	Static Thermal Line Rating
TCC	Turbomachinery Characteristic Curve
UC	Unit commitment
VOLL	Value of loss of load
WAMS	Wide Area Monitoring System
WECC	Wind Energy Conversion System

Chapter 1

Introduction

"Honesty is the first chapter in the book of wisdom"
-Thomas Jefferson

1.1 Motivation

Emerging concerns about climate change and increasing depletion of non-renewable sources of energy have become the primary drivers for a paradigm shift in electric power systems around the world. This paradigm shift has resulted in several changes in the structure and operation of existing electric power systems. On the generation side, the renewable energy sources (RES) such as wind and solar energy, are being integrated in large proportions. On the other hand, conventional electricity generators, for instance, coal-fired power plants are being eliminated from the generation mix. Consumption end of the electric power systems is also affected by these changes. The electrification of the transportation sector in the form of electric vehicles (EVs) and electric trains have increased the demand for electricity. Transitions are also occurring at the regulatory level. Deregulated electric power system structure has been adopted in many countries with electricity markets replacing the conventional single-entity electric utility framework. The amalgamation of these transitions has brought momentous challenges to the reliable yet economic planning and operation of sustainable electric power systems.

One of the significant challenges stems from the large-scale addition of RES in electric power systems. The penetration of RES in existing electric power systems has been increasing continuously over the past few decades. Figure 1.1 pictorially represents this trend [1]. It has been projected that the total global electricity generation from RES will rise above 6500 TWh by 2020 [1]. By 2035, this figure will reach 11000 TWh, representing an increase of 70% in 2020 levels. As the proportion of RES in the existing electric power systems continues to rise, their inherent variability and intermittency represent a key challenge for maintaining the balance between electricity generation and demand at all times [2], [3], [4] . Therefore, the ability of an electric power system to supply electricity to the consumers with reasonable levels of reliability is seriously threatened. This calls for higher levels of operational flexibility in an electric power

system to ensure that the reliability and security of the system are maintained [5]. In this regard, different smart grid technologies have been developed to provide operational flexibility to electric power system and hence meet these diverse challenges [3].

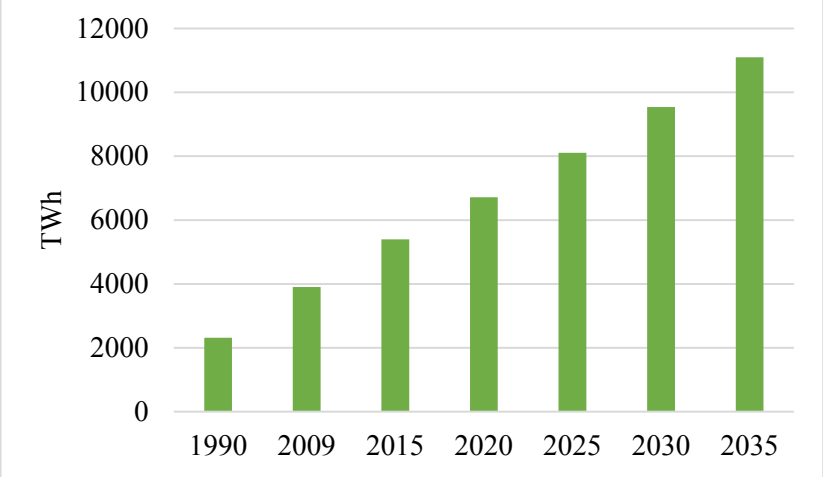

Figure 1.1 Total installed capacity of RES, 1990-2035 [1]

1.2 Energy Storage Systems

Energy storage systems (ESSs) are vital components of smart grids which can significantly increase the flexibility of an electric power system and hence assist in maintaining the balance between the generation and demand in the presence of uncertainties and variabilities of different resources [6], [7]. ESSs convert electrical energy into other storable forms such as mechanical or chemical energy and provide the stored energy back in the form of electricity when required [7]. In contrast to a transmission system which moves energy in space, ESSs move energy in time [1] [8]. ESSs increase the efficiency of an electric power system by enhancing the utilization of output from RES [9]. ESSs can also reduce the investments in the assets of an electric power system while maintaining the system reliability and meeting the targets of low carbon emissions [10], [11].

1.2.1 Classification of ESSs

ESSs can be classified according to the technology used for storing the electrical energy. Figure 1.2 indicates this classification. Pumped hydro storage (PHS), which stores electrical energy in the form of potential energy of water raised to a certain height [12], is currently the most widely used

[1] EVs can be regarded as mobile ESSs which have the ability to move energy both in time and in space.

storage technology. In fact, around 99% of the total installed energy storage capacity is in the form of PHS [13]. PHS is also the oldest storage technology, dating back to late 19th century [12]. Compressed air energy storage (CAES) is next in the list with the cumulative installed capacity of 440 MW in the world [14]. Followed by CAES are different technologies of batteries such as sodium-sulfur battery, lithium-ion battery and lead acid battery [13]. Recent advancements in different battery technologies have accelerated the deployment of both large- and small-scale batteries in electric power systems [15].

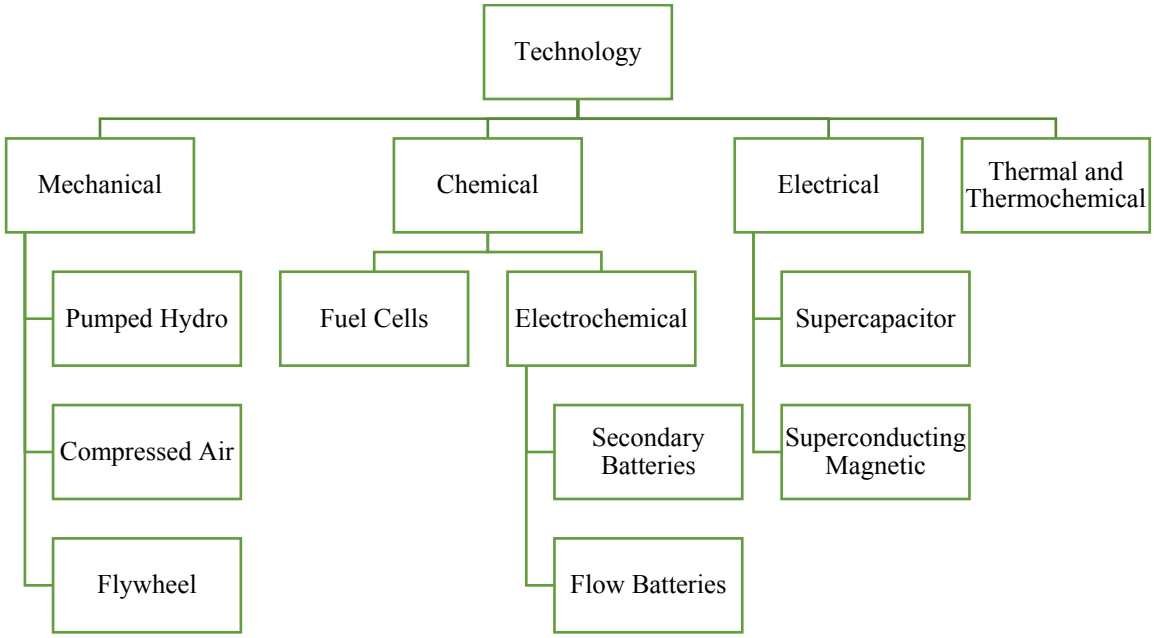

Figure 1.2 Classification of ESSs by technology

1.2.2 Applications of ESSs

Due to their versatility, ESSs can be employed in a wide array of applications in different sections of electric power systems. On the generation side, ESSs can be utilized for time shifting where excess output from RES is stored during the periods of low electricity demand, and the stored electricity is supplied when the demand is high [16]. ESSs can also assist in output smoothing and capacity firming of RES. Through output smoothing, fast varying fluctuations in the output of RES are removed whereas in capacity firming, ESSs ensures that actual RES output meets its scheduled output [9], [16]. For the transmission system, ESSs offer various applications such as frequency regulation, load leveling, peak shaving, voltage control, provision of operating reserve and inertia emulation [7]. Finally, on the demand side, ESSs can be utilized for

implementing demand-side management (DSM) programs and also by assisting the integration of distributed renewable energy resources (DRERs) such as roof-top solar panels and small-scale wind turbines. As a result of their extensive applications, it is expected that ESSs will play a crucial role in providing the required flexibility to electric power systems and hence assisting in realizing sustainable electric power systems with high penetration of RES [17].

1.2.3 Trends in ESSs

Due to the growing importance of ESSs, various different projects are being carried out around the world to install new ESSs in electric power systems. These projects have been given impetus by the continuously decreasing costs of various storage technologies. According to a report which was commissioned by International Finance Corporation (IFC) and Energy Sector Management Assistance Program (ESMAP), it is projected that this trend will continue in the near future (Figure 1.3) [13]. As a consequence of the decreasing costs, the number of installation of new ESSs has been increasing sharply. According to one estimate, it is projected that the total installed capacity of ESSs will cross 18,000 MW by 2026, representing a tremendous increase of over 180% in less than a decade [18]. Both of these trends manifest that ESSs, particularly utility-scale ESSs will be widely employed in the electric power systems in the coming years.

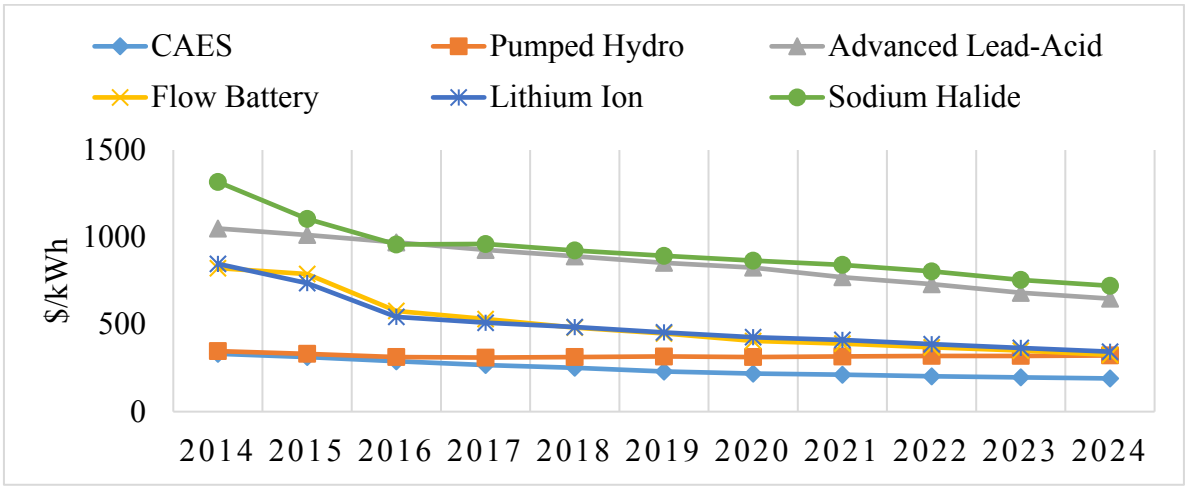

Figure 1.3 Capital costs of utility-scale ESSs [13]

1.3 Compressed Air Energy Storage

CAES is one of the two cost-effective large-, utility-scale storage technology [19], [20], the other being PHS. CAES employs high-pressure air as the storage medium for storing the electrical energy. The high-pressure compressed air is stored in either underground caverns or aboveground storage tanks.

Both the capital and operational costs of CAES are among the lowest of all storage technologies [7]. CAES is also suitable for utility-scale applications where one of the primary purposes is to store electrical energy for long durations (in the order of hours). Furthermore, CAES is not susceptible to phenomena of self-discharge and degradation [19]. This makes CAES an ideal utility-scale storage technology for large-scale applications in an electric power system such as facilitating higher penetration of RES. Although, PHS is the most widely used storage technology at present [19], the suitable geographical locations where new PHS plants can be constructed are becoming scarce [19]. Consequently, CAES remains the only feasible option for commercial, utility-scale energy storage at the present levels of ESSs' costs.

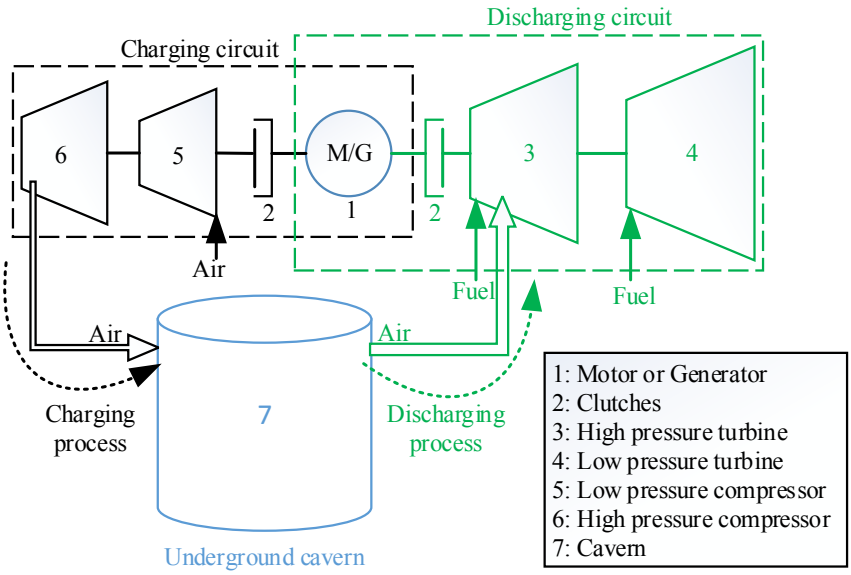

Figure 1.4 CAES operation

CAES is derived from the gas turbine technology [19]. Therefore, the operation of CAES is very similar to that of a gas-fired generator. In the charging process, CAES utilizes excess electrical energy from the electric power system to run electrically-driven compressors for compressing the ambient air. The high-pressure air is then stored in a storage facility. In the discharging mode, when the electrical energy is required, the high-pressure air is released from the storage, combusted and then expanded in a manner similar to that of a gas-fired generator (Figure 1.4).

In a conventional gas-fired generator, the compression and expansion processes take place simultaneously. Therefore, nearly two-thirds of the turbine output is consumed to run the compressors alone [21]. On the other hand, the turbines in CAES are not directly coupled with compressors, and the compression/expansion cycles occur at different times. As a result, in CAES, full output of the turbines can be used to run the generator [21]. This implies that the fuel consumption of CAES is one-third of a conventional gas-fired generator for the same output power. Similar to a gas-fired generator, CAES has a high ramping rate. However, because of the way the output of CAES is controlled, it has a better part-load efficiency [19], [21]. Therefore, it can be concluded that CAES is a better candidate than a gas-fired generator for mitigating fast fluctuations of RES.

At present, there are two existing CAES plants in the world. The world's first CAES plant is located in Huntorf, Germany. The Huntorf CAES plant has been in operation since 1978 [20]. Although the plant was initially designed to deliver 290 MW in discharging mode, its capacity was increased to 321 MW in 2006 [22]. The plant efficiency (i.e. the ratio of total output energy to total input energy) of Huntorf CAES plant is 42% [23]. The second CAES plant in the world was constructed in 1991 in McIntosh, Alabama, USA [20], [24]. The McIntosh CAES plant has a capacity of 110 MW. It can provide full output power for nearly 26 hours. The plant efficiency of McIntosh CAES plant is reported to be 54% [7].

Unlike other ESSs technology, CAES employs additional fuel during the discharging process. This type of CAES is also known as a diabatic CAES. A diabatic CAES is not a pure storage technology, *per se*. Recently, investigations have been carried out to utilize a thermal energy storage to capture the heat generated during the compression process and utilize it during the expansion process. This would eliminate the need of using fuel for the combustion process. This

type of CAES, also known as adiabatic CAES, is currently in the development phase [21]. This thesis is concerned with diabatic CAES and hereafter, diabatic CAES will be referred to as CAES.

CAES requires a high volume storage facility to store the compressed air. Underground caverns provide a more cost-effective option as compared to aboveground storage tanks for air storage [19]. This is because of the presence of existing underground formations such as salt deposits or natural gas mines, which can be used for storing the compressed air. Consequently, the capital costs for constructing an underground storage is lower than any aboveground storage site [21]. The two existing CAES plants also utilize underground caverns for air storage. Figure 1.5 shows locations of different salt mines around the world [25]. The figure indicates that there are many possible locations which can be exploited as underground caverns for CAES.

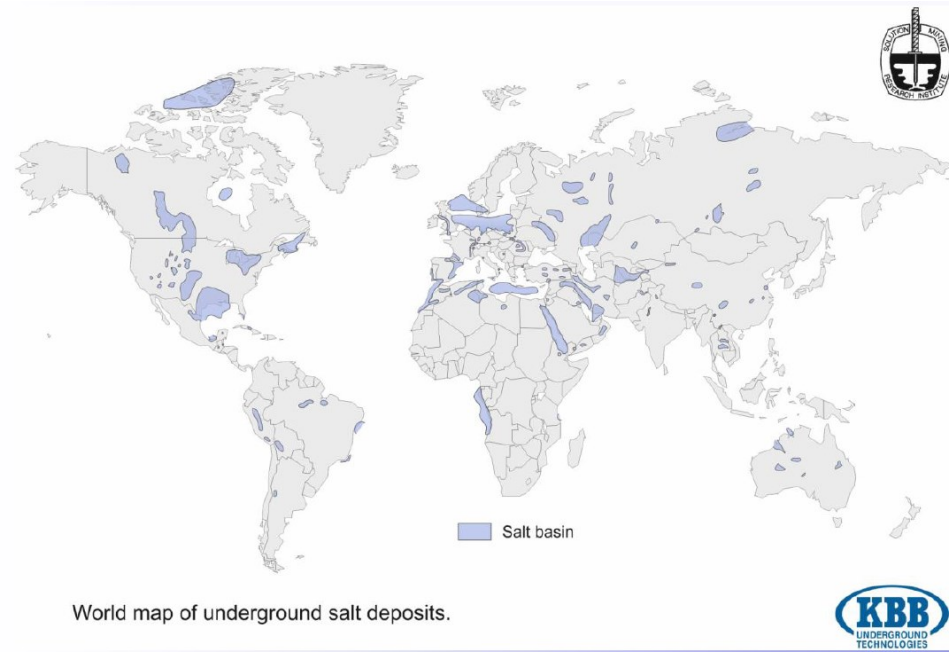

Figure 1.5 Location of salt mines around the world [25]

Saskatchewan also has several possible locations for the construction of CAES as Saskatchewan lies in the region of a geological formation known as 'prairie evaporate formation' [26] (Figure 1.6). This geological formation contains many salt and potash deposits. A number of these deposits have already been mined. Moreover, there are 26 such locations where underground storage caverns and storage fields are present. These caverns and fields are currently employed for storing natural gas [27]. These underground storage facilities represent excellent options for the construction of a CAES. Moreover, some of these storage facilities are located near the wind farms,

hence minimizing the additional costs for constructing new transmission lines to connect CAES with these wind farms. Given that the province of Saskatchewan has set a target of increasing the renewable energy penetration in their electric power systems to 50% by 2050 [28], CAES represents a viable large-scale energy storage option for the province to realize this target.

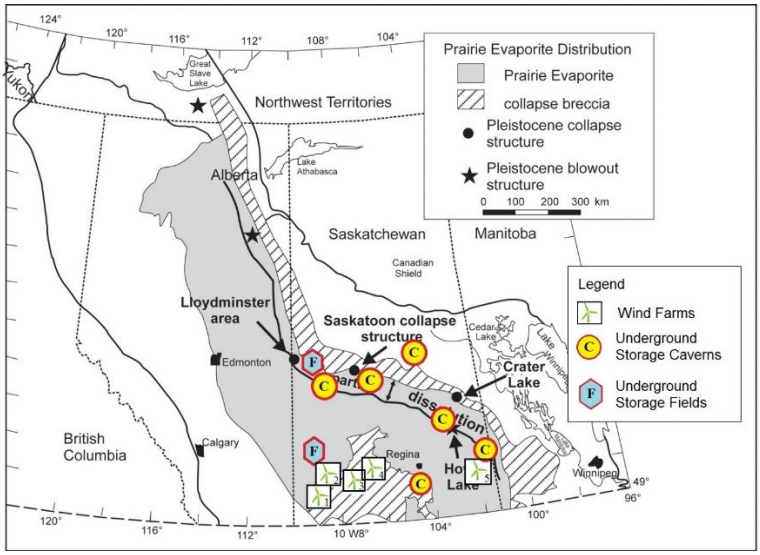

Figure 1.6 Location of underground caverns and storage fields in Saskatchewan [26]

1.4 Research Questions

Large-scale ESSs are central for realizing a sustainable electric power system with a high penetration of RES. CAES represents one large-scale ESSs option which is cost-effective and has various technical benefits. This thesis aims to extend the existing literature of CAES by exploring answers to the following important research questions:

- The first question surrounding the inclusion of CAES in future sustainable electric power systems is to determine whether there is a need for constructing a CAES or not. Moreover, CAES plants constructed at different buses of an electric power system may have different applications. If CAES is required to be installed in an electric power system, what are the most effective locations for CAES installation from an electric power system perspective? In addition, what should be the optimal size of CAES to obtain the maximum benefits at a justifiable cost?

- The efficiency of CAES is a key factor in determining its actual benefits to an electric power system. What are the existing models of CAES employed in electric power system studies? Are there any thermodynamics-based CAES models that can be utilized in electric power system studies? What are the impacts of including a comprehensive model of CAES in the problem of optimal self-scheduling of CAES in electricity markets? Are the profits from the electricity markets impacted by the changes in the efficiency of the CAES?

- Reliability is an important metric that ensures that electric power system is able to meet the load demand in the events of unexpected contingencies. The electric power systems are planned and operated considering a certain level of reliability. What are the impacts of CAES on the reliability of the electric power system? Are there any methods that can quantify the benefits of CAES on electric power system reliability? Also, what are the optimal size and location of CAES in an electric power system from a reliability perspective?

All of the above questions are further complicated by the presence of highly variable RES in an electric power system. Moreover, the variations and uncertainties of other elements of an electric power system, such as electricity market prices also render the problem complicated. It is, therefore, extremely critical to consider the stochasticity arising from different sources while devising mathematical tools and models to answer these research questions.

1.5 Research Objectives

Based on the research questions presented in the previous section, this thesis aims to develop tools and models for the modeling and applications of CAES in future sustainable electric power systems. In particular, the thesis deals with the following three objectives:

1.5.1 Development of a Planning Tool for CAES Considering Smart Grid Technologies

As a first step toward realizing an electric power system with CAES, it is crucial to design a planning tool that can be utilized by electric utilities or system operators to find optimal locations for constructing a CAES in an electric power system. Therefore, in the first work of this thesis, a framework for optimal planning of CAES is developed. The planning framework determines the

optimal locations as well as sizes of different CAES in an electric power system. As other smart grid technologies can also assist an electric power system, the proposed framework also includes other smart grid technologies.

1.5.2 Development of an Accurate Model of CAES and its Application in Electricity Market Scheduling

A thermodynamics-based model for CAES can consider the variation in its efficiency at different operating conditions. However, such a model is highly non-linear and hence cannot be employed for electric power studies. Therefore, in this objective, a novel linear, thermodynamics-based model of CAES is developed. The proposed model considers the turbomachinery characteristic curves of compressors and turbines in a CAES. The importance of the proposed model is highlighted through its application in the problem of optimal scheduling of CAES in electricity markets.

1.5.3 Development of a Reliability Model of CAES for Power Systems Reliability Evaluation

In addition to bringing economic benefits to a merchant and technical benefits to a system operator or electric utility, CAES can also improve the reliability of an electric power system with significant penetration of RES. However, to assess the actual improvement in reliability of the system, it is essential to develop a suitable reliability model of CAES that can consider its different failure mechanisms. Therefore, this objective focuses on the development of a reliability model of CAES. Afterward, a framework for power system reliability evaluation with CAES is developed. The framework integrates the reliability model of CAES and evaluate the reliability indices of the electric power system.

For all of the above objectives, the uncertainties introduced by RES and electricity market prices are handled through stochastic optimization. Stochastic optimization employs the theory of probability to consider the uncertainties through various different scenarios. A comprehensive explanation of stochastic optimization can be found in [29]. In this thesis, various stochastic optimization models are developed for each objective of the research work.

1.6 Organization of Thesis

The thesis has been organized in a manuscript-style. In particular, the content of this thesis is based on two manuscripts and one poster presentation. The three main chapters of this thesis are based on the three research works and address three research objectives separately. Sufficient details have been included in all chapters so that each chapter can be read on its own if desired. However, all of the chapters are closely linked with each other.

Chapter 1 provides the motivation behind the research work. The importance and significance of ESSs for sustainable electric power systems are highlighted. A brief overview of the existing technologies of ESSs is presented. Potential applications of ESSs in sustainable electric power systems are also identified. Following this, a review of CAES is presented. The chapter also describes the research questions concerning CAES that are addressed in this thesis. Further, the objectives of the research work are summarized.

Chapter 2 focuses on the development of a mathematical tool for planning of CAES. The chapter also discusses the application of dynamic thermal line rating (DTLR) for improving the economics of the investment plan for CAES. This chapter investigates the potential applications of CAES with due consideration given to the location and size of each CAES. The work presented in this chapter is based on [30].

Chapter 3 delves into the operational aspects of CAES. In this chapter, a thermodynamics-based model of CAES is presented. This is followed by a linearization method to develop a linear model of CAES. Afterward, the linear model is employed in the optimal scheduling problem of CAES in electricity markets. Further case studies are also included in this chapter to explain the effects of various parameters of CAES on its scheduling in electricity markets. The work in this chapter is based on [31].

Chapter 4 presents a reliability evaluation framework of an electric power system in the presence of CAES. In this chapter, a reliability model of CAES is first proposed. Following this, a reliability evaluation framework is presented to assess the impacts of CAES on power system reliability. The effects of the location and size of CAES on the power system reliability is also presented in this chapter. Reference [32] forms the basis of this work.

Chapter 5 provides the conclusion of the research work. This chapter summarizes key findings of the research work. Some suggestions for future work are also provided.

Appendix contains copyright permission letters from co-authors of the manuscripts reused in this thesis as well copyright permission letters for reuse of Figures 1.5 and 1.6.

Chapter 2

Stochastic Planning of Compressed Air Energy Storage Considering Dynamic Thermal Line Ratings[1]

"Planning is bringing the future into the present so that you can do something about it now."
- Alan Lakein

2.1 Abstract

Compressed air energy storage (CAES) can be employed for providing flexibility to power systems at a justifiable cost. Some of the major benefits of CAES to a power system include the reduction in the transmission congestion and the decrease in spillage of output from renewable energy sources (e.g., wind generation). On the other hand, dynamic thermal line ratings (DTLR) of overhead transmission lines have also shown to provide the above-mentioned benefits to power systems. However, the actual benefits derived from CAES and DTLR depend upon their locations in a power system. The benefits of CAES also depend upon their size. In this regard, this chapter of the thesis is concerned with the development of a novel framework for optimal placement of CAES and DTLR system and optimal sizing of CAES in a power system for maximizing the benefits from an electric utility's perspective. The proposed framework is applied to a 24-bus IEEE Reliability Test System. The results verify that the inclusion of DTLR in the planning model for CAES can reduce the total investment cost. Moreover, the results indicate that the location of a CAES affects its application.

[1]

2.2 Nomenclature

Sets/Indices

i	Index of bus
l	Index of line
t	Index of hour
ω	Index of scenario
Ω_B	Set of all buses
Ω_T	Set of time $\{1,2,\dots,T_\omega\}$
Ξ	Set of scenarios

Parameters

ru_i	Ramp-up rate limit of generator at bus i (MW/h)
rd_i	Ramp-down rate limit of generator at bus i (MW/h)
$d_{i,t}^{\omega}$	Electricity load demand at bus i in scenario ω at hour t (MW)
f_l^{STLR}	The maximum power flow of lines l and n, respectively (MW) (Static thermal line rating)
$f_{l,t}^{\omega,\mathrm{DTLR}}$	Dynamic thermal line rating (DTLR) in scenario ω at time t (MW)
$\bar{g}_i, \underline{g}_i$	Maximum, minimum power output of generator at bus i, respectively (MW)
k	Depth of discharge (DOD) of CAES
$\overline{p}_{\mathrm{B}}, \underline{p}_{\mathrm{B}}$	Maximum, minimum allowable power rating for CAES, respectively (MW)
$\overline{E}_{\mathrm{B}}, \underline{E}_{\mathrm{B}}$	Maximum, minimum allowable energy rating for CAES, respectively (MWh)
$\mathrm{C}_{\mathrm{S,E}}^{\mathrm{IC}}$	Energy capital cost of CAES ($/MWh)
$\mathrm{C}_{\mathrm{S,F}}^{\mathrm{IC}}$	Fixed capital cost of CAES ($)
$\mathrm{C}_{\mathrm{S,P}}^{\mathrm{IC}}$	Power capital cost of CAES ($/MW)
$\mathrm{C}_{\mathrm{DTLR}}^{\mathrm{IC}}$	Investment cost for installation of DTRL system ($/km)
T_ω	Total number of hours in each scenario (hours)
$T_{i,\min}^{\mathrm{on}}$	Minimum up time of generator i (hours)
$T_{i,\min}^{\mathrm{off}}$	Minimum down time of generator i $(hours)$

$M_{i,l}$ The element in the *i*th row and the *l*th column of node-branch incidence matrix

N_d Number of days in an year

$\overline{W}_i^{\kappa}$ Maximum wind power that can be generated at bus i (MW)

Λ_i Target expected wind curtailment (MWh)

$\tilde{\gamma}_l$ Susceptance of a line l (Siemens)

η_{ch} Charging efficiency of CAES

η_{dch} Discharging efficiency of CAES

$\rho_{i,\mathrm{S}}^{\mathrm{OC}}$ Variable operation and maintenance cost of CAES($/MWh)

$\rho_{i,\mathrm{E}}^{\mathrm{IC}}$ Prorated energy capital cost of CAES ($/MWh)

$\rho_{i,\mathrm{F}}^{\mathrm{IC}}$ Prorated fixed capital cost of CAES ($)

$\rho_{i,\mathrm{P}}^{\mathrm{IC}}$ Prorated power capital cost of CAES ($/MW)

$\rho_{l,\mathrm{DTLR}}^{\mathrm{IC}}$ Prorated investment cost of DTLR system ($/km)

ρ_i^g Generation cost of generator at bus i ($/MWh)

$\rho_{j,\mathrm{su/sd}}^{\mathrm{G}}$ Start-up/shut-down cost for conventional generator j

ρ_i^L Penalty cost for electricity load loss at bus i ($/MWh)

$\rho_{i,\mathrm{su}}^{\mathrm{G}}$ Start-up cost of generator at bus i ($)

$\rho_{i,\mathrm{sd}}^{\mathrm{G}}$ Shut-down cost of generator at bus i ($)

π Annual discount factor

γ Lifetime of CAES or DTLR system (years)

Δt Time duration (1 hour)

Variables (All variables are continuous otherwise indicated)

$f_{l,t}^{\omega}$ Total active power flow on line l in scenario ω at time t (MW)

$g_{i,t}^{\omega}$ Power output of generator at bus i (MW)

$p_{i,t}^{\mathrm{ch},\omega}$ Charging power of CAES at bus i (MW)

$p_{i,t}^{\mathrm{dch},\omega}$ Discharging power of CAES at bus i (MW)

$r_{i,t}^{\omega}$ Electricity load curtailment at bus i (MW)

$s_{i,t}^{\omega}$ Wind power curtailment at bus i (MW)

$I_{i,t}^{\omega}$	Binary variable indicating online/offline status of the generator i : 1 if it is online, 0 otherwise
$P_{i,\mathrm{R}}^{\mathrm{S}}$	Rated power of CAES at bus i (MW)
$E_{i,\mathrm{R}}^{\mathrm{S}}$	Rated energy of CAES at bus i (MWh)
$W_{i,t}^{\omega}$	Scheduled wind power generation at bus i (MW)
$\overline{W}_{i}^{\omega,t}$	Forecast wind power generation at bus i (MW)
$\alpha_{i,t}^{\mathrm{G},\omega}$	Binary variable indicating start-up of generator i
$\beta_{i,t}^{\mathrm{G},\omega}$	Binary variable indicating shut-down of generator i
$\alpha_{i,\mathrm{ch}}^{\omega,t}$	Binary variable indicating charging status of CAES at bus i : 1 if it is charging, 0 otherwise
$\alpha_{i,\mathrm{dch}}^{\omega,t}$	Binary variable indicating discharging status of CAES at bus i : 1 if it is discharging, 0 otherwise
$\theta_{l,\mathrm{fr/to}}^{\omega}$	Phase angle of from/to-side node of line l (rad)
δ_i	Binary variable indicating whether a CAES is installed at bus i
λ_l	Binary variable indicating whether a DTLR system is installed on line l

2.3 Introduction

The increased penetration of renewable sources of generation such as large-scale wind farms and solar generators have tremendously intensified the need for the addition of flexible resources in the power systems [4], [6]. Subsequently, various different resources such as energy storage systems (ESSs), demand response (DR) programs and flexible generators are being investigated as suitable options to increase the flexibility of the power system. The inclusion of large-scale ESSs is universally courted as a key to unlock the potential of renewable sources by providing the added flexibility to the power system at a justifiable cost [3], [4]. As a result, the installation of ESSs in the existing power systems is on the rise [18]. From the electric utility's perspective, utility-owned large-scale ESSs such as compressed air energy storage (CAES) can provide various technical and economic benefits to the power system. These benefits include the reduction in operating costs [33], improvement in system reliability [32], and decrease in the fluctuations of output from the wind and solar generators. In addition, CAES can also assist in relieving the transmission congestion in a power system.

The benefits obtained by including CAES in the power system are highly dependent upon their location and size [17]. In particular, when CAES is employed for easing the congestion in the transmission system, the location of the CAES becomes very critical. As a result, any decision to install a CAES should include its optimal location (siting) as well as its size (sizing) to maximize the benefits. However, the uncertainty introduced by renewable sources render this problem of finding the optimal installation plan of CAES complicated [17].

The authors in [8] presented a three-stage planning model for optimal location and size of distributed ESSs in the power system. In [33], a planning model for siting and sizing utility-owned ESSs is presented. The computational efficiency of the model has been shown by applying it to the Western Electricity Coordinating Council (WECC) system. A framework based on chance-constrained programming for sizing ESSs in a power system is developed in [34]. In this framework, ESSs are assumed to be operated under a model predictive control scheme. However, the model does not consider the optimum location of the ESSs in the power system. A framework is developed for optimal sizing of an energy storage based on a scenario tree model in [35]. The proposed framework employs Benders' decomposition to solve the problem. The work presented in [8], [33] [34] and [35] do not consider the inclusion of other possible alternatives such as construction of a new transmission line or addition of other transmission equipment (e.g. transmission line switching and dynamic thermal line rating (DTLR)) in the planning model. On the other hand, including other alternatives can also improve the system performance and hence can result in a more cost-effective plan for ESSs. For instance, DTLR system can alleviate congestion in the transmission lines during the peak period and hence minimize the ESSs' capacity required for peak shaving application. Therefore, it can be beneficial to include possible alternatives while planning for ESSs.

In this regard, [36] presents a model for planning the transmission system and ESSs at the same time. The proposed model indicates that the number of ESSs installed decreases when the planning decisions for new transmission lines are included in the planning model. In [37], the transmission planning decisions by a system operator or transmission operator are considered while determining the optimal location and size of a merchant-owned energy storage.

To the best of author's knowledge, no work has considered the inclusion of DTLR system while planning for ESSs or CAES in a power system. As mentioned earlier, DTLR system can improve the transmission utilization and hence may defer the need for installation of new CAES.

In addition, in previous studies for energy storage planning, such as one presented in [33], the spillage from renewable energy sources is controlled through a penalty cost. In practice, such penalty costs may not be easily determined. Whereas, many jurisdictions have set targets for utilizing renewable energy for a certain percentage of the total energy consumption [38]. Therefore, it may be more logical to use the expected or average output of renewable energy utilized for controlling the spillage of renewable energy output.

2.4 Contributions

In the light of the literature review presented in the previous section, this chapter of the thesis contributes to the existing literature in the following ways:

1. A framework[2] for the optimal planning of CAES considering the alternative of installing a DTLR system in the transmission system is developed. By co-optimizing the investment in the CAES and DTLR, an economic plan is obtained that can make use of the actual capacities of the existing assets of a transmission system.
2. Instead of wind spillage costs, the proposed framework employs expected wind curtailment (EWC) during the planning stage for controlling the spillage from wind generation. This ensures that the amount of wind utilized in the system does not fall below a certain threshold. This threshold can be set the by the utility, system operator or regulating agencies.

2.5 Dynamic Thermal Line Rating

DTLR of an overhead transmission line calculates the actual maximum current carrying capacity considering the real-time ambient and conductor conditions [39]. Figure 2.1 shows major factors which affect the DTLR of an overhead transmission line. Static thermal line rating (STRL), on the other hand, is a conservative, fixed estimate of the maximum current carrying capacity. In contrast

[2] A vertically-integrated power system is considered in this model. The planners of such a power system have options to consider the installation of new equipment in the transmission system. CAES installed by a vertically-integrated power system entity can help the power system in day-to-day operations such as managing peak-demands.

to STLR, DTLR is a more accurate representation of the actual maximum power that can be transferred over a transmission line. In fact, DTLR of a transmission line is found to be higher than the STLR for most periods of the time. Figure 2.2 indicates that for a particular case study, DTLR is higher than STLR for 87% of the time [39]. For the remainder of the time, the actual line capacity as measured by DTLR system is lower than STLR. In the case when DTLR is higher than STLR, higher amounts of power can be transferred through the transmission lines and hence additional investments in the transmission system for alleviation of congestion can be minimized [39], [40]. On the other hand, when DTLR is lower than STLR, the utilization of DTLR for limiting the power flow on the transmission lines can help in avoiding the overloading of the transmission lines. This can assist in preventing system blackouts [41].

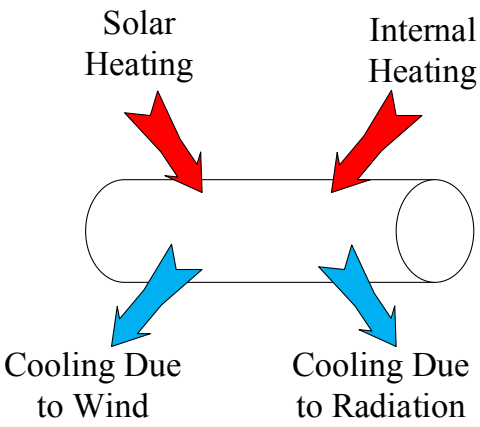

Figure 2.1 Factors affecting DTLR of an overhead transmission line

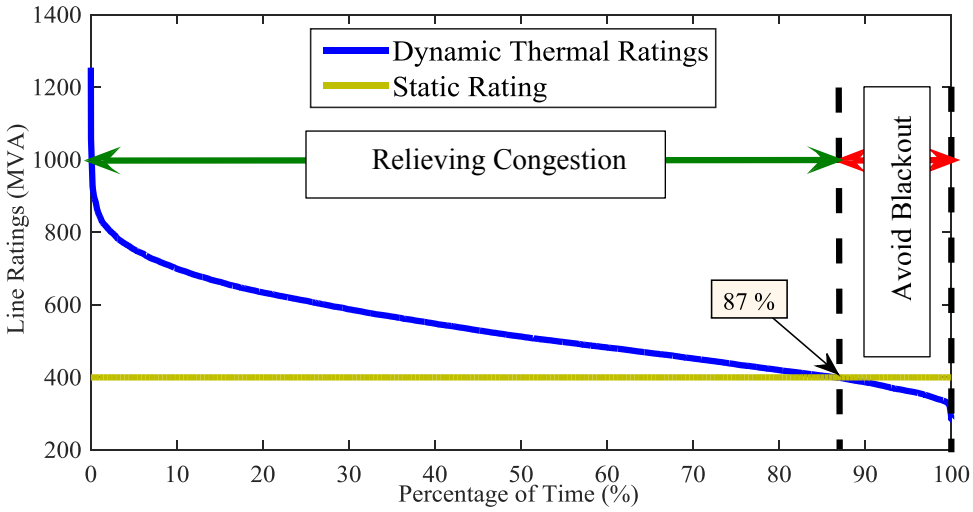

Figure 2.2 Duration Curve of DTLR

Several projects have demonstrated the application of DTLR system for improving the utilization of a transmission system. One example of these projects include a demonstration project conducted by New York Power Authority (NYPA) and Electric Power Research Institute (EPRI), which indicated that up to 25% additional capacity of the existing transmission system can be utilized during the power system operation by considering a DTLR system [42].

As DTLR can assist in improving the utilization efficiency of the transmission system, it is only logical to include the option of installing a DTLR equipment while planning for CAES in a power system.

2.6 Model

The proposed model for the optimal sizing and siting of the CAES considering the installation of DTLR system is formulated as a two-stage stochastic mixed-integer linear programming (MILP) model. The formulation of the model in the form of MILP guarantees global optimality because of the availability of efficient solution strategies for such models [43]. In the proposed two-stage model, the first stage considers the investment decisions about the planning of CAES and DTLR system. Whereas, the second stage represents the recourse function of daily operational costs of a power system. For this daily operation, a unit commitment model (UC) is adopted. UC model ensures that inter-temporal constraints, such as ramping constraints, and on-off constraints of the generators are included. The uncertainties introduced by the variability in renewable generation, load demand and DTLR are included through scenarios in this second stage.

2.6.1 Objective Function

The objective function of the model is formulated by (2.1) – (2.5).

$$\sum_{i\epsilon\Omega_{\mathrm{B}}}\left(\rho_{i,\mathrm{P}}^{\mathrm{IC}}P_{i,\mathrm{R}}^{\mathrm{S}}+\rho_{i,\mathrm{E}}^{\mathrm{IC}}E_{i,\mathrm{R}}^{\mathrm{S}}+\rho_{i,\mathrm{F}}^{\mathrm{IC}}\delta_i\right)+\sum_{l\in\Omega_{\mathrm{L}}}\left(\rho_{l,\mathrm{DTLR}}^{\mathrm{IC}}\lambda_l\right)+\sum_{\omega\epsilon\Xi}p_\omega\left(\sum_{t=1}^{T_\omega}\left(\sum_{i\epsilon\Omega_{\mathrm{B}}}\left(\rho_{i,\mathrm{su}}^{\mathrm{G}}\alpha_{i,t}^{\mathrm{G},\omega}+\rho_{i,\mathrm{sd}}^{\mathrm{G}}\beta_{i,t}^{\mathrm{G},\omega}+\rho_i^{\mathrm{G}}g_{i,t}^{\omega}\right)\right)+\sum_{i\epsilon\Omega_{\mathrm{B}}}\left(\rho_i^{\mathrm{L}}r_{i,t}^{\omega}\right)+\sum_{i\epsilon\Omega_{\mathrm{B}}}\left(\rho_{i,\mathrm{S}}^{\mathrm{OC}}\left(p_{i,t}^{\mathrm{ch},\omega}+p_{i,t}^{\mathrm{dch},\omega}\right)\right)\right) \quad (2.1),$$

$$\rho_{i,\mathrm{P}}^{\mathrm{IC}}=\mathrm{C}_{\mathrm{S,P}}^{\mathrm{IC}}\frac{\pi(1+\pi)^{\gamma}}{N_{\mathrm{d}}(1+\pi)^{\gamma}-1}, \quad (2.2)$$

$$\rho_{i,\mathrm{E}}^{\mathrm{IC}}=\mathrm{C}_{\mathrm{S,E}}^{\mathrm{IC}}\frac{\pi(1+\pi)^{\gamma}}{N_{\mathrm{d}}(1+\pi)^{\gamma}-1}, \quad (2.3)$$

$$\rho_{i,\mathrm{F}}^{\mathrm{IC}} = \mathrm{C}_{\mathrm{S,F}}^{\mathrm{IC}} \frac{\pi(1+\pi)^{\gamma}}{N_{\mathrm{d}}(1+\pi)^{\gamma}-1}, \tag{2.4}$$

$$\rho_{l,\mathrm{DTLR}}^{\mathrm{IC}} = \mathrm{C}_{\mathrm{DTLR}}^{\mathrm{IC}} \frac{\pi(1+\pi)^{\gamma}}{N_{\mathrm{d}}(1+\pi)^{\gamma}-1}, \tag{2.5}$$

The first term in the objective function (2.1) represents the investment costs of CAES. The CAES investment costs include the capital costs for rated power and rated energy of CAES as well as the fixed costs of constructing a CAES. The second term in the objective function describes the installation costs of a DTLR system. The third term represents the second-stage of the model. This stage considers the expected or average daily operational costs of the power system. The operational costs include the operating costs of generators, load curtailment costs and the costs for operating CAES. Equations (2.2)–(2.5) define the normalized investment costs of CAES and DTLR system. These equations annualize the investment costs of CAES and DTLR system based on their lifetimes and annual discount factor [33]. Different from [33], the objective function does not contain the costs associated with renewable energy spillage.

2.6.2 Constraints

2.6.2.1 Power balance constraint

Power balance constraints for each bus are formulated by (2.6). The power balance constraint includes the generation from the conventional generators, wind generation, as well as, load demand, and output from CAES.

$$\sum_{l\in\Omega} M_{i,l}\, f_{l,t}^{\omega} + g_{i,t}^{\omega} + W_{i,t}^{\omega} - s_{i,t}^{\omega} + r_{i,t}^{\omega} - d_{i,t}^{\omega} + p_{i,t}^{\mathrm{dch},\omega} - p_{i,t}^{\mathrm{ch},\omega} = 0, \quad \forall i \in \Omega_B, \forall t \in \Omega_T, \forall \omega \epsilon \Xi. \tag{2.6}$$

2.6.2.2 Power flow constraint

Equation (2.7) represents the power flow on the transmission lines. In this work, DC power flow is employed. The DC power flow considers only the active power flow on a transmission system. For planning problems, DC power flow captures enough details of the transmission system. For actual power system operation problems, AC power flow is generally preferred.

$$f_{l,t}^{\omega} - \tilde{\gamma}_l\left(\theta_{l,\mathrm{fr}}^{\omega,t} - \theta_{l,\mathrm{to}}^{\omega,t}\right) = 0, \forall l \in \Omega_{\mathrm{L}}, \forall t \in \Omega_T, \forall \omega \epsilon \Xi, \tag{2.7}$$

2.6.2.3 Power flow limit and DTLR constraint

Equation (2.8) limits the power flow on the transmission lines. In this equation, the binary variable λ_l indicates whether the transmission line has a DTLR system installed or not. If this binary variable is 1, it implies that the line is equipped with the DTLR system and hence the DTLR are used as the limits on the power flow in the transmission lines. On the other hand, if this binary variable is 0, STLR is used for the power flow limits for each line.

$$\left|f_{l,t}^{\omega}\right| \leq \lambda_l f_{l,t}^{\omega,\mathrm{DTLR}} + (1-\lambda_l) f_l^{\mathrm{STLR}},\ \forall l \in \Omega_{\mathrm{L}},\ \forall t \in \Omega_T, \forall \omega \epsilon \Xi\ , \tag{2.8}$$

2.6.2.4 Generators' constraints

The constraints on the operation of conventional generators (coal, natural gas, nuclear and hydro) are expressed by (2.9)–(2.16). Equation (2.9) limits the maximum and minimum output power of the generator. Equations (2.10) and (2.11) set the limits on the ramping capacities of conventional generators. Equation (2.12) ensures that a conventional generator cannot be started up or shut down during the same hour. Equations (2.13) and (2.14) express the constraints for minimum up time of a generator. The constraints for minimum down time of a generator are represented by (2.15) and (2.16) [44].

$$I_{i,t}^{\omega}\underline{g}_i \leq g_{i,t}^{\omega} \leq I_{i,t}^{\omega}\bar{g}_i,\ \forall i \in \Omega_B,\ \forall t \in \Omega_T, \forall \omega \epsilon \Xi\ , \tag{2.9}$$

$$g_{i,t+1}^{\omega} - g_{i,t}^{\omega} \leq ru_i,\ \forall i \in \Omega_B,\ \forall t \in \Omega_{T-1}, \forall \omega \epsilon \Xi\ \ , \tag{2.10}$$

$$g_{i,t}^{\omega} - g_{i,t+1}^{\omega} \leq rd_i,\ \forall i \in \Omega_B,\ \forall t \in \Omega_{T-1}, \forall \omega \epsilon \Xi\ \ , \tag{2.11}$$

$$\alpha_{i,t}^{\mathrm{G},\omega} - \beta_{i,t}^{\mathrm{G},\omega} = I_{i,t}^{\omega} - I_{i,t-1}^{\omega},\ \forall i \in \Omega_B,\ \forall t \in \Omega_T, \forall \omega \epsilon \Xi\ , \tag{2.12}$$

$$\sum_t^{t+T_{i,\min}^{\mathrm{on}}-1} I_{i,t}^{\omega} \geq \alpha_{i,t}^{\omega} T_{i,\min}^{\mathrm{on}}, \forall i \in \Omega_B,\ \forall t \in \left\{1, \dots, T_\omega - T_{i,\min}^{\mathrm{on}} + 1\right\}, \forall \omega \epsilon \Xi\ , \tag{2.13}$$

$$\sum_t^{T_\omega} I_{i,t}^{\omega} \geq \alpha_{i,t}^{\omega}(T_\omega - t + 1), \forall i \in \Omega_B,\ \forall t\ \left\{T_\omega - T_{i,\min}^{\mathrm{on}} + 2, \dots, T_\omega\right\}, \forall \omega \epsilon \Xi\ , \tag{2.14}$$

$$\sum_t^{t+T_{i,\min}^{\mathrm{off}}-1} \left(1 - I_{i,t}^{\omega}\right) \geq \beta_{i,t}^{\omega} T_{i,\min}^{\mathrm{off}}, \forall i \in \Omega_B,\ \forall t \in \left\{1, \dots, T_\omega - T_{i,\min}^{\mathrm{off}} + 1\right\}, \forall \omega \epsilon \Xi\ , \tag{2.15}$$

$$\sum_t^{T_\omega} \left(1 - I_{i,t}^{\omega}\right) \geq \beta_{i,t}^{\omega}(T_\omega - t + 1), \forall i \in \Omega_B,\ \forall t\ \left\{T_\omega - T_{i,\min}^{\mathrm{off}} + 2, \dots, T_\omega\right\}, \forall \omega \epsilon \Xi\ , \tag{2.16}$$

2.6.2.5 CAES constraints

The constraints on the operation of a CAES are defined by (2.17) – (2.22). The maximum power and energy ratings of the CAES are set by (2.17) and (2.18), respectively. Equations (2.19) and (2.20) ensure that the charging and discharging powers are within the ratings, respectively. The state-of-charge (SOC) of CAES in terms of its energy is expressed by (2.21). The available energy of CAES at any hour is constrained by (2.22).

$$\delta_i \underline{p}_{\mathrm{B}} \le P_{i,\mathrm{R}}^{\mathrm{S}} \le \delta_i \overline{p}_{\mathrm{B}},\ \forall i \in \Omega_B\ , \tag{2.17}$$

$$\delta_i \underline{E}_{\mathrm{B}} \le E_{i,\mathrm{R}}^{\mathrm{S}} \le \delta_i \overline{E}_{\mathrm{B}},\ \forall i \in \Omega_B\ , \tag{2.18}$$

$$0 \le p_{i,t}^{\mathrm{ch},\omega} \le \alpha_{i,t}^{\mathrm{S},\omega} P_{i,\mathrm{R}}^{\mathrm{S}},\ \forall i \in \Omega_{B,} \forall t \in \Omega_T, \forall \omega \epsilon \Xi\ , \tag{2.19}$$

$$0 \le p_{i,t}^{\mathrm{dch},\omega} \le (1-\alpha_{i,t}^{\mathrm{S},\omega}) P_{i,\mathrm{R}}^{\mathrm{S}},\ \forall i \in \Omega_{B,} \forall t \in \Omega_T, \forall \omega \epsilon \Xi\ , \tag{2.20}$$

$$E_{i,t}^{\omega} = E_{i,t-1}^{\omega} + \left(\eta_{\mathrm{ch}} p_{i,t}^{\mathrm{ch},\omega} - \frac{p_{i,t}^{\mathrm{dch},\omega}}{\eta_{\mathrm{dch}}}\right) \Delta t, \forall i \in \Omega_{B,} \forall t \in \Omega_T, \forall \omega \epsilon \Xi\ , \tag{2.21}$$

$$(1-k) E_{i,\mathrm{R}}^{\mathrm{S}} \le E_{i,t}^{\omega} \le E_{i,\mathrm{R}}^{\mathrm{S}},\ \forall i \in \Omega_{B,} \forall t \in \Omega_T, \forall \omega \epsilon \Xi\ , \tag{2.22}$$

2.6.2.6 Wind and load curtailment constraints

The constraints for wind and load curtailments are represented by (2.23) and (2.24), respectively. Equation (2.25) ensures that the wind curtailment is non-negative. Equation (2.26) defines the limit on the EWC. As mentioned earlier, this limit can allow a utility or system operator to ensure that the average amount of wind power curtailed should not exceed a certain set limit. This limit can be set according to the renewable energy utilization targets in different jurisdictions.

$$s_i^{\omega,t} + W_i^{\omega,t} = \overline{W}_i^{\omega,t},\ \forall i \in \Omega_B,\ \forall t \in \Omega_T, \forall \omega \epsilon \Xi\ , \tag{2.23}$$

$$0 \le r_{i,t}^{\omega} \le d_{i,t}^{\omega},\ \forall i \in \Omega_B,\ \forall t \in \Omega_T, \forall \omega \epsilon \Xi\ , \tag{2.24}$$

$$0 \le s_i^{\omega,t},\ \forall i \in \Omega_B,\ \forall t \in \Omega_T, \forall \omega \epsilon \Xi \tag{2.25}$$

$$\sum_{\omega} p_{\omega} \sum_{t}^{T_{\omega}} s_i^{\omega,t} \le \Lambda_i, \forall i \in \Omega_B\ , \tag{2.26}$$

2.6.2.7 Budget constraint

Equation (2.27) sets the limit on the total budget for the installation of CAES. This constraint is added in the model to ensure that the total investment in CAES does not exceed a certain limit.

$$\sum_{i\in\Omega_{\mathrm{B}}}\left(\mathrm{C}_{\mathrm{S,P}}^{\mathrm{IC}}P_{i,\mathrm{R}}^{\mathrm{S}}+\mathrm{C}_{\mathrm{S,E}}^{\mathrm{IC}}E_{i,\mathrm{R}}^{\mathrm{S}}\right)\leq Max\ Budget \tag{2.27}$$

2.6.2.8 Other constraints

The limits on the bus angles are represented by (2.28). Equation (2.29) sets the bus angle of the reference bus.

$$-\pi\leq\theta_{\mathrm{i}}^{\omega,t}\leq\pi\ ,\ \forall i\in\Omega_B, i\ \neq ref, \forall t\in\Omega_T, \forall\omega\epsilon\Xi\ , \tag{2.28}$$

$$\theta_{\mathrm{ref}}^{\omega,t}=0,\ \forall t\in\Omega_T, \forall\omega\epsilon\Xi\ , \tag{2.29}$$

The complete planning model is then represented as:

Min. (2.1)

Subject to: (2.2)–(2.29) (2.30)

2.6.2.9 Linearization of the model

The proposed model (2.30) is a mixed integer nonlinear programming model (MINLP). The nonlinearity of the model stems from the product of binary and continuous variables in (2.19) and (2.20). Although, nonlinear solvers exist which can solve the above problem, their computational performance is often poor. Moreover, as the number of scenarios grows, the computational burden increases significantly. Reference [33] presented a method for linearizing (2.19) and (2.20). In this work, the same linearization method is adopted. Equations (2.19) and (2.20) are replaced by:

$$0\leq p_{i,t}^{\mathrm{ch},\omega}\leq\vartheta_{i,t}^{\omega},\ \forall i\in\Omega_{B,}\forall t\in\Omega_T, \forall\omega\epsilon\Xi \tag{2.31}$$

$$0\leq p_{i,t}^{\mathrm{dch},\omega}\leq P_{i,\mathrm{R}}^{\mathrm{B}}-\vartheta_{i,t}^{\omega},\ \forall i\in\Omega_{B,}\forall t\in\Omega_T, \forall\omega\epsilon\Xi \tag{2.32}$$

$$0\leq\vartheta_{i,t}^{\omega}\leq\alpha_{i,t}^{\mathrm{B},\omega}\overline{p}_{\mathrm{B}},\ \forall i\in\Omega_{B,}\forall t\in\Omega_T, \forall\omega\epsilon\Xi \tag{2.33}$$

$$0\leq P_{i,\mathrm{R}}^{\mathrm{B}}-\vartheta_{i,t}^{\omega}\leq(1-\alpha_{i,t}^{\mathrm{B},\omega})\overline{p}_{\mathrm{B}}, \forall i\in\Omega_{B,}\forall t\in\Omega_T, \forall\omega\epsilon\Xi\ , \tag{2.34}$$

where, $\vartheta_{i,t}^{\omega}$ is the continuous auxillary variable.

The complete MILP model is then obtained as:

Min. (2.1)

Subject to: (2.2)–(2.17), (2.21)–(2.29), (2.31)–(2.34) (2.35)

The complete methodology for the proposed planning framework is shown in Figure 2.3. Meteorological data obtained from weather stations are used to generate wind power time series and DTLR time series [39]. In particular, the data for wind speed are usually obtained at a height which is lower than the actual height of the wind turbine. Therefore, the wind speed at a different height is obtained by:

$$v^{h_1}/_{v^{h_2}} = \left(h_1/_{h_2}\right)^{\alpha}, \tag{2.36}$$

where, v^{h_1} and v^{h_2} are the wind speed values at height h_1 and h_2, respectively. α is constant which is determined based on type of terrain [45]. After obtaining the time series for wind speed at a suitable height, wind speed is converted to wind power using wind power curve of a wind generator [32].

Next, a scenario reduction technique is adopted. The accuracy and efficiency of a stochastic programming model depends upon the number of scenarios utilized in the model [46]. However, the computational time increases exponentially with the increase in the number of scenarios. As a result, different scenario reduction techniques have been utilized to obtain a smaller set of scenarios [47]. These techniques combine similar scenarios based on some statistical and probabilistic metrics. In this work, forward selection algorithm (FSA) is used to obtain the reduced set of scenarios [30]. The FSA utilizes Kantorovich distance between the scenarios as the probability metric for reducing the number of scenarios. Further, SCENRED2, a scenario reduction toolbox provided by GAMS [48], is employed for implementing FSA. After obtaining the reduced set of scenarios, the optimization model (2.35) is solved to obtain the investment plan.

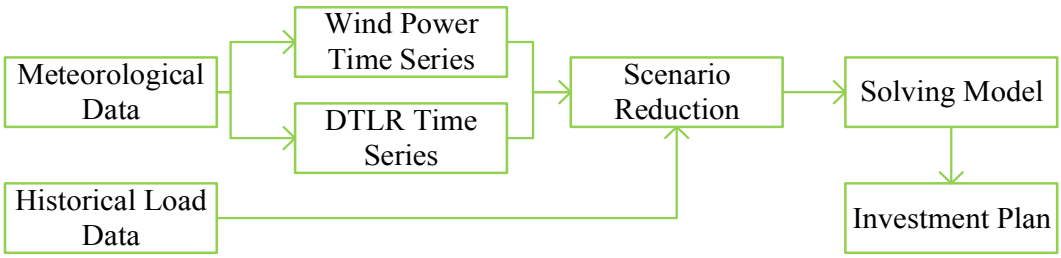

Figure 2.3 Proposed planning framework

2.7 Case Studies and Results

2.7.1 Test System

The proposed model is applied to a 24-bus IEEE Reliability Test System (RTS) [49]. The complete data for generators, transmission lines and load can be obtained from [50]. Two wind farms are added on bus 3 and bus 4 of the test system as shown in Figure 2.4. The penetration of the wind farm is set to 37.4% of the total generation capacity. In order to represent the load growth, the load at all buses have been increased by 30%. To model the degradation of transmission system assets, the line capacities are reduced by 20%. For forecast wind power and DTLR, the historical data of Wawa, Canada in the year 2005 has been utilized [39].

The load curtailment cost is set to \$5000/MWh. This high cost ensures that the load curtailment is always minimized. The actual load curtailment cost can be set by carrying out a value-based reliability assessment [51]. The load curtailment cost is then set to the value of loss of load (VOLL). Since, such studies are out of the scope of this work, the load curtailment cost is arbitrarily set to a high value. The data for CAES are given in Table 2.1 and Table 2.2. The cost data, in particular, has been adopted from [7].

For the DTLR, the installation costs are obtained from [52]. According to the information presented in [52], the per kilometer cost of installing a DTLR system is \$860,000. It is assumed that the lifetime of a DTLR system is 20 years and the annual discount factor is 5%.

The target EWC index at each bus is set to 15% of the total installed wind generation capacity on that bus.

The optimization model is solved using CPLEX 12.6.3. and MATLAB 2015. The optimality gap is set to a value of 0.1%. The computational time for all cases is under 8 minutes.

Table 2.1 Technical data of CAES

η_{ch}	η_{dch}	$\overline{p}_{\mathrm{B}}/\underline{p}_{\mathrm{B}}$ (MW)	$\overline{E}_{\mathrm{B}}/\underline{E}_{\mathrm{B}}$ (MWh)	k	γ (years)
0.85	0.85	300/0	1500/0	0	20

Table 2.2 Cost data of CAES

$C_{S,F}^{IC}$ ($)	$C_{S,P}^{IC}$ ($/MW)	$C_{S,E}^{IC}$ ($/MWh)	$\overline{E}_B/\underline{E}_B$ (MWh)	$\rho_{i,S}^{OC}$ ($/MWh)	γ (years)
0	400,000	2000	1500/0	3.59	20

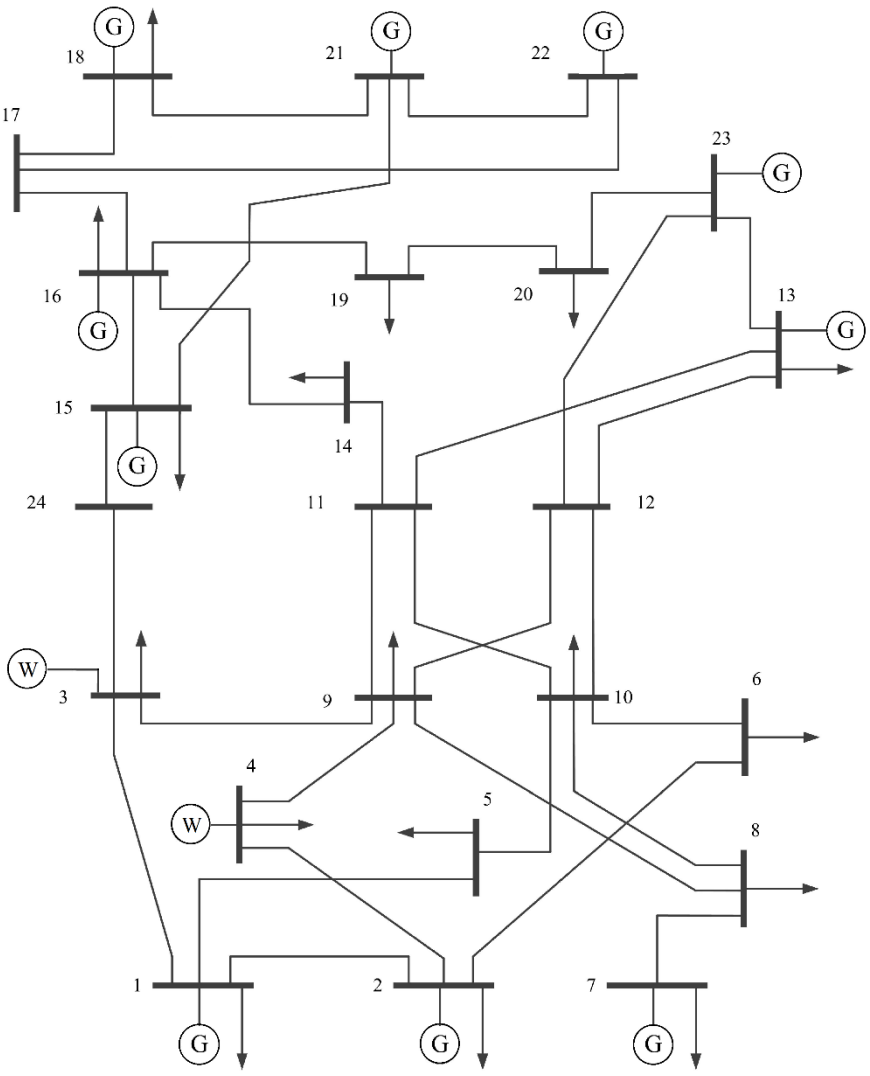

Figure 2.4 IEEE 24 Bus RTS

2.7.2 Wind, DTLR and Load Scenarios

After scenario reduction, five scenarios representing five days are obtained. Figure 2.5 and Figure 2.6 show the generated five scenarios for wind power and load, respectively. Figure 2.7 depicts five scenarios for DTLR of a transmission line. In these studies, it is assumed that the DTLR of other transmission lines vary in a similar manner. However, for more accurate results, different variations of DTLR for different transmission lines can be easily included. Table 2.3 shows the probability of these scenarios.

Table 2.3 Probability of reduced scenarios

Scenario 1	Scenario 2	Scenario 3	Scenario 4	Scenario 5	Sum
0.1790	0.0440	0.1620	0.4700	0.1460	=1

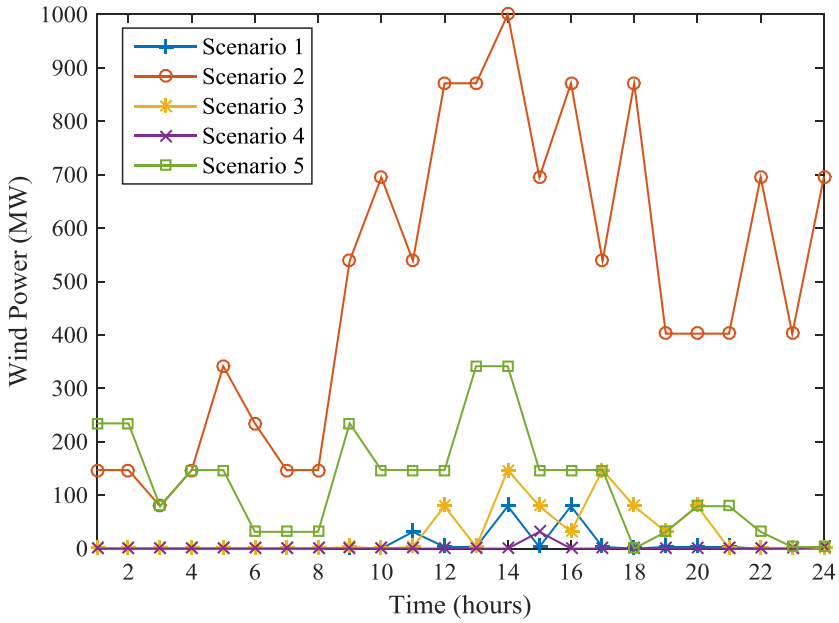

Figure 2.5 Wind power scenarios

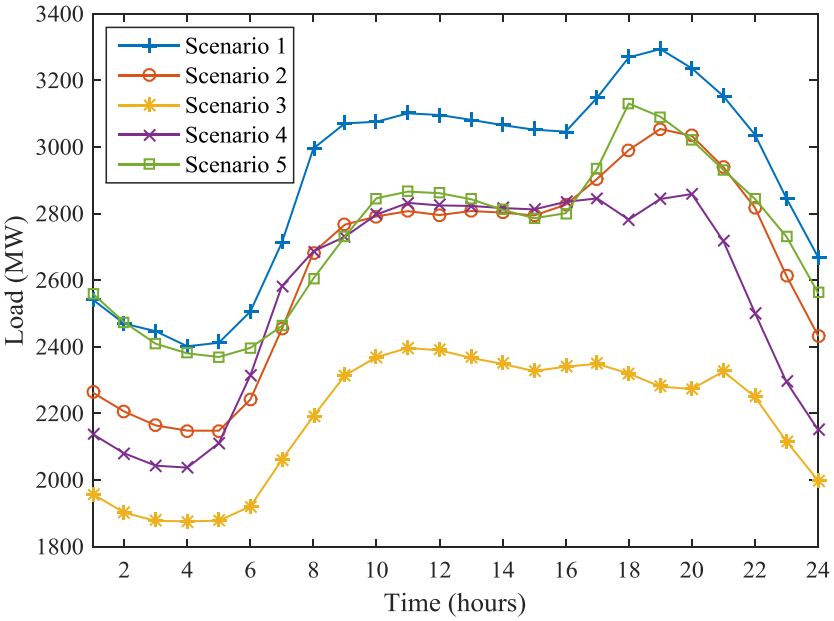

Figure 2.6 Load scenarios

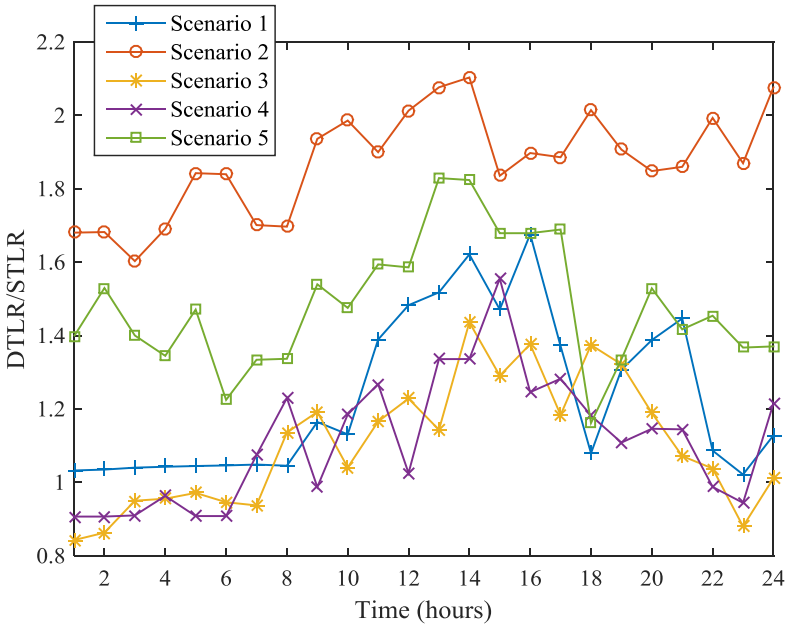

Figure 2.7 DTLR scenarios

2.7.3 Sizing and Siting Results

The sizing and siting results obtained from the proposed model are shown in Table 2.4 for the following two cases:

Case A: CAES sizing and siting only

Case B: CAES sizing and siting with DTLR siting

It can be observed from Table 2.4 that the investment cost decreases significantly when DTLR is included during the planning for CAES. A reduction of 36% in the investment cost was observed. For case A, a total of 4 CAES are deployed. In case B, instead of constructing 4 CAES, the model determines that it is more economical to construct 2 CAES and install 2 DTLR system on the transmission lines. These two lines have a common bus (bus 4) which has a wind generation.

Table 2.4 Investment plan for two cases

Case	Investment Cost ($)	Expected Operational Cost ($)	CAES Location (Buses)	DTLR Location
Case A	50.392 M	6.0327 M	2, 4, 12, 24	-
Case B	32.2153 M	6.0187 M	5, 17	Line 4-9 Line 2-4

The reason for the decrease in the investment costs can be shown from Figure 2.8 and Figure 2.9. These two figures pictorially depict the power balance constraint ((2.6)) for Scenario 2. As it can be observed, for case A (Figure 2.8), the power flow on the transmission lines between buses 4 to 2 and 4 to 9 are constrained to their maximum static rating (140 MW). In order to reduce wind curtailment at bus 4, a large CAES at this bus is constructed to store the power from wind generation and hence reduce its spillage.

On the other hand, for case B (Figure 2.9), after installing a DTLR system on the two transmission lines connected at this bus, higher amounts of wind power can be utilized. In fact, during the high wind period, the two transmission lines carry significantly higher amount of power as compared to their static ratings. Subsequently, there is a significant reduction in the spillage of wind power. This is achieved without the construction of a large-scale CAES at this bus. Therefore, this results in the reduction of investment costs for CAES.

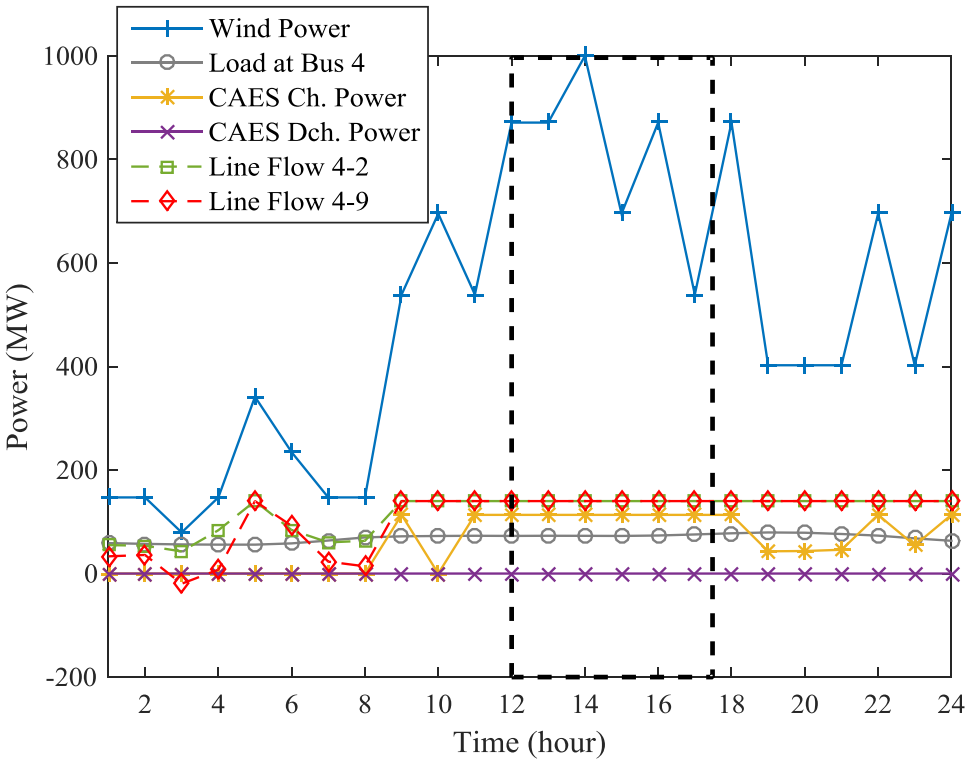

Figure 2.8 Power balance at bus 4 for Case A

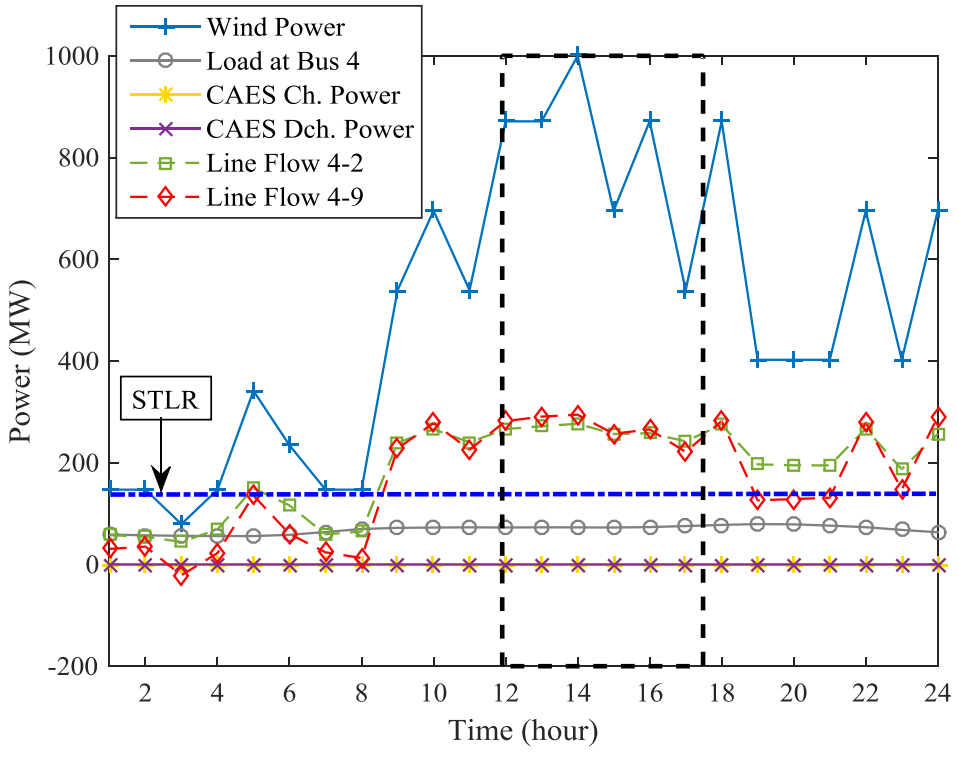

Figure 2.9 Power balance at bus 4 for Case B

2.7.3.1 CAES applications for two cases

To understand the applications of CAES in two cases, the SOC in terms of the energy of CAES is plotted for different scenarios. Figure 2.10 and Figure 2.11 show the energy of CAES installed at different buses for case A. From these figures; it can be concluded that for CAES plants installed on bus 2 and bus 12, the primary application is to offset the conventional generation during peak hours. Also, bus 2 is connected to bus 4 which has wind generation. Hence, CAES plant at bus 2 can utilize wind generation from bus 4. For these two locations, CAES plant acts as peaking unit. On the other hand, for bus 4, the main application of CAES is to support the wind generation at that bus and reduce the spillage of wind power. This is also evident from Figure 2.10 which shows that in a certain scenario (high wind scenario), CAES stores the excess output from wind to keep the wind curtailment to a pre-defined value. For bus 24 which is connected to bus 3 through a transformer (bus 3 and bus 24 are located on the same substation), CAES stores wind generation at bus 3 during high wind hours and utilizes it for supplying load during peak hours. Hence, for this bus, CAES is used for time shifting of wind power.

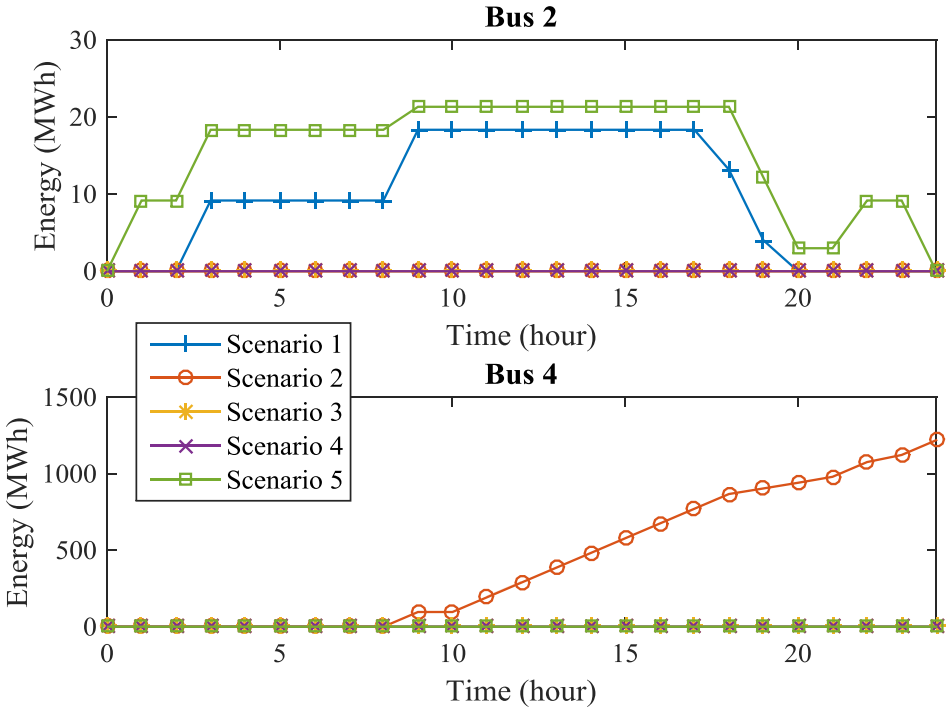

Figure 2.10 SOC (Energy) of CAES at bus 2 and 4

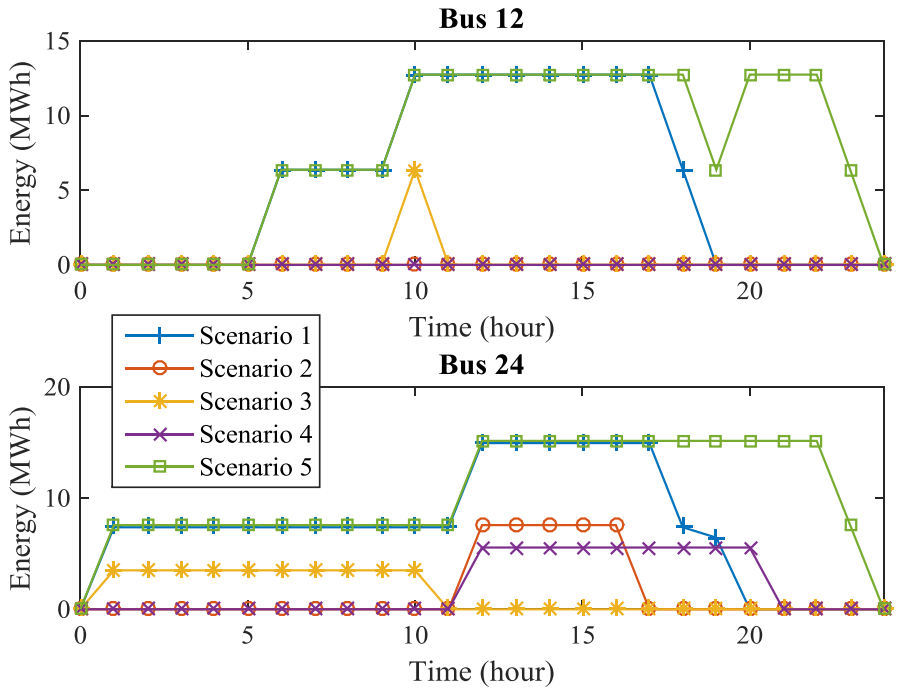

Figure 2.11 SOC (Energy) of CAES at bus 12 and 24

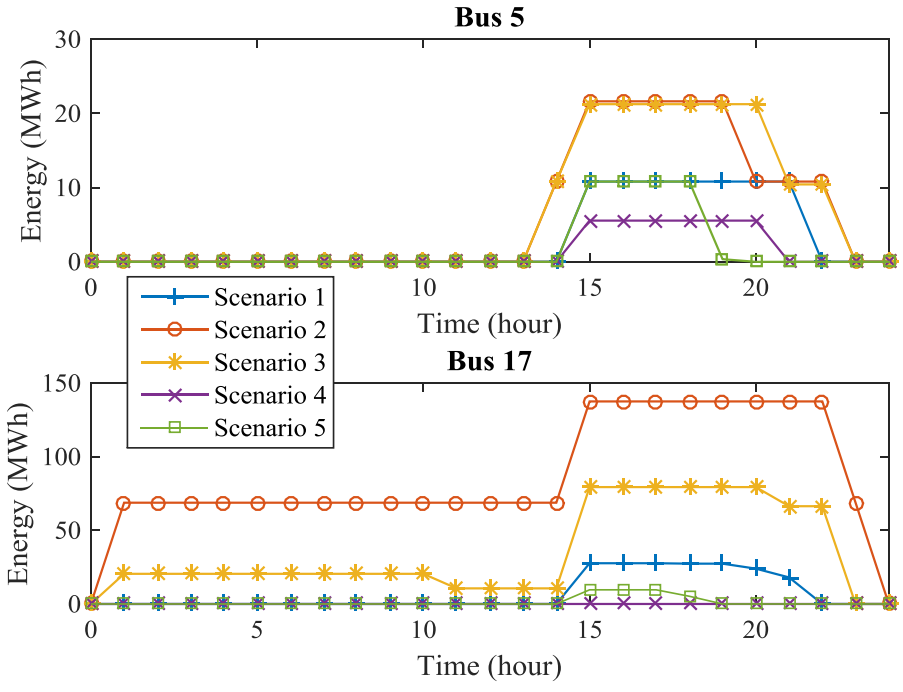

Figure 2.12 SOC (Energy) of CAES at bus 5 and 17

Figure 2.12 indicates the energy of two CAES installed for case B. For CAES installed at bus 5, it is also employed to offset the generation and reduce the generation costs from conventional generators. CAES located at bus 17 also acts as peaking unit and performs peak shaving. It is also observed that CAES at this bus supplies the load during the last 4 hours of the day (hour 21-24). During these hours, the conventional generators on the buses connected to bus 17 (which are, bus 16, bus 18, and bus 22) are shut-down to satisfy their minimum down-time constraints. Particularly, the conventional generators connected to bus 16 and bus 18 have high minimum power generation limit. Hence, keeping these generators on would result in higher generation costs.

2.8 Conclusion

In this chapter, a framework for optimal planning of CAES was developed. The proposed framework included the installation decisions of DTLR system. The wind spillage was controlled through EWC instead of utilizing a wind spillage cost. The results have indicated that a more economic plan for CAES is obtained when DTLR system is considered during the planning of CAES. It was observed that DTLR coupled with CAES can significantly reduce the wind spillage. Further insight into the results have shown that the applications of CAES vary depending upon the location of CAES in the power system. In particular, when CAES is closed to a bus with wind generation, the primary function of the CAES is to reduce wind spillage. On the other hand, CAES also acts as a peaking unit to reduce the operational costs of a power system.

Chapter 3

Optimal Scheduling of Compressed Air Energy Storage in Electricity Markets Considering Turbomachinery Charactersitc Curves[1]

"Problems worthy of attack prove their worth by fighting back."
- Piet Hein, *Grooks*

3.1 Abstract

Compressed air energy storage (CAES) is a promising large-scale energy storage technology with relatively low capital and operational costs that justify its participation in electricity markets. However, the actual profits obtained from CAES are highly dependent on its efficiency. In this regard, this part of the thesis proposes an accurate model of CAES that represents the variation in its efficiency under different operating conditions. In the proposed model, the efficiency of CAES is expressed in terms of the isentropic efficiencies of individual components using their turbomachinery characteristic curves. The proposed model can also consider additional components in CAES, such as a pre-heater (PH) and changes in ambient conditions, such as ambient temperature. The proposed model is then linearized so that it can be solved with a high computational efficiency. After validating its accuracy using the data of an existing CAES plant, the linearized model is applied to the problem of optimal scheduling of CAES in electricity markets. The results indicate that efficiency variation significantly affects the bidding schedule of CAES in electricity markets. Moreover, feasible schedules with actual profits that do not violate the operating pressure constraints of CAES are obtained. Further case studies also indicate the benefits of including a PH in CAES.

[1]

3.2 Nomenclature

Sets/Indices

κ	Index
t	Index of hours
Ξ	Set of scenarios
Ω_T	Set of hours

Subscripts and Superscripts for the CAES Model

is	Isentropic
In	Inlet conditions of a component
out	Outlet conditions of a component
s	Storage conditions
AC	Aftercooler
IC	Intercooler
CC	Combustion chamber
PH	Pre-heater
HPC	High pressure compressor
LPC	Low pressure compressor
HPT	High pressure turbine
HPT	Low pressure turbine

Parameters

c^{OM}	Operational and maintenance (O&M) cost ($/MWh)
$c_p^{(.)}$	Specific heat of air at constant pressure of component (.) (kJ/K)
f_e	Electrical grid's frequency (Hz)
g	Gear ratio
$p_{\text{dch}}^{\max}$	Maximum discharging power (MW)
$p_{\text{dch}}^{\min}$	Minimum discharging power (MW)
$p_{\text{ch}}^{\max}$	Maximum charging power (MW)
$p_{\text{ch}}^{\min}$	Minimum charging power (MW)

p_κ	Probability of the κth scenario
LHV	Lower heating value of fuel (natural gas) (MJ/kg)
$\mathrm{P_{atm}}$	Atmospheric pressure (1 bar)
$\overline{P}_s$	Maximum allowable air pressure inside the cavern (bar)
$\underline{P_s}$	Minimum allowable air pressure inside the cavern (bar)
$\mathrm{P}_{s,\mathrm{final}}$	Final air pressure inside the cavern (bar)
R	Gas constant ($\mathrm{bar} \cdot \mathrm{m}^3 \cdot \mathrm{kg}^{-1} \cdot \mathrm{K}^{-1}$)
T_s	Temperature of air stored in the cavern (K)
V_s	Volume of the cavern (m^3)
ε	Effectiveness of a pre-heater
$\gamma^{(.)}$	Ratio of specific heats of component (.)
η^{CC1}	Efficiency of the combustion chamber 1
η^{CC2}	Efficiency of the combustion chamber 2
ρ_{sr}	Probability of spinning reserve deployment
$\pi_{\mathrm{E}}^{\kappa,t}$	Price of energy at hour t in scenario κ (\$/MWh)
$\pi_{\mathrm{R}}^{\kappa,t}$	Price of reserve at hour t in scenario κ (\$/MWh)
π_{NG}^{t}	Price of natural gas at hour t (\$/GJ)
Δt	Time step (1 hour)

Variables

p_{ch}^{t}	Charging power of CAES (MW)
p_{dch}^{t}	Discharging power of CAES (MW)
$p_{\mathrm{sr,ch}}^{t}$	Spinning reserve in charging mode (MW)
$p_{\mathrm{sr,ch}}^{t}$	Spinning reserve in discharging mode (MW)
$q_{(.)}^{t}$	Dimensionless rotational speed of component (.)
$x_{(.)}^{t}$	Dimensionless mass flow rate of component (.)
$y_{(.)}^{t}$	Dimensionless pressure ratio of component (.)
M_s^{t}	Mass of air in the cavern (kg)
$\dot{M}_{\mathrm{s,in}}^{t}$	Mass flow in of the storage in charging mode (kg/s)
$\dot{M}_{\mathrm{s,out}}^{t}$	Mass flow out of the storage in discharging mode (kg/s)

$\dot{M}_{(.)}^{t}$	Mass flow rate in component (.) (kg/s)
$\dot{M}_{\mathrm{fu,CC1}}^{t}$	Fuel flow rate in the combustion chamber 1 (kg/s)
$\dot{M}_{\mathrm{fu,CC2}}^{t}$	Fuel flow rate in the combustion chamber 2 (kg/s)
P_{s}^{t}	Pressure of air inside the cavern (bar)
$P_{(.)}^{t,\mathrm{in}}$	Inlet pressure of component (.) (bar)
$P_{(.)}^{t,\mathrm{out}}$	Outlet pressure of component (.) (bar)
$T_{(.)}^{\mathrm{in}}$	Inlet temperature of component (.) (K)
$T_{(.)}^{\mathrm{out}}$	Outlet temperature of component (.) (K)
$T_{(.)}^{t,\mathrm{out,is}}$	Outlet temperature of component (.) considering isentropic thermodynamic processes (K)
$T_{\mathrm{PH}}^{\mathrm{A}}$	Outlet temperature of air of a PH (K)
$T_{\mathrm{PH}}^{\mathrm{E}}$	Inlet temperature of exhaust gases of a PH (K)
$W_{(.)}^{t}$	Mechanical power consumed or generated (MW)
$\alpha_{\mathrm{c,ch/dch}}^{t}$	Binary variable indicating charging status of CAES: 1 if it is charging, 0 otherwise
$\alpha_{\mathrm{c,dch}}^{t}$	Binary variable indicating charging status of CAES: 1 if it is discharging, 0 otherwise
$\eta_{\mathrm{is},(.)}^{t}$	Isentropic efficiency of component (.)
$\omega_{(.)}^{t}$	Rotational speed of component (.) (rad/s)

3.3 Introduction

Compressed air energy storage (CAES) technology can store electrical energy in the form of compressed air for long durations at high power ratings. The operational and maintenance (O&M) costs of CAES are among the lowest of all storage technologies [7]. Also, unlike batteries, CAES does not suffer from self-discharge losses and lifecycle reduction [7], [19]. Moreover, being a large-scale energy storage, CAES can assist in integrating higher proportions of renewable energy sources into existing power systems [53]. Currently, two CAES plants are operational around the world: one in Huntorf, Germany and the other in McIntosh, Alabama, USA [7], [19]. These plants

have exhibited high values of availability and starting reliability[2] [19], [20]. Several new CAES projects are also in the planning and construction phases [20].

As a result of its economic and technical benefits, some researchers have considered the participation of CAES in electricity markets to bring economic benefits to the owners. In [54] and [55], CAES participates in the energy market to obtain profit through arbitrage. Because a single source of revenue might not justify the involvement of CAES in electricity markets, in [56], a privately-owned CAES also provides transmission congestion relief as an ancillary service. The authors in [57] considered both energy and reserve markets for devising the optimal schedules for CAES.

The profits obtained from the participation of CAES in electricity markets critically depend upon its efficiency. If CAES operates at low efficiency, substantial energy loss would therefore significantly reduce the profits [54]. Existing CAES models can be broadly classified into two types: models with constant efficiency and models with variable efficiency.

The first type of model assumes the efficiency of the whole CAES plant is constant irrespective of the operating conditions. These models are linear and hence can be directly employed in power systems optimization problems (e.g., [54], [55], [56], [58], [59], [60]). However, the efficiency of CAES depends upon its operating conditions, such as charging/discharging power, ambient conditions, and the use of additional components, e.g., a pre-heater (PH) [61], [62], [63]. As a result, constant-efficiency models are inaccurate and may lead to suboptimal or even infeasible solutions. Hence, to obtain optimal bidding schedules for CAES that are within its operational limits, it is imperative to consider variation in the efficiency of CAES.

Variable efficiency models make use of thermodynamic relationships for the compression, expansion, and combustion processes of CAES [62], [63]. The efficiency is expressed in terms of individual efficiencies of different components of CAES, such as compressors and turbines [61]. For compressors and turbines (also collectively known as turbomachinery), the variation in their efficiencies under different operating conditions is obtained from their turbomachinery characteristic curves (TCCs) [61]. *Briola* et al. proposed TCCs for CAES based on data from the

[2] Availability is concerned with the probability of a component being found in the normal and completely working state for some time in future. Starting reliability relates to the probability that a component is started successfully from its off or down state.

Huntorf plant [62]. The simulations indicate a close match between the plant data and the proposed model for rated conditions. The authors in [63] also developed a model for CAES considering TCCs and compared the performance of CAES for different discharging modes. The variable efficiency models, such as those presented in [62] and [63], suffer from the major drawback that they are highly nonlinear and, hence, cannot be utilized directly in the optimization problems for power systems. In this regard, *Shafiee* et al. linearized the results of [63] using binary techniques to consider the effects of TCCs of CAES [57]. The results indicate the operating schedule of CAES could be affected by taking into account the variation in its efficiency. However, the model presented in [57] depends upon the results of the thermodynamic analysis of CAES presented in [63]. Also, because thermodynamic relationships and TCCs are not explicitly included in [57], the model may not be applicable if CAES includes additional components such as a PH or if there is a change in ambient conditions such as ambient temperature. On the other hand, it has been demonstrated at the McIntosh CAES plant that a PH can improve the overall efficiency of CAES by 12% and reduce fuel consumption by 22-25% [7], [19]. This implies that the profits obtained by CAES in the electricity market could be affected by considering a PH.

3.4 Contributions

To address these issues, this chapter develops an accurate model of CAES that takes into account its variable efficiency. The model explicitly includes the thermodynamic relationships and TCCs and therefore can consider the effects of the inclusion of additional components and variation in operating conditions on CAES operation. First, a complete nonlinear model of CAES is developed. Reasonable assumptions are then made to simplify the model, which is subsequently converted into a bilinear model by piecewise linearization of nonlinear terms. Last, the bilinear terms are relaxed using piecewise McCormick relaxation to obtain a mixed-integer linear model. Because the model contains a large number of binary variables that can increase the computational burden, the aforementioned piecewise linearization is reformulated using a logarithmic number of binary variables. The proposed model is then validated using data from the Huntorf plant. To show its effectiveness and importance, the model is applied to an optimal scheduling problem in the energy and reserve markets. In summary, the main contributions of this chapter to the existing literature on CAES are two-fold.

1. This work develops a linear, accurate, and comprehensive model of CAES that directly considers the thermodynamic relationships and TCCs and hence can incorporate their effects on CAES operation. Another advantage of the proposed model is that it can also consider the inclusion of a PH in CAES and changes in the ambient conditions.
2. This work proposes an optimal scheduling model that includes the detailed linear CAES model.

3.5 Modeling CAES

Conventional CAES can be regarded as a modified gas turbine with separated compression and expansion processes (Figure 3.1). In the following subsections, each process of CAES is modeled individually using the thermodynamic relationships of compression, combustion, and expansion processes.

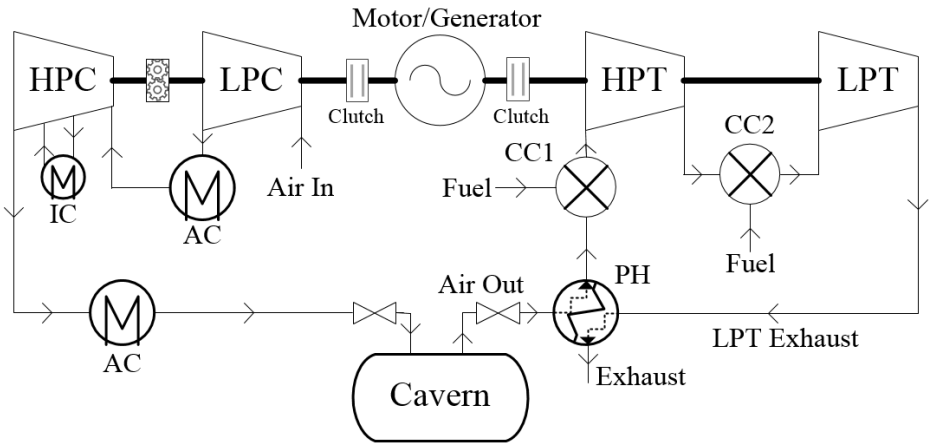

Figure 3.1 Schematic diagram of CAES

3.5.1 Charging Circuit

In a typical configuration, the charging circuit includes a low-pressure compressor (LPC) and a high-pressure compressor (HPC). The electric motor drives the compressors using electricity from a power grid, and the air at ambient conditions is compressed and stored in the cavern. As a result of using intercoolers (ICs) and aftercoolers (ACs), the inlet air temperatures at all stages of compression remain constant, provided the ambient air temperature at the inlet of the LPC is constant. The thermodynamic equations representing the energy balance and mass balance during the compression process are given by (3.1)–(3.8) [61], [62] and defined for each time period in

$\Omega_T = \{1, \dots, \mathrm{T}\}$, where T is the scheduling horizon i.e., $\forall t \in \Omega_T$. The variables are defined in Section 3.2 of this chapter.

$$W^t_{\mathrm{LPC}} \eta^t_{\mathrm{is,LPC}} = \dot{M}^t_{\mathrm{LPC}} c_p^{\mathrm{LPC}} \left(T^{t,\mathrm{out,is}}_{\mathrm{LPC}} - T^{\mathrm{in}}_{\mathrm{LPC}}\right), \tag{3.1}$$

$$W^t_{\mathrm{HPC}} \eta^t_{\mathrm{is,HPC}} = \dot{M}^t_{\mathrm{HPC}} c_p^{\mathrm{HPC}} \left(T^{t,\mathrm{out,is}}_{\mathrm{HPC}} - T^{\mathrm{in}}_{\mathrm{HPC}}\right), \tag{3.2}$$

$$T^{t,\mathrm{out,is}}_{\mathrm{LPC}} = T^{\mathrm{in}}_{\mathrm{LPC}} \left(P^{t,\mathrm{out}}_{\mathrm{LPC}} / P^{t,\mathrm{in}}_{\mathrm{LPC}}\right)^{\left(1 - \frac{1}{\gamma^{\mathrm{LPC}}}\right)}, \tag{3.3}$$

$$T^{t,\mathrm{out,is}}_{\mathrm{HPC}} = T^{\mathrm{in}}_{\mathrm{HPC}} \left(P^{t,\mathrm{out}}_{\mathrm{HPC}} / P^{t,\mathrm{in}}_{\mathrm{HPC}}\right)^{\left(1 - \frac{1}{\gamma^{\mathrm{HPC}}}\right)}, \tag{3.4}$$

$$\dot{M}^t_{\mathrm{LPC}} = \dot{M}^t_{\mathrm{HPC}} = \dot{M}^t_{\mathrm{s,in}}, \tag{3.5}$$

$$P^{t,\mathrm{in}}_{\mathrm{LPC}} = \mathrm{P}_{\mathrm{atm}}, \tag{3.6}$$

$$P^{t,\mathrm{in}}_{\mathrm{HPC}} = P^{t,\mathrm{out}}_{\mathrm{LPC}}, \tag{3.7}$$

$$\omega^t_{\mathrm{LPC}} = g\omega^t_{\mathrm{HPC}} = \omega^t_{\mathrm{Motor}} = 2\pi f_e. \tag{3.8}$$

Equations (3.1) and (3.2) represent the energy balance for the LPC and HPC, respectively. The adiabatic relationships between the inlet/outlet temperatures and inlet/outlet pressures for LPC and HPC are defined by (3.3) and (3.4), respectively. Equation (3.5) describes the mass balance for the charging circuit. Equations (3.6) and (3.7) define constraints on inlet pressures of the LPC and HPC, respectively. The rotational speed of the LPC, HPC, and motor are described by (3.8). In the above formulation, the efficiencies of LPC and HPC are defined by isentropic efficiencies $\eta^t_{\mathrm{is},(.)}$. The isentropic efficiency measures the deviation of an actual thermodynamic process from the idealized one. The determination of isentropic efficiencies will be shown later in Section 3.5.3.

3.5.2 Discharging Circuit

During discharging stage, the compressed air from the cavern is released and regulated through the valve at the inlet of the PH. The PH utilizes the exhaust gases from the last turbine to heat the air before entering the first combustion chamber (CC1), thereby reducing the amount of fuel required for combustion in CC1. In CC1, the compressed air is combusted using fuel, which is typically natural gas [19]. The high-temperature mixture of air and fuel is then expanded in the high-pressure turbine (HPT). Afterward, it is again combusted in the second combustion chamber (CC2) and finally expanded in the low-pressure turbine (LPT). As a result of using the valve at the

inlet of the PH, the mass flow rate and inlet pressure at the HPT for a given output power remain constant [63]. Based on the energy balance and mass balance, thermodynamic equations for the expansion process are given by (2.9)–(2.21) [61], [62] and defined for each time period in Ω_T i.e., $\forall t \in \Omega_T$.

$$\dot{M}^t_{\mathrm{s,out}} c_p^{\mathrm{PH}} \left(T^{\mathrm{A}}_{\mathrm{PH}} - T_s\right) - \dot{M}^t_{\mathrm{LPT}} c_p^{\mathrm{LPT}} \left(T^{\mathrm{out,is}}_{\mathrm{LPT}} - T^{\mathrm{E}}_{\mathrm{PH}}\right) = 0, \tag{3.9}$$

$$\varepsilon = \left(c_p^{\mathrm{PH}} \left(T^{\mathrm{A}}_{\mathrm{PH}} - T_s\right)\right) / \left(c_p^{\mathrm{LPT}} (T^{\mathrm{out,is}}_{\mathrm{LPT}} - T_s)\right), \tag{3.10}$$

$$\dot{M}^t_{\mathrm{s,out}} + \dot{M}^t_{\mathrm{fu,CC1}} = \dot{M}^t_{\mathrm{HPT}}, \tag{3.11}$$

$$\dot{M}^t_{\mathrm{fu,CC1}} \left(c_p^{\mathrm{fu}} T^{\mathrm{fu}}_{\mathrm{CC1}} + \mathrm{LHV}\eta^{\mathrm{CC1}}\right) + \dot{M}^t_{\mathrm{s,out}} c_p^{\mathrm{CC1}} T^{\mathrm{A}}_{\mathrm{PH}} - \dot{M}^t_{\mathrm{HPT}} c_p^{\mathrm{HPT}} T^{\mathrm{in}}_{\mathrm{HPT}} = 0, \tag{3.12}$$

$$W^t_{\mathrm{HPT}} = \dot{M}^t_{\mathrm{HPT}} c_p^{\mathrm{HPT}} \left(T^{t,\mathrm{in}}_{\mathrm{HPT}} - T^{t,\mathrm{out,is}}_{\mathrm{HPT}}\right) \eta^t_{\mathrm{is,HPT}}, \tag{3.13}$$

$$W^t_{\mathrm{LPT}} = \dot{M}^t_{\mathrm{LPT}} c_p^{\mathrm{LPT}} \left(T^{t,\mathrm{in}}_{\mathrm{LPT}} - T^{t,\mathrm{out,is}}_{\mathrm{LPT}}\right) \eta^t_{\mathrm{is,LPT}}, \tag{3.14}$$

$$T^{t,\mathrm{out,is}}_{\mathrm{HPT}} = T^{\mathrm{in}}_{\mathrm{HPT}} \left(P^{t,\mathrm{out}}_{\mathrm{HPT}} / P^{t,\mathrm{in}}_{\mathrm{HPT}}\right)^{\left(1 - \frac{1}{\gamma^{\mathrm{HPT}}}\right)}, \tag{3.15}$$

$$T^{t,\mathrm{out,is}}_{\mathrm{LPT}} = T^{\mathrm{in}}_{\mathrm{LPT}} \left(P^{t,\mathrm{out}}_{\mathrm{LPT}} / \mathrm{P}^{t,\mathrm{in}}_{\mathrm{LPT}}\right)^{\left(1 - \frac{1}{\gamma^{\mathrm{LPT}}}\right)}, \tag{3.16}$$

$$\dot{M}^t_{\mathrm{HPT}} + \dot{M}^t_{\mathrm{fu,CC2}} = \dot{M}^t_{\mathrm{LPT}}, \tag{3.17}$$

$$\dot{M}^t_{\mathrm{fu,CC2}} \left(c_p^{\mathrm{fu}} T^{\mathrm{fu}}_{\mathrm{CC2}} + \mathrm{LHV}\eta^{\mathrm{CC2}}\right) + \dot{M}^t_{\mathrm{HPT}} c_p^{\mathrm{HPT}} T^{t,\mathrm{out}}_{\mathrm{HPT}} - \dot{M}^t_{\mathrm{LPT}} c_p^{\mathrm{LPT}} T^{\mathrm{in}}_{\mathrm{LPT}} = 0, \tag{3.18}$$

$$P^{t,\mathrm{out}}_{\mathrm{HPT}} = P^{t,\mathrm{in}}_{\mathrm{LPT}}, \tag{3.19}$$

$$P^{t,\mathrm{out}}_{\mathrm{LPT}} = \mathrm{P}_{\mathrm{atm}}, \tag{3.20}$$

$$\omega^t_{\mathrm{HPT}} = \omega^t_{\mathrm{LPT}} = \omega^t_{\mathrm{Generator}} = 2\pi f_e. \tag{3.21}$$

The PH is modeled by (3.9)–(3.10) in terms of its effectiveness ε. The effectiveness of a PH defines its efficiency. Higher values of ε imply higher reduction in fuel consumption. Equation (3.11) represents the mass balance and (3.12) describes the energy balance for CC1. Equations (3.13)–(3.14) represent the energy balance for the turbines. Equations (3.15)–(3.16) are the adiabatic relationships between temperatures and pressures of the turbines. The inlet temperatures of the turbines are generally kept constant for better heat utilization [19]. The mass balance and energy balance for CC2 are described by (3.17) and (3.18), respectively. Equations (3.19) and

(3.20) are the additional constraints on the outlet pressures. Equation (3.21) ensures that all turbines and the generator rotate at the same rotational speed.

3.5.3 Turbomachinery Characteristic Curves

In the previous formulation for the charging and discharging circuits, the isentropic efficiencies $\eta^{t}_{\mathrm{is},(.)}$ are not constant. Instead, they vary with the charging and discharging power levels, mass flow rates, ratio of inlet to outlet pressures, and rotational speed of the turbomachinery. The isentropic efficiency of the turbomachinery determines the deviation of the actual compression or expansion process from idealized isentropic processes. The variation in the isentropic efficiency for different operating conditions is obtained from the TCCs. The TCCs of turbomachinery define the relationships between the mass flow rate, pressure ratio, isentropic efficiencies, and rotational speed at various operating conditions [61], [62]. These relationships are expressed in terms of dimensionless variables. These curves are determined either empirically [62] or analytically [63].

To include the TCCs of the compressors and turbines in the model, additional dimensionless variables are defined. These variables include dimensionless mass flow rate, pressure ratio, and dimensionless rotational speed.

For the charging circuit, these additional variables are defined by (3.22)–(3.24). Then, the TCCs are expressed by (3.25)–(3.29) [63], [64]. For the sake of simplicity, the superscripts for time and subscripts for compressors are dropped. However, it should be noted that these variables are defined for each compressor in the charging circuit, and $\forall t \in \Omega_T$.

$$x = \left(\dot{M}\sqrt{T^{\mathrm{in}}}/P^{\mathrm{in}}\right)/\left(\dot{M}_{\mathrm{dp}}\sqrt{T^{\mathrm{in}}_{\mathrm{dp}}}/P^{\mathrm{in}}_{\mathrm{dp}}\right), \tag{3.22}$$

$$q = \left(\omega/\sqrt{T^{in}}\right)/\left(\omega_{dp}/\sqrt{T^{in}_{dp}}\right), \tag{3.23}$$

$$y = P^{\mathrm{out}}/P^{\mathrm{in}}, \tag{3.24}$$

$$\eta_{\mathrm{is}}/\eta_{\mathrm{is,dp}} = \left(1.4 - 0.3(1-q)^2\right)(q/x)(2 - q/x), \tag{3.25}$$

$$y/y_{\mathrm{dp}} = ax^2 + bx + c, \tag{3.26}$$

$$a = q/(p_1(1 - p_2 q^{-1}) + q(q - p_2)^2), \tag{3.27}$$

$$b = (p_1 - 2p_2 q^2)/(p_1(1 - p_2 q^{-1}) + q(q - p_2)^2), \tag{3.28}$$

$$c = -(p_1 p_2 q - {p_2}^2 q^3)/(p_1(1 - p_2 q^{-1}) + q(q - p_2)^2), \tag{3.29}$$

where dp represents the design point (rated) conditions and p_1, p_2 are constants

Similar to the charging circuit, additional dimensionless variables are defined for the discharging circuit. Equations (3.22) and (3.23) are also employed to define x and q for the discharging circuit. However, the definition of y is reversed and is given by (3.30). The TCCs for turbines are given by (3.31)–(3.33) [63], [64].

$$y = P^{\text{in}}/P^{\text{out}}, \tag{3.30}$$

$$\dot{M}/\dot{M}_{\text{dp}} = \alpha\left(\sqrt{T^{\text{in}}}/\sqrt{T^{\text{in}}_{\text{dp}}}\right)\left(\sqrt{y^2 - 1}/\sqrt{y_{dp}^2 - 1}\right), \tag{3.31}$$

$$\alpha = \left(1.4 - 0.4(\omega/\omega_{\text{dp}})\right)^{1/2}, \tag{3.32}$$

$$\eta_{\text{is}}/\eta_{\text{is,dp}} = (1.4 - 0.3(1 - q)^2)\,(q/x)(2 - q/x). \tag{3.33}$$

The turbomachinery characteristic curves for the isentropic efficiencies of the turbines (3.33) and compressors (3.25) are shown in Figure 3.2(a) and Figure 3.2(b), respectively.

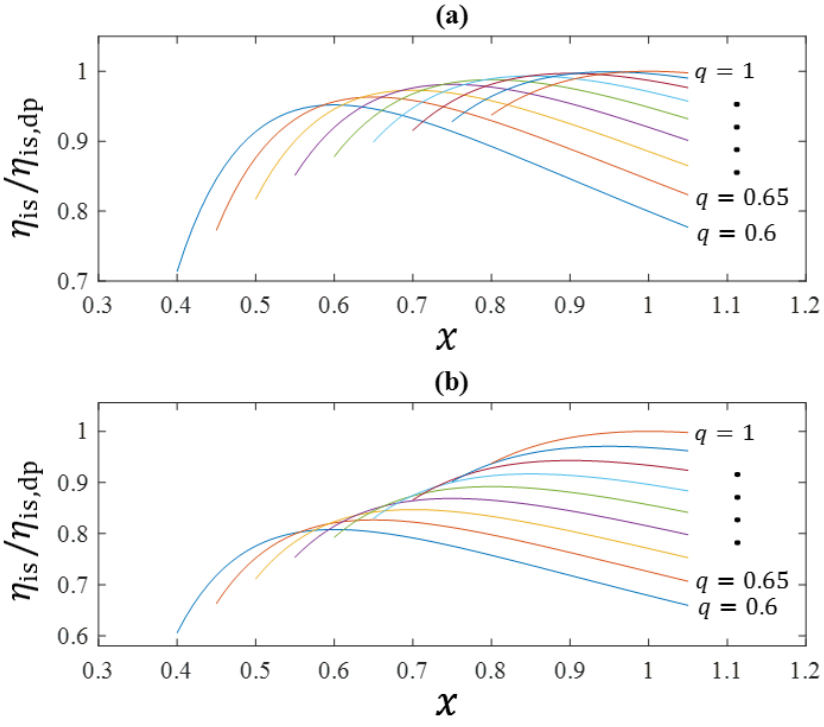

Figure 3.2 TCCs for isentropic efficiencies

3.5.4 Cavern Model

The thermodynamic equations for the cavern are formulated by (3.34)–(3.37).

$$P_{\mathrm{s}}^{t} V_{\mathrm{s}} = M_{\mathrm{s}}^{t} R T_{\mathrm{s}}\,,\ \forall t \in \Omega_T, \tag{3.34}$$

$$\dot{M}_{\mathrm{s}}^{t} = \dot{M}_{\mathrm{s,in}}^{t} - \dot{M}_{\mathrm{s,out}}^{t},\ \forall t \in \Omega_T, \tag{3.35}$$

$$M_{\mathrm{s}}^{t} = M_{\mathrm{s}}^{t-1} + \dot{M}_{\mathrm{s}}^{t}\,\Delta t,\ \forall t \in \Omega_T, \tag{3.36}$$

$$\underline{P_{\mathrm{s}}} \le P_{\mathrm{s}}^{t} \le \overline{P}_{\mathrm{s}},\ \forall t \in \Omega_T. \tag{3.37}$$

Equation (3.34) is the equivalent form of ideal gas equation for the air inside the cavern [60]. Equations (3.35)–(3.36) determine the mass of air inside the cavern. The operating pressure of the cavern is limited by (3.37). Equations (3.34)–(3.37) determine the state-of-charge (SOC) of the CAES. These equations model the SOC of the CAES in terms of its physical quantities, which are the mass and pressure of the air inside the cavern.

3.6 MILP Formulation of the Model

The CAES model presented in the previous section ((3.1)–(3.37)) is highly nonlinear. The nonlinearity of the model arises from the bilinear terms in the energy balance equations ((3.1)–(3.2), (3.9), (3.12)–(3.14), and (3.18)), and the nonlinear terms of adiabatic relationships ((3.3)–(3.4), and (3.15)–(3.16)) and the TCCs in the charging and discharging circuits ((3.22)–(3.33)). The cavern model is already linear. To simplify the model, the rotational speeds of turbomachinery are assumed to be constant at all times. This is a reasonable assumption because the rotational speed of turbomachinery is governed by the rotational speed of the motor/generator unit, which in turn is determined by the electrical grid's frequency as given by (3.8) and (3.21). Also, because the electrical grid's frequency is generally not considered in the day-ahead hourly scheduling problems (e.g., [55], [56], [57]), it is assumed to be constant at all given times. Moreover, the solution of the nonlinear model indicates that for an allowable variation of ±1% in the electrical grid's frequency [65], the deviation in the mass flow rates, the air pressure inside the cavern, and hence the SOC, is insignificant. After making this assumption, the simplified model is first converted to a bilinear model through piecewise linearization of nonlinear terms using convex combination linearization [66]. Then, all bilinear terms in the model are relaxed using piecewise

McCormick linearization [66], [67]. The detailed process of linearization is given in the following subsections.

3.6.1 Bilinear Formulation of Charging Circuit Model

For the charging circuit, because the inlet temperatures are constant for each compressor, (3.1) and (3.2) each contain two bilinear terms. Using (3.24), (3.3) and (3.4) are reformulated as:

$$T_{\mathrm{LPC}}^{t,\mathrm{out,is}} = T_{\mathrm{LPC}}^{\mathrm{in}} \hat{y}_{\mathrm{LPC}}^{t}, \quad \forall t \in \Omega_T, \tag{3.38}$$

$$T_{\mathrm{HPC}}^{t,\mathrm{out,is}} = T_{\mathrm{HPC}}^{\mathrm{in}} \hat{y}_{\mathrm{HPC}}^{t}, \quad \forall t \in \Omega_T, \tag{3.39}$$

where $\hat{y}_{\mathrm{LPC}}^{t} = (y_{\mathrm{LPC}}^{t})^{\left(1-\frac{1}{\gamma^{\mathrm{LPC}}}\right)}$ and $\hat{y}_{\mathrm{HPC}}^{t} = (y_{\mathrm{HPC}}^{t})^{\left(1-\frac{1}{\gamma^{\mathrm{HPC}}}\right)}$.

For the TCCs of the compressors, (3.22) and (3.24) each contain a bilinear term. As a result of assuming a constant rotational speed, a, b, c, and q all become constants and hence (3.25) and (3.26) can be rewritten as:

$$\eta_{\mathrm{is}}/\eta_{\mathrm{is,dp}} = d\,\overline{x}, \tag{3.40}$$

$$y/y_{\mathrm{dp}} = \hat{x}, \tag{3.41}$$

where $\hat{x} = ax^2 + bx + c$, $d = (1.4 - 0.3(1-q)^2)$, and $\overline{x} = (q/x)(2 - q/x)$. For brevity, the superscripts for time and subscripts for the compressors in (3.40) and (3.41) are omitted.

The nonlinear terms on the right-hand side of (3.38)–(3.41) are piecewise-linearized using convex combination linearization [66]. For a general non-linear function $f(x)$, using convex combination linearization results in the function being approximated as $\tilde{f}(x)$:

$$\tilde{f}(x) = \textstyle\sum_{p\in\Omega_P} f(x_p)\lambda_p, \tag{3.42}$$

$$x = \textstyle\sum_{p\in\Omega_P} x_p\lambda_p, \tag{3.43}$$

$$\textstyle\sum_{p\in\Omega_P} \lambda_p = \alpha_{\mathrm{c,ch}}^{t}, \tag{3.44}$$

$$x_p = x^{\min} + (p-1)\left(x^{\max} - x^{\min}\right)/P, \ \forall p \in \Omega_P, \tag{3.45}$$

where $\Omega_P = \{1,2,\dots,P\}$ is the set of breakpoints for piecewise linearization and $\lambda_p \in \mathbb{R}$, $0 \leq \lambda_p \leq 1$ are the additional continuous variables. Additionally, λ should satisfy the condition that only two λs at most can be non-zero. This condition is also known as special order set of type two

or SOS Type 2. SOS Type 2 is explicitly formulated by assigning a binary variable to each segment between two consecutive breakpoints and adding the following constraints:

$$\sum_{p\in\Omega_{\overline{P}}} \delta_p = \alpha^t_{\mathrm{c,ch}}, \tag{3.46}$$

$$\lambda_1 \leq \ \delta_1, \tag{3.47}$$

$$\lambda_p \leq \delta_{p-1} + \delta_p \ \ \forall p \in \Omega_{\overline{P}}, \tag{3.48}$$

$$\lambda_P \leq \ \delta_{P-1}, \tag{3.49}$$

where $\Omega_{\overline{P}} = \{1,2,\dots,P-1\}$ is the set of segments for piecewise linearization and $\delta_p \in \{0,1\}, \forall p \in \Omega_{\overline{P}}$ are the additional binary variables.

After the piecewise linearization of (3.38)–(3.41) using (3.42)–(3.49), the charging circuit is represented as a bilinear model.

3.6.2 Bilinear Formulation of Charging Circuit Model

For the discharging circuit, (3.9), (3.12), and (3.18) contain bilinear terms. Equations (3.13) and (3.14) contain bilinear and trilinear terms. Each trilinear term is converted into two bilinear terms using auxiliary variables. For instance,

$$\dot{M}^t_{(.)} T^{t,\mathrm{out,is}}_{(.)} \eta^t_{\mathrm{is},(.)} = \dot{M}'^{,t}_{(.)} T^{t,\mathrm{out,is}}_{(.)}, \forall t \in \Omega_T, \tag{3.50}$$

where $\dot{M}'^{,t}_{(.)} = \dot{M}^t_{(.)} \eta^t_{\mathrm{is},(.)}$ is the auxiliary variable and $(.)$ represents HPT or LPT.

Similar to the charging circuit, (3.15) and (3.16) are reformulated using (3.30).

$$T^{t,\mathrm{out,is}}_{\mathrm{HPT}} \hat{y}^t_{\mathrm{HPT}} = T^{\mathrm{in}}_{\mathrm{HPT}}, \ \ \forall t \in \Omega_T, \tag{3.51}$$

$$T^{t,\mathrm{out,is}}_{\mathrm{LPT}} \hat{y}^t_{\mathrm{LPT}} \ = T^{\mathrm{in}}_{\mathrm{LPT}}, \ \ \forall t \in \Omega_T, \tag{3.52}$$

where $\hat{y}^t_{\mathrm{HPT}} = (y^t_{\mathrm{HPT}})^{\left(1-\frac{1}{\gamma^{\mathrm{HPT}}}\right)}$ and $\hat{y}^t_{\mathrm{LPT}} = (y^t_{\mathrm{LPT}})^{\left(1-\frac{1}{\gamma^{\mathrm{LPT}}}\right)}$.

For the TCCs of turbines, (3.22) and (3.30) each contain a bilinear term. Using the assumption of constant rotational speed, (3.31) and (3.33) are reformulated as:

$$\dot{M}/\dot{M}_{\mathrm{dp}} = \hat{\alpha}\tilde{y}, \tag{3.53}$$

$$\eta_{\mathrm{is}}/\eta_{\mathrm{is,dp}} = \ e\ \overline{x}, \tag{3.54}$$

where $\tilde{y} = \sqrt{y^2 - 1}/\sqrt{y_{\mathrm{dp}}^2 - 1}$, $\hat{\alpha} = \alpha\sqrt{T^{\mathrm{in}}}/\sqrt{T_{\mathrm{dp}}^{\mathrm{in}}}$, and $\overline{x} = (q/x)(2 - q/x)$. For brevity, the subscripts and superscripts are omitted in (3.53)–(3.54).

Subsequently, the nonlinear terms in (3.51)–(3.54) are linearized using convex combination linearization (3.42)–(3.49) with $\alpha_{\mathrm{c,ch}}^t$ replaced by $\alpha_{\mathrm{c,dch}}^t$ in (3.44) and (3.46). To avoid the violation of the PH constraint in the case of zero output power, (3.10) is reformulated as:

$$\varepsilon c_p^{\mathrm{LPT}}\left(T_{\mathrm{LPT}}^{\mathrm{out,is}} - T_s\right) = c_p^{\mathrm{PH}}\left(T_{\mathrm{PH}}^{\mathrm{A}} - T_s\right) - (1 - \alpha_{\mathrm{c,dch}}^t)(T_s\left(\varepsilon c_p^{\mathrm{LPT}} - c_p^{\mathrm{PH}}\right)), \forall t \in \Omega_T \quad (3.55)$$

The model for the discharging circuit is now reduced to a bilinear model.

3.6.3 Linearization of Bilinear Terms

Several bilinear terms in the model such as $W_{(.)}^t \eta_{\mathrm{is},(.)}^t$, $\dot{M}_{(.)}^t T_{(.)}^{t,\mathrm{out,is}}$, $T_{(.)}^{t,\mathrm{out,is}} \hat{y}_{(.)}^t$,and $yP^{\mathrm{in/out}} = P^{\mathrm{out/in}}$are relaxed using piecewise McCormick relaxation [66], [67]. This relaxation replaces a bilinear term by a set of linear inequalities. In piecewise McCormick relaxation, the domain of one of the two variables in the bilinear term is partitioned into several subdomains. Then, the standard McCormick relaxation is applied to each subdomain. Consequently, the relaxation obtained by this method is considerably tighter than the standard McCormick relaxation. The difference between the standard and piecewise McCormick relaxations is shown in Figure 3.3 for five partitions. The lines with diamonds represent envelopes for standard McCormick. In piecewise McCormick relaxation, only one of the envelopes is active at any given time. This is achieved through disjunctive programming. For a given bilinear term in the model, represented by a general term, ab with $a^{\min} \le a \le a^{\max}$, and $b^{\min} \le b \le b^{\max}$, and $a, b \in \mathbb{R}$, the bilinear term is replaced by

$$w = ab, \quad (3.56)$$

with the following disjunctive constraints:

$$\bigvee_{s \in \Omega_S} \begin{bmatrix} \sigma_s \\ w \ge ab^{\min} + a_s^{\min} b - a_s^{\min} b^{\min} \\ w \ge ab^{\max} + a_s^{\max} b - a_s^{\max} b^{\max} \\ w \le ab^{\min} + a_s^{\max} b - a_s^{\max} b^{\min} \\ w \le ab^{\max} + a_s^{\min} b - a_s^{\min} b^{\max} \end{bmatrix}, \quad (3.57)$$

where $\Omega_S = \{1,2,\dots,S\}$ and S is the total number of partitions.

The above disjunctive constraints are reformulated using the convex-hull reformulation as:

$$w \geq \sum_s \left(\delta_a^s b^{\min} + a_s^{\min}\delta_b^s - a_s^{\min} b^{\min}\sigma_s\right), \tag{3.58}$$

$$w \geq \sum_s (\delta_a^s b^{\max} + a_s^{\max}\delta_b^s - a_s^{\max} b^{\max}\sigma_s), \tag{3.59}$$

$$w \leq \sum_s \left(\delta_a^s b^{\min} + a_s^{\max}\delta_b^s - a_s^{\max} b^{\min}\sigma_s\right), \tag{3.60}$$

$$w \leq \sum_s \left(\delta_a^s b^{\max} + a_s^{\min}\delta_b^s - a_s^{\min} b^{\max}\sigma_s\right), \tag{3.61}$$

$$a = \sum_s \delta_a^s, \tag{3.62}$$

$$b = \sum_s \delta_b^s, \tag{3.63}$$

$$\sigma_s a_s^{\min} \leq \delta_a^s \leq \sigma_s a_s^{\max}, \forall s \in \Omega_S, \tag{3.64}$$

$$\sigma_s b_s^{\min} \leq \delta_b^s \leq \sigma_s b_s^{\max}, \forall s \in \Omega_S, \tag{3.65}$$

$$\sum_s \sigma_s = \alpha_{\text{c,ch/dch}}, \tag{3.66}$$

$$a_s^{\min} = a^{\min} + (s-1)\left(a^{\max} - a^{\min}\right)/S, \forall s \in \Omega_S, \tag{3.67}$$

$$a_s^{\max} = a^{\min} + (s)\left(a^{\max} - a^{\min}\right)/S, \forall s \in \Omega_S, \tag{3.68}$$

where $\delta_a^s, \delta_b^s \in \mathbb{R}, \sigma_s \in \{0,1\}, \forall s \in \Omega_S$ are the additional variables for the convex-hull reformulation.

After relaxing all bilinear terms in the charging and discharging circuits using (3.56) and (3.58)–(3.68), the resulting model is reduced to an MILP model.

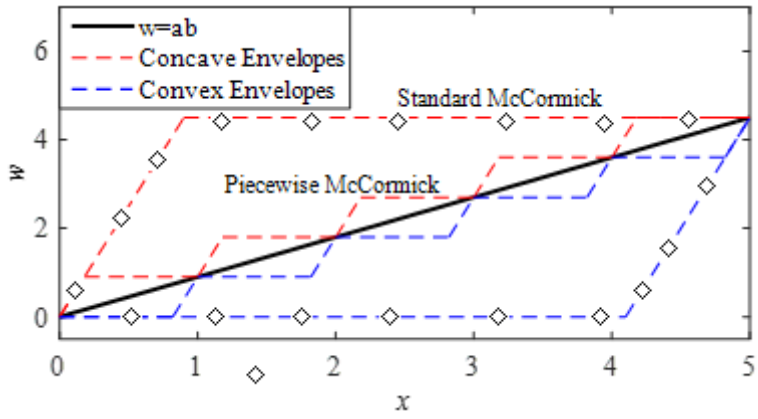

Figure 3.3 Standard McCormick envelopes and piecewise McCormick envelopes for a bilinear term $w = ab$, where $0 \leq a \leq 5$, and $0 \leq b \leq 5$, projected on $b = 0.9$.

3.6.4 Logarithmic Formulation of Piecewise Linearization

The linearized model of CAES developed in the previous sub-section represents a large-scale MILP problem, even for a single hour. The linearization procedures introduce a large number of binary variables to the model which can increase the computational burden. Moreover, the number of binary variables required for convex combination linearization scales linearly with the number of breakpoints. To make the model tractable without reducing its accuracy, the number of binary variables required for piecewise linearization is reduced. For this purpose, logarithmic convex combination linearization (Log-CCL) is implemented [68]. In this method, each linear segment between two breakpoints of the function is assigned a binary vector $\boldsymbol{\nu} \in \{0,1\}^{\lceil \log_2 |P-1| \rceil}$. The binary vector is obtained through an injective function $B : \Omega_{\overline{P}} \rightarrow \{0,1\}^{\lceil \log_2 |P-1| \rceil}$. This injective function B follows the properties of gray code, i.e., only one digit varies in consecutive binary numbers. Afterward, a branching scheme is formed that consists of a sequence of sets $\{L_\varsigma, R_\varsigma\}, \forall \varsigma \in \Omega_V, \Omega_V = \{1, \dots, \lceil \log_2 |P-1| \rceil\}$ of dichotomies. The detailed process for generating these sets, $\{L_\varsigma, R_\varsigma\}$, can be obtained from [68]. Then, the following constraints are defined:

$$\sum_{p \in L_\varsigma} \lambda_p \leq \nu_\varsigma, \forall \varsigma \in \Omega_V, \tag{3.69}$$

$$\sum_{p \in R_\varsigma} \lambda_p \leq (1 - \nu_\varsigma), \forall \varsigma \in \Omega_V, \tag{3.70}$$

where $\nu_\varsigma \in \{0,1\}, \forall \varsigma \in \Omega_V$ is the $(\lceil \log_2 |P-1| \rceil - \varsigma + 1)$th element of vector $\boldsymbol{\nu}$. These constraints replace (3.46)–(3.49). The number of binary variables required is $\lceil \log_2 |P-1| \rceil$.

3.7 Optimal Scheduling Model

To show the effectiveness of the proposed model, the optimal scheduling problem of CAES considering energy and reserve markets is formulated by (3.71)–(3.81). The formulation is in the form of an MILP model. Uncertainties in electricity market prices are included in the model through various scenarios whereas uncertainties associated with the deployment of reserves are considered through the probability of reserve deployment [69]. In line with [56], [57], CAES is assumed to be a price taker as the size of an individual CAES plant is considerably smaller than the rest of the system.

The objective function (3.71) includes the profit obtained from the energy and reserve markets as well as the operational cost of CAES. Equations (3.72) and (3.73) describe the profits obtained from the energy and reserve markets, respectively. Equation (3.74) represents the operational costs of CAES. The electric charging and discharging powers of CAES are related to the mechanical work of the compressors and turbines by (3.75)–(3.77). The spinning reserve power is constrained by (3.78)–(3.80). The final pressure is constrained by (3.81).

$$\text{Max.} \sum_{\kappa\in\Xi} p_{\kappa} \sum_{t\in\Omega_T} \left(\varphi_{\mathrm{E}}^{\kappa,t} + \varphi_{\mathrm{R}}^{\kappa,t} - \varphi_{\mathrm{OC}}^{\kappa,t}\right) \tag{3.71}$$

s.t. $$\varphi_{\mathrm{E}}^{\kappa,t} = \pi_{\mathrm{E}}^{\kappa,t}(p_{\mathrm{dch}}^{t} - p_{\mathrm{ch}}^{t}) + \pi_{\mathrm{E}}^{\kappa,t}\left(p_{\mathrm{sr,dch}}^{t}\rho_{\mathrm{sr}} + p_{\mathrm{sr,ch}}^{t}\rho_{\mathrm{sr}}\right), \forall t \in \Omega_T, \forall\kappa, \tag{3.72}$$

$$\varphi_{\mathrm{R}}^{\kappa,t} = \pi_{\mathrm{R}}^{\kappa,t}\left(p_{\mathrm{sr,dch}}^{t} + p_{\mathrm{sr,ch}}^{t}\right), \quad \forall t \in \Omega_T, \forall\kappa, \tag{3.73}$$

$$\varphi_{\mathrm{OC}}^{\kappa,t} = c^{\mathrm{OM}}\left(p_{\mathrm{dch}}^{t} + p_{\mathrm{ch}}^{t} + p_{\mathrm{sr,dch}}^{t}\rho_{\mathrm{sr}} - p_{\mathrm{sr,ch}}^{t}\rho_{\mathrm{sr}}\right) + (\dot{M}_{\mathrm{fu,CC1}}^{t} + \dot{M}_{\mathrm{fu,CC2}}^{t})\Delta\mathrm{t}\cdot\mathrm{LHV}\cdot\pi_{\mathrm{NG}}^{\kappa,t}, \ \forall t \in \Omega_T, \forall\kappa, \tag{3.74}$$

$$W_{\mathrm{LPC}}^{t} + W_{\mathrm{HPC}}^{t} = p_{\mathrm{ch}}^{t} - p_{\mathrm{sr,ch}}^{t}\rho_{\mathrm{sr}}, \forall t \in \Omega_T \tag{3.75}$$

$$W_{\mathrm{LPT}}^{t} + W_{\mathrm{HPT}}^{t} = p_{\mathrm{dch}}^{t} + p_{\mathrm{sr,dch}}^{t}\rho_{\mathrm{sr}}, \forall t \in \Omega_T \tag{3.76}$$

$$\alpha_{\mathrm{c,ch}}^{t} + \alpha_{\mathrm{c,dch}}^{t} \leq 1, \ \forall t \in \Omega_T, \tag{3.77}$$

$$p_{\mathrm{dch}}^{t} + p_{\mathrm{sr,dch}}^{t} \leq p_{\mathrm{dch}}^{\max}\alpha_{\mathrm{c}}^{t,\mathrm{dch}}, \forall t \in \Omega_T, \tag{3.78}$$

$$p_{\mathrm{ch}}^{t} - p_{\mathrm{sr,ch}}^{t} \geq p_{\mathrm{ch}}^{\min}\alpha_{\mathrm{c}}^{t,\mathrm{ch}}, \forall t \in \Omega_T, \tag{3.79}$$

$$p_{\mathrm{ch}}^{t} \leq p_{\mathrm{ch}}^{\max}\alpha_{\mathrm{c}}^{t,\mathrm{ch}}, p_{\mathrm{sr,ch}}^{t} \leq p_{\mathrm{ch}}^{\max}\alpha_{\mathrm{c}}^{t,\mathrm{ch}}, \forall t \in \Omega_T, \tag{3.80}$$

$$P_{\mathrm{s}}^{\mathrm{T}} \geq \mathrm{P}_{s,\mathrm{final}}, \ \forall t \in \Omega_T. \tag{3.81}$$

3.8 Case Studies and Results

3.8.1 Model Verification

The proposed model is verified using data of the CAES plant in Huntorf, Germany. Table 3.1 provides the model data for the Huntorf CAES plant [62], [63], [70].

Table 3.1 Operational data of CAES

Parameter	Value
Ambient conditions	1 bar, 283 K
Rated power of compressors	23.8 MW for LPC, 35.6 MW for HPC
Rated power of turbines	200 MW for LPT, 90 MW for HPT
Rated mass flow rate	108 kg/s for LPC and HPC
	422 kg/s for HPT, 427 kg/s for LPT
Inlet temperature of compressors	283 K for LPC, 323 K for HPC
Inlet temperature of turbines	823 K for HPT, 1098 K for LPT
Rated inlet pressure of LPC/HPC	1 bar for LPC, 8.43 bar for HPC
Rated inlet pressure of LPT/HPT	43 bar for HPT, 11 bar for LPT
Natural gas LHV, η^{CC}, c_p^{fu}	47.141 MJ/kg, 0.98, 2.34 kJ/K
Cavern minimum and maximum pressure	46 bar and 66 bar
Cavern volume and temperature	310,000 m^3, 323 K

Figure 3.4 shows the results of model verification for the discharging circuit. The data for the Huntorf plant are obtained from [71]. For the sake of comparison, the results are compared with a constant efficiency model [60]. The results indicate a close match between the actual data, the nonlinear model, and the proposed linear model (Figure 3.4(a)). This is achieved due to the use of a large number of piecewise segments (30 in this case). Figure 3.4(a) also depicts the inaccuracy of the constant efficiency model. Figure 3.4(b) shows that the efficiency of the discharging circuit varies with the discharging power. In fact, at lower discharging power, the amount of air required to produce an output of 1 MW is higher compared to that at higher discharging power. On the other hand, for the constant efficiency model the amount of air consumed per unit MW is the same at all discharging powers. Figure 3.4(c) depicts the accuracy of the proposed model for the fuel flow at different discharging power. Figure 3.4(c) also shows the effect of inclusion of a PH (with an effectiveness of 75%) in CAES. When a PH is included in the system, the fuel flow rate decreases thereby reducing fuel consumption. The Huntorf plant did not originally include a PH. However,

it has been used at the McIntosh plant. The effect of including a PH on the scheduling of CAES is shown later in section 3.8.3.

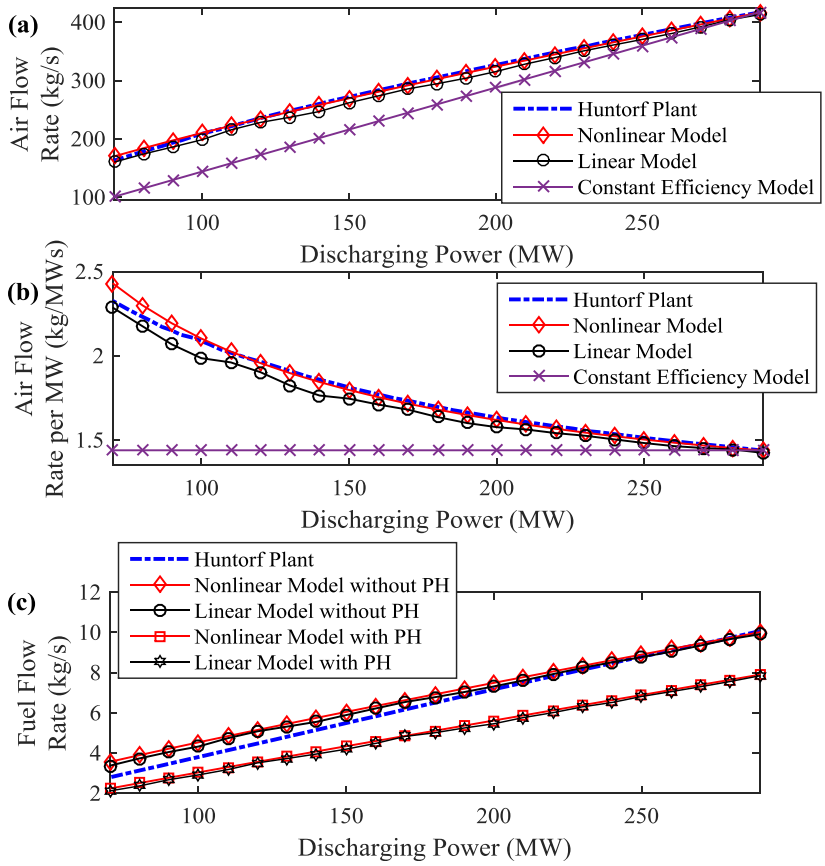

Figure 3.4 Comparison of the accuracy of different models

3.8.2 Scheduling Results

For the optimal scheduling problem, electricity market price data of the PJM market from October 2012 to December 2014 are used [72]. The number of scenarios is reduced to 5 using a scenario reduction technique (SCENRED2) provided in GAMS [46]. The initial and final pressures are set to 56 and 50 bar, respectively. The probability of spinning reserve deployment is set to 5% [69]. The price of natural gas is set to $1.5 per GJ. All of the simulations are performed on a PC with a 3.4-GHz Intel Core i7-6700 and 16 GB RAM. MATLAB R2015b and GUROBI 7.5.1 were used to solve the model.

Two cases are considered to show the effectiveness of the model, first case with the constant efficiency model and the second with the proposed linear model of CAES with variable efficiency.

The results in Figure 3.5 show that the optimal bidding schedule of CAES is considerably affected when its variable efficiency is taken into account. For the constant efficiency model (Figure 3.5(a)), the CAES discharges at low output power most of the time and the remaining capacity is made available for the spinning reserve bids. In contrast, when the accurate model is considered, the CAES outputs maximum power in discharging mode most of the time (Figure 3.5(b)). The reason for this behavior is evident from Figure 3.4(b); at lower output power, the efficiency of CAES drops significantly and, hence, high losses are incurred. Therefore, the optimal solution is to operate the plant at high output power, corresponding to higher efficiency. The total profit gained by considering the accurate model is \$17,848 but for the constant efficiency model is \$18,497. Hereafter, the second case will be referred to as a base case.

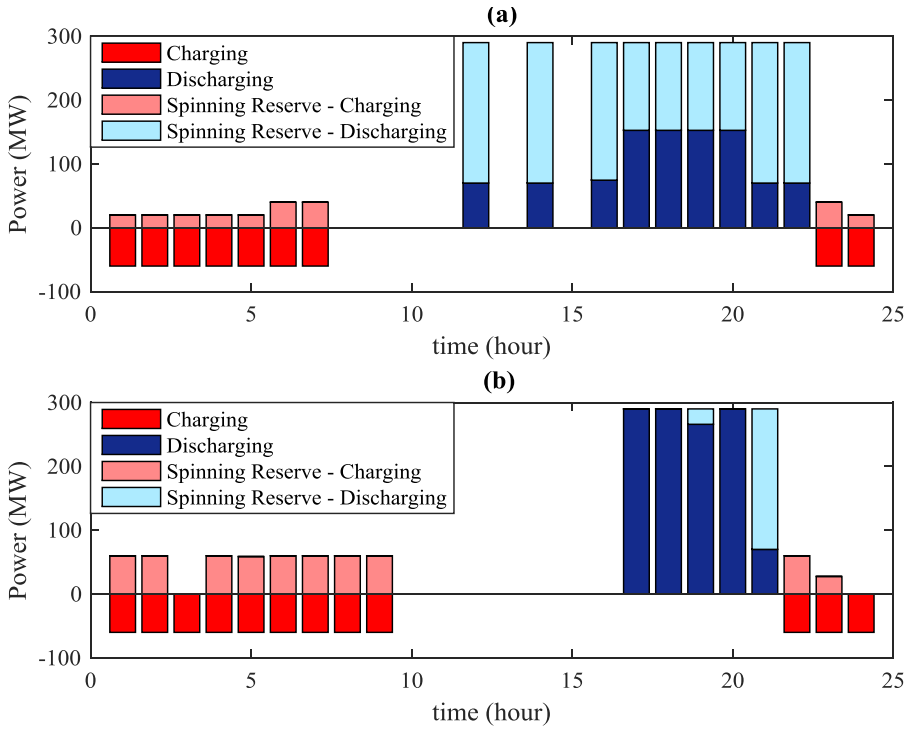

Figure 3.5 Optimal bidding schedule for two cases

The schedule obtained from the constant efficiency model may not satisfy all CAES constraints. This is depicted in Figure 3.6, which shows the variation of cavern pressure when the schedules obtained from the constant efficiency and proposed models are input to the nonlinear model hour by hour. Following the schedule obtained from the constant efficiency model, the cavern pressure would violate the operating limits of the plant from hour 20 to hour 24. In fact, the cavern pressure would go below the minimum operating pressure of 46 bar and hence (3.37) is violated. The reason

for this behavior can be explained by examining Figure 3.4(a) and Figure 3.5(a). As the CAES discharges at low power during hours 12, 14, and 16 to 22, the actual amount of air being consumed is significantly higher than that obtained from the constant efficiency model. Hence, according to (3.34)–(3.37), the actual decrease in pressure is higher than that obtained from the constant efficiency model. Also for the constant efficiency model, the final pressure would fall well below the set point of 50 bar. On the other hand, the proposed model ensures that the cavern pressure is within the operating limits at all times and the final pressure is not below set point.

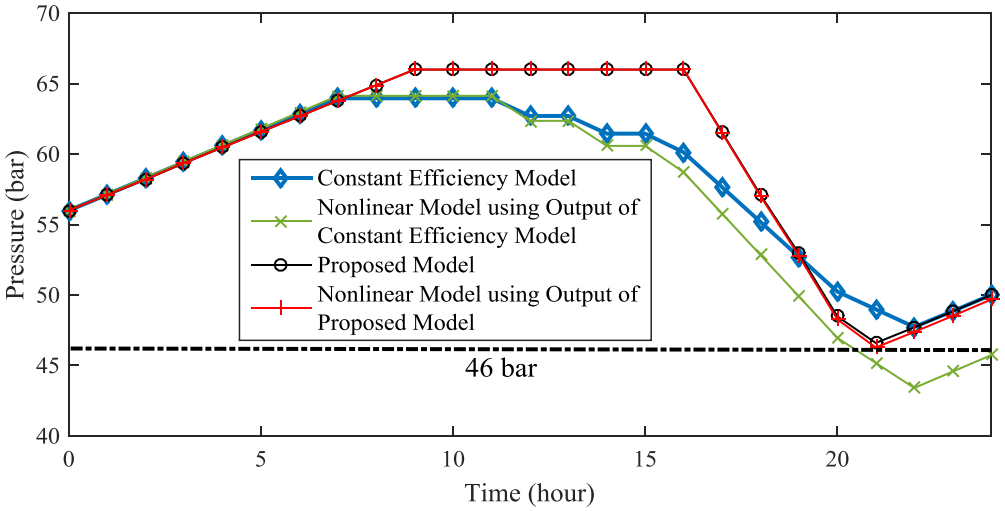

Figure 3.6 Air pressure inside the cavern for different models

3.8.3 Effect of a PH on CAES Scheduling

As mentioned in the introduction and shown in Figure 3.4(c), the inclusion of a PH can improve the fuel consumption efficiency of CAES and hence the overall efficiency of the plant. To depict the effects of a PH on the bidding schedule of CAES, a PH with an effectiveness ε of 80% is considered. For this case, the bidding schedule is the same as shown in Figure 3.5(b). This is due to the fact that the fuel flow rate does not affect the mass of air in the cavern and hence the SOC of CAES. However, the profit obtained in this case is $20,201, which is 13% higher than the base case without a PH. Therefore, the inclusion of a PH in CAES can bring economic benefits.

A major portion of the operating costs of CAES comes from natural gas consumption during discharging mode. Therefore, the price of natural gas and the effectiveness of a PH can significantly affect the profits gained by CAES in electricity markets. Figure 3.7 shows the variation in CAES profits for different natural gas prices and values of PH effectiveness. The

results show that natural gas prices have a larger impact on CAES profits than the effectiveness of PH.

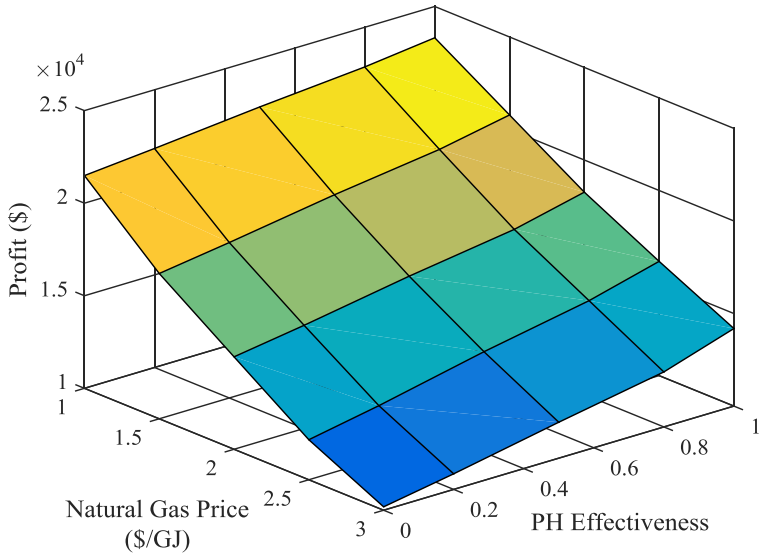

Figure 3.7 Variation in profits for different values of PH effectiveness and natural gas prices

3.8.4 Effect of Ambient Temperature on CAES Scheduling

Ambient air temperature also has an effect on the operation of the compressors, particularly on LPC [61]. As the ambient air temperature increases, the mass flow rate for the given charging power decreases. This is because it is difficult to compress hot air, which has a lower density [73]. This effect is important to consider when scheduling CAES as it can affect the charging/discharging bids. The proposed model can consider these effects. Fig. 8 depicts the optimal CAES schedule when the ambient temperature ($T_{\mathrm{LPC}}^{\mathrm{in}}$) is 313 K as opposed to 283 K in the base case. The charging mass flow rate in this case reduces to 95.2 kg/s from 108 kg/s for rated power (59.4 MW). The total profit obtained in this case is $15,070, which is 15% less than the base case.

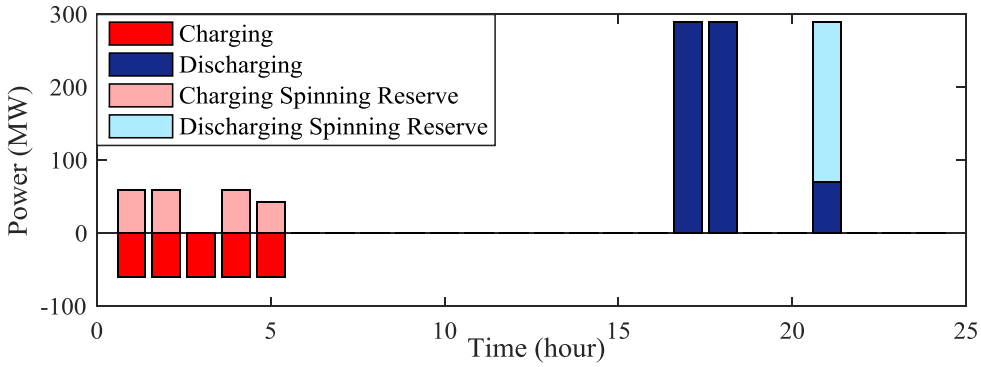

Figure 3.8 Optimal schedule of CAES for an ambient temperature of 313 K

3.9 Conclusion

In this chapter, an accurate and a comprehensive model of the CAES was developed. The model considered the thermodynamic relationships and the turbomachinery characteristic curves of the compressors and turbines. The model was linearized so that it can be solved efficiently by the commercial solvers. The accuracy of the proposed linear model was verified using the data of an existing plant. The model was then applied to an optimal scheduling problem considering energy and reserve markets to show its necessity and effectiveness. Results showed that a more realistic estimate of profits gained by CAES in the electricity market was found by considering the more accurate CAES model. Further, the optimal schedule satisfied all of the operating constraints of CAES. The results also indicated that the inclusion of a PH improves the profits. Further case studies indicated that ambient air temperature also affects the optimal schedule of CAES in the electricity markets.

Chapter 4

Reliability Evaluation of Bulk Power System Considering Compressed Air Energy Storage[1]

"The price of reliability is the pursuit of the utmost simplicity. It is a price which the very rich may find hard to pay."
- Tony Hoare

4.1 Abstract

The integration of large-scale energy storage systems (ESSs) has been identified as a viable option to mitigate the adverse effects of renewable energy sources (RES) on the power system operation and reliability. Currently, compressed air energy storage (CAES) is one of the two large-scale energy storage technologies with low capital and operational costs. This chapter presents a method to integrate a new CAES reliability model in the bulk power system reliability evaluation and investigates quantitative benefits derived from the CAES. A state-duration sampling method is adopted for the reliability evaluation. A detailed reliability model of the CAES that considers its actual operating mechanism is first developed. Each system contingency state is then analyzed using a unit commitment (UC) method instead of hourly optimal power flow (OPF). This ensures that the inter-temporal constraints introduced by the CAES, such as its state-of-charge (SOC), are included in the analysis. Case studies are performed on a six-bus test system containing a wind farm and a CAES. The results indicate that the CAES can improve the overall reliability of the system. In particular, the reliability indices of the bus where the CAES is connected show the greatest improvement. Further case studies have demonstrated that CAES location and size is also important factors affecting the reliability of a power system.

[1] O. A. Ansari, S. Bhattarai, R. Karki and C. Y. Chung, "Reliability evaluation of bulk power system considering compressed air energy storage," in *2017 IEEE Electric Power and Energy Conference (EPEC)*, Saskatoon, Oct. 2017 (in press).

4.2 Nomenclature

Sets/Indices

i	Index of bus
l	Index of line
κ	Index of scenario
t	Index of hour
Ω_{G}	Set of conventional generators
Ω_{B}	Set of all buses
Ω_C	Set of buses with a CAES

Parameters

c_i^{vom}	Variable operation and maintenance cost ($/MWh)
ru_i	Ramp-up rate limit of generator at bus i (MW/h)
rd_i	Ramp-down rate limit of generator at bus i (MW/h)
$d_i^{\kappa,t}$	Electricity load demand at bus i (MW)
$f_l^{\kappa,\max}$, $f_n^{\kappa,\max}$	The maximum power flow of lines l and n, respectively (MW)
$\overline{g}_i^{\kappa}$, $\underline{g}_i^{\kappa}$	Maximum, minimum power output of generator at bus i (MW)
$\rho_{j,\mathrm{su/sd}}^{\mathrm{G}}$	Start-up/shut-down cost for conventional generator j
$\overline{p}_{i,\mathrm{ch}}^{\kappa}$	Maximum charging power
$\overline{p}_{i,\mathrm{dch}}^{\kappa}$	Maximum discharging power
$\underline{p}_{i,\mathrm{ch}}^{\kappa}$	Minimum charging power
$\underline{p}_{i,\mathrm{dch}}^{\kappa}$	Minimum discharging power
T_{κ}	Total number of hours in each contingency scenario
$M_{i,l}$	The element in the *i*th row and the *l*th column of node-branch incidence matrix
$\overline{W}_i^{\kappa}$	Maximum wind power that can be generated at bus i (MW)
$\tilde{\gamma}_l$	Susceptance of a line l (Siemens)
ρ_i^g	Generation cost of generator i ($/MWh)

ρ_i^L Penalty cost for electricity load loss at bus i (\$/MWh)

ρ_i^S Penalty cost for wind spillage at bus i (\$/MWh)

Δt Time duration (1 hour)

Variables

f_l^κ Total active power flow on line l (MW)

g_i^κ Power output of generator at bus i (MW)

$p_{i,\mathrm{ch}}^{\kappa,t}$ Charging power of CAES at bus i (MW)

$p_{i,\mathrm{dch}}^{\kappa,t}$ Discharging power of CAES at bus i (MW)

r_i^κ Electricity load loss at bus i (MW)

$I_{i,t}^\kappa$ Binary variable indicating online/offline status of the generator i : 1 if it is online, 0 otherwise

S_i^κ Wind power curtailment at bus i (MW)

$W_i^{\kappa,t}$ Scheduled wind power generation at bus i (MW)

$\alpha_i^{\kappa,t}$ Binary variable indicating start-up of generator i

$\beta_i^{\kappa,t}$ Binary variable indicating shut-down of generator i

$\alpha_{i,\mathrm{ch}}^{\kappa,t}$ Binary variable indicating charging status of CAES at bus i : 1 if it is charging, 0 otherwise

$\alpha_{i,\mathrm{dch}}^{\kappa,t}$ Binary variable indicating discharging status of CAES at bus i : 1 if it is discharging, 0 otherwise

$\theta_{l,\mathrm{fr/to}}^\kappa$ Phase angle of from/to-side node of line l (rad)

4.3 Introduction

Owing to the adverse effects of conventional sources of electricity generation on the environment, the penetration of renewable energy sources (RES), such as solar and wind power, in the existing power system is gradually increasing throughout the world. In this regard, renewable portfolio standards (RPS) have been widely accepted in many different countries [38]. These standards bound the electric utilities to produce a certain percentage of their total generation from RES. From the electric utilities' point of view, the integration of RES brings many new challenges to the reliable planning and operation of a power system. RES are inherently

intermittent and stochastic in nature and hence high penetration of such sources can cause large imbalances between the load and generation. Furthermore, in certain situations, the power system may not be able to utilize the available output from RES due to congestion. In these cases, the output of RES has to be curtailed. To mitigate these negative impacts of RES, energy storage systems (ESSs) have become indispensable components of a power system containing a large proportion of renewable energy generation. ESSs can provide grid related ancillary services such as voltage regulation, power quality and black start [7], [74]. Various ESSs technologies include compressed air energy storage (CAES), pumped hydro storage (PHS), flywheel, battery ESSs (BESSs) etc. [7].

ESSs require substantial initial investment for their construction. The inclusion of ESSs in the existing power system can be justified if specific benefits in terms of reduction in operational costs, and improvement in system reliability are obtained. The impacts of ESSs on the overall system reliability and economy have been studied from various perspectives. The reliability evaluation of a small isolated wind energy conversion system (WECS) with BESSs has been performed in [75]. Reference [76] presents a Monte-Carlo simulation based technique to assess the reliability benefits of ESSs considering different operating strategies and wind energy dispatch restrictions. The analysis is carried out for the generation system, that is, at HL-1. In [77], a reliability assessment method based on the combination of analytical and simulation based approaches has been proposed for a WECS with BESS. The BESS is connected to the doubly-fed induction generator (DFIG)-based wind turbine at the DC-link of the power converter. In [78], the operational strategies for ESSs are proposed to improve the reliability of a distribution system with load aggregation. In [79], a method based on sequential Monte-Carlo simulation (SMCS) is proposed to evaluate the reliability and economy of distribution system containing ESSs. The method considers the optimal operation of distribution system's load aggregator and islanding feature of the system. Reference [80] considers the ramp up and ramp down capabilities of conventional generators and ESSs in the evaluation of the operational reliability of the system. In [81], ESSs operated by the wind farm operator is utilized to decrease the operating risk of the power system.

The previous work presented in the literature utilizes a generic reliability model of the ESSs. However, different ESSs may have entirely different operating mechanisms. Hence, it is essential to take into account the actual operation scheme which is specific for a particular type of ESSs.

Therefore, in this chapter, a reliability model of CAES is developed. The model takes into account different failure events that may occur during the operation of CAES. Afterward, the reliability model is included in the simulation-based method to evaluate the reliability of a bulk power system (HL-II). In the simulation-based evaluation methods, a large number of contingency states are generated based on the failure and repair rates of components. Then in each contingency state, optimal power flow (OPF) is used to reschedule the generation to minimize the load curtailment. However, the single-hour OPF cannot consider the coupling between different hours. This link which is introduced by the SOC of CAES can be taken into account by considering the daily unit commitment (UC). Hence, for the system analysis, 24-hour UC is utilized to reschedule the generation, CAES and other resources to minimize the load curtailment.

4.4 Reliability Modeling of CAES

In order to accurately determine the reliability impacts of the CAES, it is important to consider the actual operation of such a system. The block diagram of a conventional CAES is shown in Figure 4.1. The principle of operation of a CAES is similar to the operation of a conventional gas turbine. The only difference is that, in CAES, the compression and expansion cycles are separated in two different stages. During charging, the air at ambient conditions is compressed using multi-stage compressors and is stored inside the cavern at high pressure. During discharging, the air from the cavern is released, combusted and expanded in the turbines.

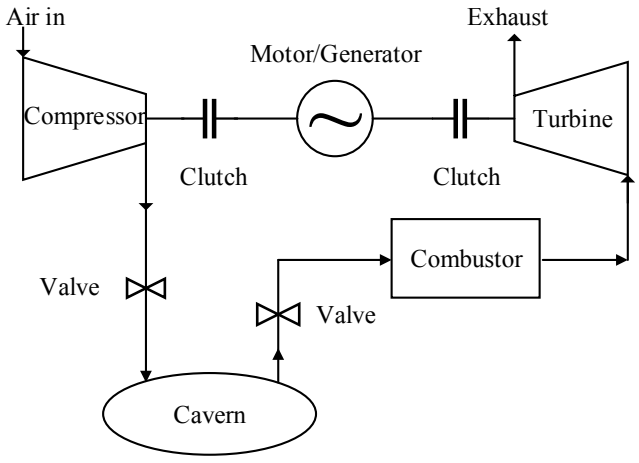

Figure 4.1 CAES simplified diagram

An accurate reliability model of CAES should consider the interaction between different parts of the system and the possible failure events of different components in the system. For the reliability modeling of a conventional gas turbine, the two-state continuous-time Markov model has been widely used that represents the complete system either in upstate or in downstate as illustrated in Figure 4.2 [82]. A similar two-state model can be used in case of CAES with appropriate values of transition rates between the two states. However, this two-state model does not accurately represent the operation of the CAES.

Since the charging and discharging parts of CAES are separated, the failures of the components in the charging part will not affect the operation of discharging part and vice versa.

To represent this behavior, a four-state model is developed as shown in Figure 4.3. In this model, the charging and discharging processes are decoupled. The up-state (state 1) represents the situation when all the components of CAES are available. State 2 corresponds to the failure in the charging part. State 3 relates to the failure in the discharging part. State 0 represents the complete failure state. This state occurs when either both charging and discharging parts are failed or when the motor/generator set is failed. Hence, CAES can neither be used for charging or discharging.

The different transition rates among the states represent the possible failure events. In the subsequent studies, it is assumed that during one time period, only one transition can occur. Hence, the transition rates between states 2 and 3 are assumed to be zero. Also, it is assumed that once CAES is in down state (state 0), it is brought to the up state after a complete repair process. And, therefore, the transition rates from state 0 to states 2 and 3 are assumed to be zero. In the following sections, this model for the CAES is utilized for the reliability studies.

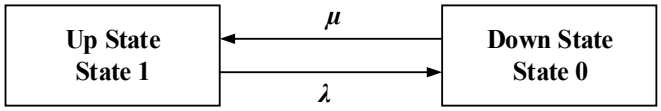

Figure 4.2 Two-state model

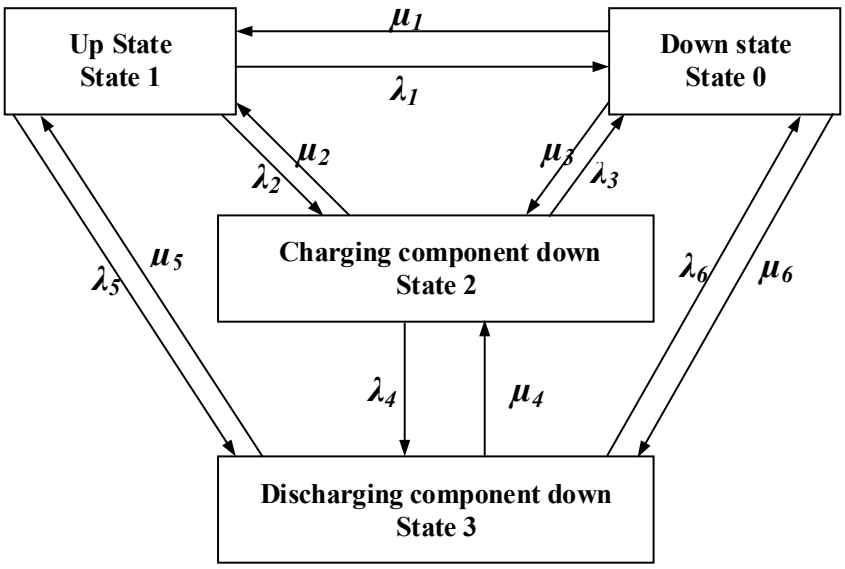

Figure 4.3 Four-state model

4.5 Simulation Methodology

In power system reliability studies, SMCS is widely employed to simulate the system and obtain the reliability indices [83], [84]. The main advantages of the SMCS are that this simulation is independent of the size of the system and that the chronology of the events is maintained. This chronology is important when CAES is included in the system. This is because of the fact that the SOC of the CAES links different hours in the simulation period. Hence, the chronology of the events will affect the operation of the CAES. A major drawback of SMCS is that it requires a large number of iterations before it converges. In this regard, different variance reduction techniques such as Latin Hypercube Sampling (LHS), importance sampling and dagger sampling etc. have been utilized to speed up the rate of convergence of the simulation [83]. In this paper, LHS is employed for the simulation. Unlike Monte-Carlo (MC) simulation which utilizes random numbers to generate the samples from a probability distribution, LHS stratifies the probability distribution so that the samples are obtained from equally spaced intervals of the distribution. This ensures that those events which are less probable but have high impact are also included in the samples. In this work, state-duration method is adopted for the simulation. In this method, the component state duration distribution functions are used to generate the chronological component state transition process. Afterward, the system's chronological state transition process is created from the combination of components' processes [83].

4.6 System Analysis

In power system reliability studies, after generating different contingencies states, single-hour OPF is utilized to reschedule the generation as a result of contingencies [83]. The objective is to minimize load curtailment. However, as mentioned earlier this method is not suitable in the presence of CAES. The reason being is that the different hours of operation of the system are coupled through the SOC of CAES. Therefore, in this work, a daily UC is used to reschedule the generation in the presence of contingencies. After simulating a large number of contingency states of the system, these states for 24 hours are aggregated to form contingency scenarios and then the daily UC optimization problem is solved.

The optimization problem for a daily UC is given by (4.1) – (4.20).

$$\text{Min. } \sum_{t=1}^{T}\sum_{j\in\Omega_{\mathrm{G}}}\left(\rho_{j,\mathrm{su}}\alpha_{j,\kappa,t}^{\mathrm{G}}+\rho_{j,\mathrm{sd}}\beta_{j,\kappa,t}^{\mathrm{G}}\right)+\sum_{i\in\Omega_B}\left(\sum_{t=1}^{T_\kappa}\left(\rho_j^{\mathrm{G}}g_i^{\kappa,t}\Delta t+\rho_i^{\mathrm{W}}S_i^{\kappa,t}\Delta t+\rho_i^{\mathrm{L}}r_i^{\kappa,t}\Delta t+c_i^{\mathrm{vom}}\left(p_{i,\mathrm{ch}}^{\kappa,t}+p_{i,\mathrm{dch}}^{\kappa,t}\right)\Delta t\right)/T_\kappa\right) \tag{4.1}$$

s.t.

$$\sum_{l\in\Omega}M_{i,l}\,f_l^{\kappa,t}+g_i^{\kappa,t}+W_i^{\kappa,t}+r_i^{\kappa,t}-d_i^{\kappa,t}+p_{i,\mathrm{dch}}^{\kappa,t}-p_{i,\mathrm{ch}}^{\kappa,t}=0,\ \ \forall i\in\Omega_B,\forall t\in\Omega_T,\forall\kappa, \tag{4.2}$$

$$f_l^{\kappa,t}-\tilde{\gamma}_l\left(\theta_{l,\mathrm{fr}}^{\kappa,t}-\theta_{l,\mathrm{to}}^{\kappa,t}\right)=0,\forall l\in\Omega,\forall t\in\Omega_T,\forall\kappa\ , \tag{4.3}$$

$$\left|f_l^{\kappa,t}\right|\le f_l^{\kappa,\max},\ \forall l\in\Omega_{\mathrm{L}},\ \forall t\in\Omega_T,\forall\kappa, \tag{4.4}$$

$$I_{i,t}^{\kappa}\underline{g}_i^{\kappa}\le g_{i,t}^{\kappa}\le I_{i,t}^{\kappa}\overline{g}_i^{\kappa},\ \ \forall i\in\Omega_B,\ \forall t\in\Omega_T,\forall\kappa, \tag{4.5}$$

$$g_{i,t+1}^{\kappa}-g_{i,t}^{\kappa}\le ru_i,\ \ \forall i\in\Omega_B,\ \forall t\in\Omega_T,\forall\kappa, \tag{4.6}$$

$$g_{i,t}^{\kappa}-g_{i,t+1}^{\kappa}\le rd_i,\ \ \forall i\in\Omega_B,\ \forall t\in\Omega_T,\forall\kappa, \tag{4.7}$$

$$\alpha_{i,t}^{\mathrm{G},\kappa}-\beta_{i,t}^{\mathrm{G},\kappa}=I_{i,t}^{\kappa}-I_{i,t-1}^{\kappa},\ \ \forall i\in\Omega_B,\ \forall t\in\Omega_T,\forall\kappa, \tag{4.8}$$

$$\sum_{t}^{t+T_{i,\min}^{\mathrm{on}}-1}I_{i,t}^{\kappa}\ge\alpha_{i,t}^{\kappa}T_{i,\min}^{\mathrm{on}},\ \ \forall i\in\Omega_B,\ \forall t\in\left\{1,\dots,T_\kappa-T_{i,\min}^{\mathrm{on}}+1\right\},\forall\kappa, \tag{4.9}$$

$$\sum_{t}^{T_\kappa}I_{i,t}^{\kappa}\ge\alpha_{i,t}^{\kappa}(T_\kappa-t+1),\ \ \forall i\in\Omega_B,\ \forall t\in\left\{T_\kappa-T_{i,\min}^{\mathrm{on}}+2,\dots,T_\kappa\right\},\forall\kappa, \tag{4.10}$$

$$\sum_{t}^{t+T_{i,\min}^{\mathrm{off}}-1}\left(1-I_{i,t}^{\kappa}\right)\ge\beta_{i,t}^{\kappa}T_{i,\min}^{\mathrm{off}},\forall i\in\Omega_B,\ \forall t\in\left\{1,\dots,T_\kappa-T_{i,\min}^{\mathrm{off}}+1\right\},\forall\kappa, \tag{4.11}$$

$$\sum_{t}^{T_\kappa}\left(1-I_{i,t}^{\kappa}\right)\geq\beta_{i,t}^{\kappa}(T_\kappa-t+1),\forall i\in\Omega_B,\ \forall t\ \left\{T_\kappa-T_{i,\min}^{\text{off}}+2,\dots,T_\kappa\right\},\forall\kappa, \tag{4.12}$$

$$S_i^{\kappa,t}+W_i^{\kappa,t}=\overline{W}_i^{\kappa,t},\ \ \forall i\in\Omega_B,\ \forall t\in\Omega_T,\forall\kappa, \tag{4.13}$$

$$0\leq W_i^{\kappa,t},\ \ \forall i\in\Omega_B,\ \forall t\in\Omega_T,\forall\kappa, \tag{4.14}$$

$$0\leq S_i^{\kappa,t},\ \ \forall i\in\Omega_B,\ \forall t\in\Omega_T,\forall\kappa, \tag{4.15}$$

$$r_i^{\kappa,t}\leq d_i^{\kappa,t},\ \ \forall s\in\Omega_B,\ \forall t\in\Omega_T,\forall\kappa, \tag{4.16}$$

$$\alpha_{i,\text{ch}}^{\kappa,t}+\alpha_{i,\text{dch}}^{\kappa,t}\leq 1,\ \ \forall s\in\Omega_C,\ \forall t\in\Omega_T,\forall\kappa, \tag{4.17}$$

$$E_s^{\kappa,t}=E_s^{\kappa,t-1}-\left(p_{i,\text{ch}}^{\kappa,t}-p_{i,\text{dch}}^{\kappa,t}\right)\Delta t\ ,\forall s\in\Omega_C,\ \forall t\in\Omega_T,\forall\kappa, \tag{4.18}$$

$$\alpha_{i,\text{ch}}^{\kappa,t}\underline{p}_{i,\text{ch}}^{\kappa}\leq p_{i,\text{ch}}^{\kappa,t}\leq\alpha_{i,\text{ch}}^{\kappa,t}\overline{p}_{i,\text{ch}}^{\kappa},\ \ \forall s\in\Omega_C,\ \forall t\in\Omega_T,\forall\kappa, \tag{4.19}$$

$$\alpha_{i,\text{dch}}^{\kappa,t}\underline{p}_{i,\text{dch}}^{\kappa}\leq p_{i,\text{dch}}^{\kappa,t}\leq\alpha_{i,\text{dch}}^{\kappa,t}\overline{p}_{i,\text{ch}}^{\kappa},\ \ \forall s\in\Omega_C,\ \forall t\in\Omega_T,\forall\kappa \tag{4.20}$$

The objective function is given in (4.1). The objective function includes the start-up, shut-down and the running costs of the conventional generators, wind spillage costs, load shedding costs and operational costs of the CAES. The power balance and line flow constraints are given by (4.2) and (4.3) respectively. The limits on the line flows, and conventional generators' output are given by (4.4) and (4.5). Constraints (4.6) and (4.7) represent the ramp down and ramp up limits respectively. The constraints for minimum up and down times of the conventional generators are formulated by (4.8) – (4.12). Constraints (4.13) – (4.15) represent the limits on the wind spillage. The load curtailment is limited by (4.16). Moreover, the constraints for CAES and its SOC are represented by (4.17) – (4.20). This problem is solved for each contingency scenario.

4.7 Reliability Evaluation Method

The complete methodology of the reliability evaluation is shown in Figure 4.5. In the first step, the up times and down times for all of the components in the system are generated using the method described Section 4.5. These components include generators, transmission lines, and the CAES. For each of these components, except CAES, a two-state Markov model is used. For CAES, the four-state model developed in Section 4.4 is employed. These up times and down times are generated for a large number of sample years to ensure that all the possible combinations of up and down states of different components are sampled. The wind power is then simulated for the

same duration. The wind power can be simulated either by sampling the probability distribution of the wind speed using inverse transformation and then converting it to wind power [84], or by generating the time-series from different time-series models [76]. The load can also be generated using the same method as that of wind power.

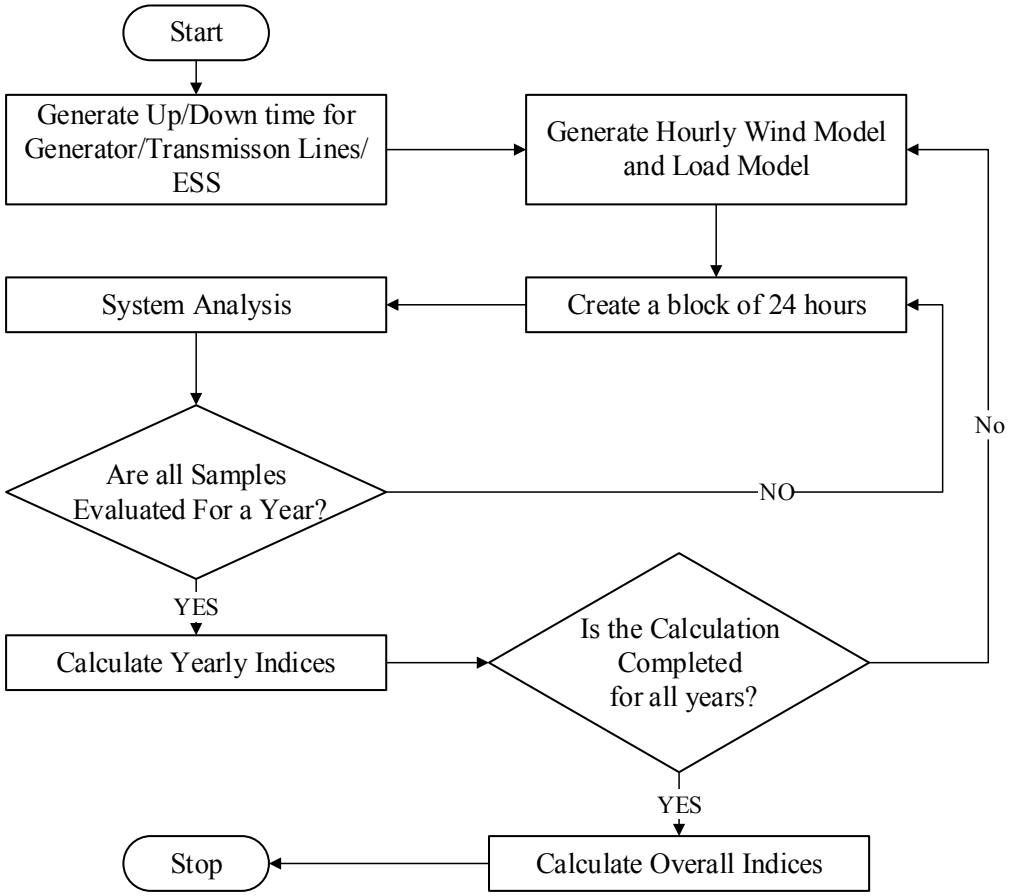

Figure 4.4 Proposed complete methodology

Afterward, the up and down times, as well as wind power and load, are divided into blocks of 24 hours. For each block of 24 hours, some of the components can be in the down state while other components can be in the up state. Then, for each 24-hours block, the optimization problem presented in Section 4.6 is solved. The solution determines the optimal generation output and CAES output (charging or discharging) for each hour of the 24-hours block. It also determines the total load that is curtailed during each of the 24-hours blocks due to components' failures. The load curtailment in each hour contributes to the system unreliability and hence take part in the evaluation of reliability indices. Subsequently, further blocks of 24-hours are analyzed until one year is completed. At the end of each year, the reliability indices are evaluated. The calculations

are repeated for a large number of simulation years. Certain convergence criteria such as one based on the coefficient of variation can be employed for convergence of the simulation.

4.8 Case Studies and Results

4.8.1 Test System

The reliability evaluation method is applied to a six-bus test system shown in Figure 4.6 [85].The reliability data for the generators are obtained from [86], and are shown in Table 4.1. For the transmission lines, the failure rate and repair rate are assumed to be 0.150 f/yr and 547.5 r/yr respectively [86]. The test system is modified by introducing one wind farm at bus 4 and one CAES at bus 5. The rating of the wind farm is set to 100 MW. The operational data related to CAES are shown in Table 4.2. Table 4.3 provides the assumed transition rates for the four-state model of the CAES. All the other transition rates, except the ones provided in the table, are assumed to be zero. These values of transition rates are selected such that the availability of the CAES matches the actual values [7]. The load model is obtained from Roy Billinton Test System (RBTS) whereas the wind profile is simulated using the time-series provided in [76]. The peak load of the system is 256 MW. The costs of load curtailment and wind spillage are set to $1000/MWh and $500/MWh respectively.

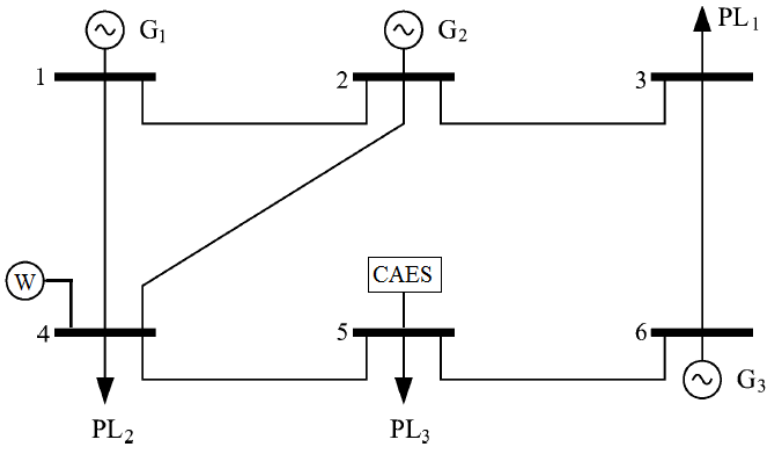

Figure 4.5 Six-bus test system

Table 4.1 Operational data of the test system

Generator	Maximum Power (MW)	Minimum Power (MW)	Operating Cost ($/MWh)	Start-up Cost ($)	Shut-down Cost ($)	Min. Up Time (h)	Min. Down Time (h)	Failure Rate (f/yr)	Repair Rate (r/yr)
1	220	100	13.5	300	50	4	4	4	196
2	100	10	32.6	200	0	2	3	2.4	157.6
3	20	10	17.7	250	30	1	1	3.0	147.0

Table 4.2 Operational data of CAES

Max. Discharging Power (MW)	Max. Charging Power (MW)	Energy Capacity (MWh)	Operational Cost ($/MWh)
60	290	580	3.59

Table 4.3 Reliability data of CAES

Failure Rates	f/yr	Repair Rates	r/yr
λ_1	5	μ_1	250
λ_2	4	μ_2	150
λ_3	5	μ_5	200
λ_5	4.5		
λ_6	5		

4.8.2 Reliability Indices

The reliability indices used in the current study include the probability of load curtailment (PLC), the expected energy not supplied (EENS), the expected demand not supplied (EDNS), the bulk power energy curtailment index (BPECI) and the severity index (SI). PLC measures the reliability of the system in terms of simple probability. EENS measures the expected amount of energy that the system is unable to supply due to random outages, EDNS describes EENS in terms of load

demand, BPECI normalizes the EENS with respect to peak load so that different systems can be compared, SI, also known as system minutes, implies that if an outage happens during the occurrence of the peak load, how much time would that outage last for. These indices are evaluated at the system level as well as at individual load points. The detailed descriptions and formulations of all indices are given in [82].

4.8.3 Results

In order to quantify the benefits derived from the CAES in terms of system reliability and operational cost, the following two different cases are analyzed:

Case 1: Bulk power system without CAES

Case 2: Bulk power system with CAES

The results for both cases are shown in Tables 4.4 and 4.5. System indices are shown in Table 4.4. Whereas Table 4.5 indicates the load point indices. It can be seen that CAES can bring significant benefit to the system in terms of reliability. There has been a marked decrease in the values of PLC, EENS, EDNS, BPECI and SI, from case 1 to case 2. Similarly, the load point indices' reliability is also improved. The load point PL_3 is at bus 5 where the CAES is connected. In case 2, it can be seen that this load point has the highest reliability among all the other load points. This is because the output of CAES can directly support the load point PL_3 in the case of contingencies and the output of CAES to that load point is not constrained by transmission line flows.

Table 4.4 System level reliability indices

Case	PLC	EENS (MWh/yr)	EDNS (10^{-3} MW/yr)	BPECI (MWh/MW-yr)	SI (syst-min)
Case 1	0.0415323	137.514	15.698	0.537164	32.2298
Case 2	0.0016597	5.440	0.621	0.021250	1.27505

Table 4.5 Reliability indices for load points

Case	Load	PLC (10^{-3})	EENS (MWh/yr)	EDNS (10^{-3} MW/yr)	BPECI (MWh/MW-yr)	SI (syst-min)
Case 1	PL_1	9.33557	19.434	2.218551	0.3795	22.77
	PL_2	35.9368	107.56	12.22791	1.0504	63.02
	PL_3	4.61055	10.514	1.200314	0.1026	6.169
Case 2	PL_1	0.33827	0.6511	0.07432	0.0127	0.762
	PL_2	1.46634	4.4089	0.50329	0.0430	2.581
	PL_3	0.15453	0.3801	0.04339	0.0037	0.220

In order to understand the economic effect of the inclusion of CAES in the system, it is important to evaluate the yearly operating costs. Also, the total wind spillage in both cases can further justify the inclusion of CAES in the system. The yearly operating costs for case 1 and case 2 are $ 19.561M/yr and $ 16.265M/yr respectively. Most of the additional cost in case 1 is because of the load curtailment costs. Moreover, there is a decrease in the wind spillage from case 1 to case 2. The wind spillage in case 2 reduces by 87% as compared to that in case 1. This shows that the CAES is highly effective in integrating the wind power and thereby supporting the integration of renewable energy.

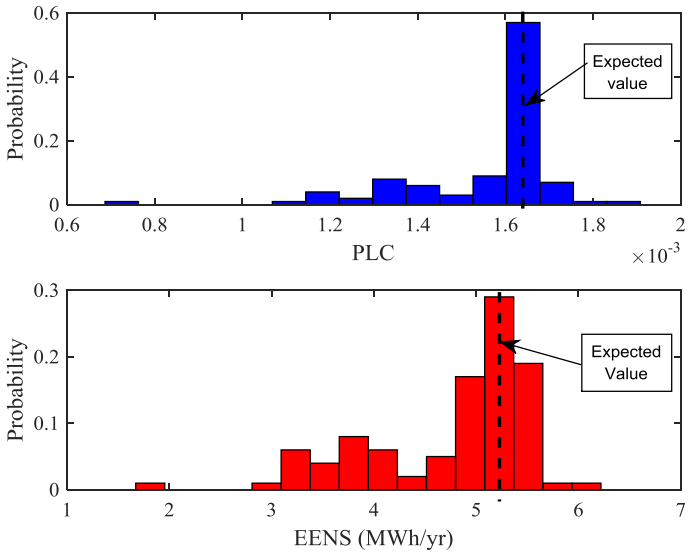

Figure 4.6 Probability distribution of PLC and EENS

For case 2, the probability distributions of PLC and EENS are shown in Figure 4.7. It can be observed that the distribution of PLC is mainly concentrated around the average value, whereas for EENS, it is fairly distributed.

4.8.4 Sensitivity Analysis

In order to understand the effect of CAES capacity on the reliability indices, sensitivity analysis is performed. The size of CAES is changed and the corresponding changes in the values of PLC and EENS are observed. The results are shown in Figure 4.8 which indicates that the reliability of system increases as the energy capacity of CAES is increased. However, after a certain increase in the capacity, the reliability of the system does not improve but saturates to a constant value. In other words, the incremental increase in reliability decreases as the capacity of CAES increases. This is because of the inherent energy limitations of the wind generation. In order to further increase the reliability, additional wind farms may be installed, rather than installing a CAES with larger capacity.

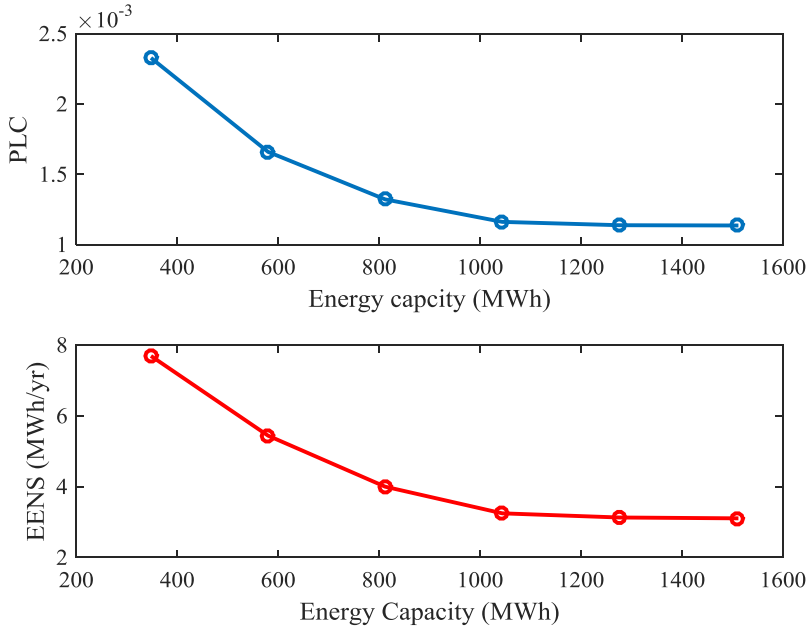

Figure 4.7 Effect of energy capacity of CAES on reliability indices

To study the effect of the siting of CAES in the system, a sensitivity study is performed by changing the location of the CAES. Since there are six buses in the system, therefore there are six positions for siting CAES. The results are shown in Table 4.6. From the results, it can be observed

that in terms of PLC and EENS, bus 4 is the most suitable location for constructing CAES. Also, the load buses are more suitable than generation buses for constructing CAES. This is again because of the fact that the output of CAES is not constrained by the transmission line limits if CAES is at the same bus as that of the load. The maximum difference in the values of PLC and EENS for different buses is 21.9% and 2.76% respectively.

Table 4.6 Effect of CAES location on reliability indices

Bus No.	PLC	EENS (MWh/yr)	EDNS (10^{-3} MW/yr)	BPECI (MWh/MW-yr)	SI (syst-min)
1	0.0021119	5.5080735	0.62877	0.02151	1.2909
2	0.0020650	5.5939675	0.63858	0.02185	1.3110
3	0.0016586	5.4683164	0.62423	0.02136	1.2816
4	0.0016529	5.4390326	0.62089	0.02124	1.2747
5	0.0016597	5.4402205	0.62102	0.02125	1.2750
6	0.0017090	5.4787719	0.62543	0.02140	1.2840

4.9 Conclusion

In this part of the thesis, the reliability evaluation of a bulk power system (HL-II) considering wind power and CAES is performed. The results indicated that the addition of CAES can bring significant benefits to the power system. It has been shown that CAES cannot only improve reliability but it can also increase the wind penetration in the system by reducing the wind spillage. It was observed that the bus where CAES was connected showed the greatest improvement in reliability. Sensitivity studies were also performed to understand the effects of the sizing and siting of CAES on the reliability indices. Further studies can be performed to understand the effect of changing load curtailment and wind curtailment cost on the reliability metrics.

Chapter 5

Summary and Conclusions

"Imagination is more important than knowledge. Knowledge is limited. Imagination encircles the world."
- Albert Einstein

5.1 Conclusions and Contributions

This thesis has examined the inclusion of CAES in future sustainable power systems from the planning, operation and reliability point of views. The studies performed in these three domains have indicated the technical, economic and societal benefits obtained from CAES. The framework and models for CAES presented in this thesis can be useful for electric utilities, private investors, and regulatory agencies to broaden their understanding of the operation of CAES in a future sustainable power system.

The following list summarizes key contributions and findings of the research presented in this thesis:

- The actual benefits and operation of the CAES are dependent upon its location in the power systems as well as its size. In this regard, the thesis has proposed a novel planning tool to obtain optimal locations and size of CAES in the power systems. It has been demonstrated that other smart grid technologies, particularly DTLR, can further assist in arriving at an economical investment plan for CAES.

- CAES can be employed by a merchant or a private owner for financial gains in an electricity market. However, the profits gained by CAES rely on its operational efficiency. The thesis has proposed a novel model for the CAES that describes the variation in its efficiency at different operating conditions. The thesis has demonstrated that by considering this detailed model, optimal schedules of CAES in electricity markets are obtained. These optimal schedules satisfy all operational constraints of a CAES.

- The reliability of a power system can be enhanced by utilizing CAES. However, this increase in reliability is dependent upon the operational strategy of CAES. In this regard, this thesis has proposed a reliability evaluation framework which considers a detailed reliability model of CAES. The thesis has validated that CAES can significantly improve the reliability of a power system. Further case studies have indicated that location and size of a CAES can also impact the reliability of the power system.

5.2 Future Work

The models and frameworks proposed in this thesis can be enhanced in different ways. The following points serve to present some suggestions to perform future work on improving the models and frameworks:

5.2.1 Improvement in the Planning Framework

- *Inclusion of other smart grid technologies in the planning problem*: The proposed planning framework considers one of the many different smart grid technologies that are aimed at assisting the transmission system. It would be interesting to consider how other smart grid technologies, such intelligent transmission switching and wide area monitory systems (WAMS), can also be included in the planning framework to arrive at an economical investment plan for CAES. The current costs of such smart grid technologies may not justify their inclusion in the planning framework. However, it is expected that large-scale adoption of new smart grid technologies will drive the prices of such technologies toward a lower spectrum.

- *Application of planning framework on a real-world test system*: For the purpose of demonstration, the proposed planning framework was applied on a 24-bus test system. However, the efficiency and tractability of the framework can be better depicted through its application on a larger and more realistic test system. The computational time of framework may increase significantly with larger test systems. Different solution strategies may be devised for improving the computational performance of the planning framework.

5.2.2 Improvement in Operational Model of CAES

- *Extending the model to consider adiabatic CAES:* The proposed model can be extended to include the concepts of adiabatic CAES. Adiabatic CAES employs a thermal energy storage to store the heat during the compression process and utilize it during the expansion of the compressed air. The thermodynamic-based model presented in this thesis can be easily extended to include thermodynamic equations for the thermal energy storage. However, the actual thermodynamic data for a thermal energy storage may not be readily available. However, with the recent advancements in thermal energy storage technology, it may be predicted that adiabatic CAES will be commercialized sooner rather than later.

- *Considering the price-maker operation of CAES in the bidding problem:* It is assumed in this thesis that CAES was operated based on electricity market prices set by the market operator i.e. price-taker operation of CAES was assumed. However, CAES can bid strategically in a competitive market to maximize the profits. This can affect electricity market prices. The effects of thermodynamics on the operation of a price-maker CAES may be explored. However, the computational burden may be a serious issue in such studies. In this regard, the model can be further simplified to make it suitable for such studies.

- *Utilizing robust or chance-constrained optimization:* In this thesis, the uncertainties introduced by market prices are handled through scenario-based stochastic optimization. One disadvantage of stochastic optimization is that it may require a large number of scenarios to arrive at a more accurate and realistic result. Robust or chance-constrained optimization do not suffer from this drawback. However, the formulation of robust or chance-constrained optimization is known to be cumbersome and often results in non-linear and non-convex optimization problems. Further studies can be performed to develop robust or chance-constrained optimization models for thermodynamics-based CAES operation.

5.2.3 Improvement in the Reliability Evaluation Framework

- *Considering multiple CAES in the reliability evaluation framework*: In the current work, only a single CAES is considered to establish the effectiveness of CAES in improving the reliability of the power system. It would be of great interest to consider the operation of multiple CAES located in different parts of the power system for the reliability enhancement of the system.

- *DC-OPF vs. UC*: In the proposed reliability evaluation framework, a UC model was adopted for evaluating the reliability indices of the power system. A DC-OPF based model can result in lesser computational burden than a UC model. However, the reliability indices obtained may not be very realistic. Therefore, the comparison between the two models can be drawn based on the computational time and accuracy of the models.

References

[1] International Energy Agency, "World Energy Outlook 2011," 2011.

[2] A. Bloom, U. Helman, H. Holttinen, K. Summers, J. Bakke, G. Brinkman and A. Lopez, "It's indisputable: five facts about planning and operating modern power systems," *IEEE Power and Energy Magazine,* vol. 15, no. 6, pp. 22-30, Nov.-Dec. 2017.

[3] H. Farhangi, "The path of the smart grid," *IEEE Power and Energy Magazine,* vol. 8, no. 1, pp. 18-28, Jan.-Feb. 2010.

[4] B. Kroposki, B. Johnson, Y. Zhang, V. Gevorgian, P. Denholm, B.-M. Hodge and B. Hannegan, "Achieving a 100% renewable grid: operating electric power systems with extremely high levels of variable renewable energy," *IEEE Power and Energy Magazine,* vol. 15, no. 2, pp. 61-73, Mar.-Apr. 2017.

[5] H. Rudnick and L. Barroso, "Flexibility Needed: Challenges for Future Energy Storage Systems [Guest Editorial]," *IEEE Power and Energy Magazine,* vol. 15, no. 5, pp. 12-19, Sep./Oct. 2017.

[6] C. O'Dwyer, L. Ryan and D. Flynn, "Efficient large-scale energy storage dispatch: challenges in future high renewable systems," *IEEE Trans. Power Syt.,* vol. 32, no. 5, pp. 3439-3450, Sep. 2017.

[7] X. Luo, J. Wang, M. Dooner and J. Clarke, "Overview of current development in electrical energy storage technologies and the application potential in power system operation," *Applied Energy,* vol. 137, pp. 511-536, Jan. 2015.

[8] H. Pandžić, Y. Wang, T. Qiu, Y. Dvorkin and D. S. Kirschen, "Near-optimal method for siting and sizing of distributed storage in a transmission network," *IEEE Trans. Power Syst.,* vol. 30, no. 5, pp. 2288-2300, Sep. 2015.

[9] H. Zhao, Q. Wu, S. Hu, H. Xu and C. N. Rasmussen, "Review of energy storage system for wind power integration support," *Applied Energy,* vol. 137, pp. 545-553, May 2014.

[10] T. Qiu, B. Xu, Y. Wang, Y. Dvorkin and D. S. Kirschen, "Stochastic multistage coplanning of transmission expansion and energy storage," *IEEE Trans. Power Syst.,* vol. 32, no. 1, pp. 643-651, Jan. 2017.

[11] G. Strbac, M. Aunedi, I. Konstantelos, R. Moreira, F. Teng, R. Moreno, D. Pudjianto, A. Laguna and P. Papadopoulos, "Opportunities for energy storage: assessing whole-system economic benefits of energy storage in future electricity systems," *IEEE Power and Energy Magazine,* vol. 15, no. 5, pp. 32-41, Sep.-Oct. 2017.

[12] W. F. Pickard, "The history, present state, and future prospects of underground pumped hydro for massive energy storage," *Proceedings of the IEEE,* vol. 100, no. 2, pp. 473-483, 2012.

[13] A. Eller and D. Gauntlett, "Energy Storage Trends and Opportunities in Emerging Markets," Navigant Consulting, Inc, Boulder, 2017.

[14] Electric Power Research Institute (EPRI), "Electrical Energy Storage Technology Options: A White Paper Primer on Applications, Costs, and Benefits," EPRI, Palo Alto, 2010.

[15] X. Hu, C. Zou, C. Zhang and Y. Li, "Technological developments in batteries: a survey of principal roles, types and management needs," *IEEE Power and Energy Magazine,* vol. 15, no. 5, pp. 20-31, Sep.-Oct. 2017.

[16] S. A. Abdelrazek and S. Kamalasadan, "Integrated PV capacity firming and energy time shift battery energy storage management using energy-oriented optimization," *IEEE Trans. Ind. Appl.,* vol. 52, no. 3, pp. 2607-2617, May/Jun. 2016.

[17] Y. Dvorkin, *Operations and Planning in Sustainable Power Systems,* Seattle: University of Washington, 2016.

[18] A. Eller and A. Dehamna, "Country Forecasts for Utility-Scale Energy Storage," Navigant Consulting Inc, 2016.

[19] F. S. Barnes and J. G. Levine, Large Energy Storage Systems Handbook, New York, NY, USA: Taylor & Francis, 2011.

[20] M. Budt, D. Wolf, R. Span and J. Yan, "A review on compressed air energy storage: basic principles, past milestones, and recent developments," *Applied Energy,* vol. 170, pp. 250-268, May 2016.

[21] S. Succar and R. H. Williams, "Compressed Air Energy Storage: Theory, Resources, and Applications for Wind Power," Princeton Environmental Institute, Princeton University, Apr. 2008.

[22] "Long-term energy storage with compressed air storage," EES International, 23 07 2014. [Online]. Available: http://www.ees-magazine.com/long-term-energy-storage-with-compressed-air-storages/.

[23] "Kraftwerk Huntorf," DOE Global Energy Storage Database, [Online]. Available: https://www.energystorageexchange.org/projects/1245. [Accessed 17 Oct. 2017].

[24] "McIntosh CAES Plant," DOE Global Energy Storage Database, [Online]. Available: https://www.energystorageexchange.org/projects/136. [Accessed 17 Oct. 2017].

[25] A. Gillhaus, F. Crotogino, D. Albes and L. van Sambeek, "Compilation and evaluation of bedded salt cavern characteristics important to successful cavern sealing and abandonment," SMRI Research Project Report No. 2006-2-SMRI, Clarks Summit (PA), 2006.

[26] S. E. Grasby and Z. Chen, "Subglacial recharge into the western canada sedimentary basin - impact of pliestocene glaciation on basin hydrodynamics," *Geological Society of America Bulletin,* vol. 117, no. 3-4, pp. 500-514, Mar./Apr. 2005.

[27] "Storage," TransGas, [Online]. Available: https://www.transgas.com/services/storage/storage.asp.

[28] "Renewables Roadmap," SaskPower, 2017. [Online]. Available: http://www.saskpower.com/our-power-future/renewables-roadmap/.

[29] J. R. Birge and F. Louveaux, Introduction to Stochastic Programming, New York, USA: Springer, 2011.

[30] O. A. Ansari, J. P. Zhan and C. Y. Chung, "Stochastic planning of ESSs considering dynamic thermal rating," in *Poster Presenation at 2017 IEEE PES General Meeting*, Chicago, Jul. 2017.

[31] O. A. Ansari, J. P. Zhan and C. Y. Chung, "Optimal scheduling of compressed air energy storage in electricity markets considering turbomachinery characteristic curves," *IEEE Trans. Sustain. Energy (Under Review).*

[32] O. A. Ansari, S. Bhattarai, R. Karki and C. Y. Chung, "Reliability evaluation of bulk power system considering compressed air energy storage," in *2017 IEEE Electric Power and Energy Conference (EPEC)*, Saskatoon, Oct. 2017.

[33] R. Fernández-Blanco, Y. Dvorkin, B. Xu, Y. Wang and D. Kirschen, "Optimal energy storage siting and sizing: a WECC case study," *IEEE Trans. Sustain. Energy,* vol. 8, no. 2, pp. 733-743, Apr. 2017.

[34] K. Baker, G. Hug and X. Li, "Energy storage sizing taking into account forecast uncertainties and receding horizon operation," *IEEE Trans. Sustain. Energy,* vol. 8, no. 1, pp. 331-340, Jan. 2017.

[35] P. Xiong and C. Singh, "Optimal planning of storage in power systems integrated with wind power generation," *IEEE Trans. Sustain. Energy,* vol. 7, no. 1, pp. 232-240, Jan. 2016.

[36] T. Qiu, B. Xu, Y. Wang, Y. Dvorkin and D. S. Kirschen, "Stochastic multistage coplanning of transmission expansion and energy storage," *IEEE Trans. Power Syst.,* vol. 32, no. 1, pp. 643-651, Jan. 2017.

[37] Y. Dvorkin, R. Fernández-Blanco, Y. Wang, B. Xu, D. S. Kirschen, H. Pandzic, J.-P. Watson and C. A. Silva-Monroy, "Co-planning of investments in transmission and merchant energy storage," *IEEE Trans. Power Syst.,* vol. PP, no. 99, pp. 1-1, 2017.

[38] M. Jaccard, Renewable Portfolio Standard, New York: Elsevier, 2004, pp. 413-421.

[39] J. Zhan, C. Y. Chung and E. Demeter, "Time series modeling for dynamic thermal rating of overhead lines," *IEEE Trans. Power Syst.,* vol. 32, no. 3, pp. 2172-2182, May 2017.

[40] D. M. Greenwood and M. T. Philip, "Unlocking the benefits of real-time thermal ratings through probabilistic power network planning," *IET Gener. Transm. Distrb.,* vol. 8, no. 12, pp. 2055-2064, Oct. 2014.

[41] U.S. Department of Energy, "Dynamic line rating systems for transmission lines- Smart Grid Demonstration Program: Topical Report," 2014.

[42] US Department of Energy, "Improving Efficiency with Dynamic Line Ratings," Sep. 2015.

[43] J. Kallrath, "Mixed integer optimization in the chemical process industry: experience, potential and future perspectives," *Chemical Engineering Research and Design,* vol. 78, no. 6, pp. 809-822, Sep. 2000.

[44] M. Shahidehpour and Y. Fu, "Benders decomposition in restructred power systems," *IEEE Techtorial,* Apr. 2005.

[45] T.-H. Yeh and L. Wang, "A study on generator capacity for wind turbines under various tower heights and rated wind speeds using weibull distribution," *IEEE Trans. Energy Convers.,* vol. 23, no. 2, pp. 592-602, Jun. 2008.

[46] J. Zhan, C. Y. Chung and A. Zare, "A fast solution method for stochastic transmission expansion planning," *IEEE Trans. Power Syst.,* vol. pp, no. 99, pp. 1-1, 2017.

[47] Y. Dvorkin, Y. Wang, H. Pandzic and D. Kirschen, "Comparison of scenario reduction technqies for the stochastic unit commitment," in *2014 IEEE PES General Meeting | Conference & Exposition*, National Harbor, 2014.

[48] "GAMS SCENRED2," GAMS, [Online]. Available: https://www.gams.com/24.8/docs/tools/scenred2/index.html.

[49] C. Grigg, P. Wong, P. Albrecht, R. Allan, M. Bhavaraju, R. Billinton, Q. Chen, C. Fong, S. Haddad, S. Kuruganty, W. Li, R. Mukerji, D. Patton, N. Rau, D. Reppen, A. Schneider, M. Shahidehpour and C. Singh, "The IEEE reliability test system - 1996: a report prepared by the reliability test system task force of the application of probability methods subcomittee," *IEEE Trans. Power Syst.,* vol. 14, no. 3, pp. 1010-1020, Aug. 1999.

[50] "Power Systems Test Case Archive," University of Washington, [Online]. Available: https://www2.ee.washington.edu/research/pstca/rts/pg_tcarts.htm.

[51] J. G. Dalton, D. L. Garrison and C. M. Fallon, "Value-based reliability transmission planning," *IEEE Trans. Power Syst.,* vol. 11, no. 3, pp. 1400-1408, Aug. 1996.

[52] New York Power Authority, "New York Power Authority (Evaluation of Instrumentation and Dynamic Thermal Ratings for Overhead Lines)," 2015. [Online]. Available: https://www.smartgrid.gov/project/new_york_power_authority_evaluation_instrumentation_and_dynamic_thermal_ratings_overhead/latest_data.html.

[53] B. Cleary, A. Duffy, A. O'Connor, M. Conlon and V. Fthenakis, "Assessing the economic benefits of compressed air energy storage for mitigating wind curtailment," *IEEE Trans. Sustain. Energy,* vol. 6, no. 3, pp. 1021-1028, Jul. 2015.

[54] H. Khani and M. R. D. Zadeh, "Online adaptive real-time optimal dispatch of privately owned energy storage systems using public-domain electricity market prices," *IEEE Trans. Power Syst.,* vol. 30, no. 2, pp. 930-938, Mar. 2015.

[55] S. Shafiee, H. Zareipour, A. M. Knight, N. Amjady and B. Mohammadi-Ivatloo, "Risk-constrained bidding and offering strategy for a merchant compressed air energy storage plant," *IEEE Trans. Power Syst.,* vol. 32, no. 2, pp. 946-957, May 2016.

[56] H. Khani, M. R. D. Zadeh and A. H. Hajimiragha, "Transmission congestion relief using privately owned large-scale energy storage systems in a competitive electricty market," *IEEE Trans. Power Syst.,* vol. 31, no. 2, pp. 1449-1458, Mar. 2016.

[57] S. Shafiee, H. Zareipour and A. Knight, "Considering thermodynamic characteristics of a CAES facility in self-scheduling in energy and reserve markets," *IEEE Trans. Smart Grid,* vol. pp, no. 99, pp. 1-1, 2017.

[58] H. Bitaraf and S. Rahman, "Reducing curtailed wind energy through energy stroage and demand response," *IEEE Trans. Sustain. Energy,* vol. pp, no. 99, pp. 1-1, 2017.

[59] H. Bitaraf, S. Rahman and M. Pipattanasomporn, "Sizing energy storage to mitigate wind power forecast error impacts by signal processing techniques," *IEEE Trans. Sustain. Energy,* vol. 6, no. 4, pp. 1457-1465, Oct. 2015.

[60] T. Das, V. Krishnan, Y. Gu and J. D. McCalley, "Compressed air energy storage: state space modeling and performance analysis," in *2017 IEEE Power and Energy Society General Meeting (GM)*, Detroit, 24-29 Jul. 2011.

[61] H. Cohen, G. F. C. Rogers and H. I. H. Saravanamutto, Gas Turbine Theory, 6th Ed, Upper Saddle River, USA: Pearson Education, 2009.

[62] S. Briola, P. D. Maro, R. Gabbrielli and J. Riccardi, "A novel mathematical model for the performance assessment of diabatic compressed air energy storage systems including the turbomachinery characteristic curves," *Applied Energy,* vol. 178, pp. 758-772, Sep. 2016.

[63] P. Zhao, L. Gao, J. Wang and Y. Dai, "Energy efficiency analysis and off-design analysis of two different discharge modes for compressed air energy storage system using axial turbines," *Renewable Energy,* vol. 85, pp. 1164-1177, Jan. 2015.

[64] N. Zhang and R. X. Cai, "Analytical solutions and typical characteristics of part-load performance of single shaft gas turbine and its cogeneration," *Energy Convers. Manag.,* vol. 43, pp. 1323-1337, 2002.

[65] "ENTSO-E Network Code on Load-Frequency Control and Reserves," ENTSO, 2017.

[66] C. E. Gounaris, R. Misener and C. A. Floudas, "Computational comparison of piecewise-linear relaxations for pooling problems," *Industrial & Engineering Chemistry Research,* vol. 48, no. 12, pp. 5742-5766, May 2009.

[67] L. S. de Assis, E. Camponogara, B. Zimberg, E. Ferreira and I. E. Grossmann, "A piecewise McCormick relaxation-based strategy for scheduling operations in a crude oil terminal," *Computers and Chemical Engineering,* vol. 106, pp. 309-321, Nov. 2017.

[68] J. P. Vielma and G. L. Nemhauser, "Modeling disjunctive contraints with a logarithmic number of binary variables and constraints," *Mathematical Programming,* vol. 128, no. 1-2, pp. 49-72, Jun. 2011.

[69] G. He, Q. Chen, C. Kang, P. Pinson and Q. Xia, "Optimal bidding strategy of battery storage in power markets considering performance-based regulation and battery cycle life," *IEEE Trans. Smart Grid,* vol. 7, no. 5, pp. 2359-2367, Sept. 2016.

[70] P. Quast and F. Crotogino, "Initial experience with the compressed-air energy storage (CAES) project of Nordwestdeutsche Kraftwerke AG (NWK) at Huntorf/West Germany," *Oil and Natural Gas Magazine - Special Print,* vol. 85, no. 9, pp. 310-314, 1979.

[71] W. Mattick, H. G. Haddenhorst, O. Weber and Z. S. Stys, "Huntorf - the world's first 290-MW gas turbine air-storage peaking plant," in *Proceedings of the American Power Conference*, 1975, 1975.

[72] "Data Miner, PJM," [Online]. Available: http://www.pjm.com/markets-and-operations/etools/data-miner.aspx.

[73] A. D. Sa and S. Al Zubaidy, "Gas turbine performance at varying ambient temperature," *Applied Thermal Engineering,* vol. 31, no. 14-15, pp. 2735-2739, Oct.2011.

[74] D. Manx, R. Piwko and N. Miller, "Look before your leap: the role of energy storage in the grid," *IEEE Power and Energy Magazine,* vol. 10, no. 4, pp. 75-84, Jul./Aug. 2012.

[75] R. Billinton, Bagen and Y. Cui, "Reliability evaluation of small stand-alone wind energy conversion systems using a time series simulation model," *IEE Proceedings- Generation, Transmission and Distribution,* vol. 150, no. 1, pp. 96-100, Apr. 2003.

[76] P. Hu, R. Karki and R. Billinton, "Reliability evaluation of generating systems containing wind power and energy storage," *IET Generation, Transmission and Distribution,* vol. 3, no. 8, pp. 783-791, Aug. 2009.

[77] F. A. Bhuiyan and A. Yazdani, "Reliability assessment of a wind-power system with intelligent operation strategy," *IEEE Trans. Smart Grid,* vol. 3, no. 3, pp. 211-220, May 2010.

[78] Y. Xu and C. Singh, "Power system reliability impact of energy storage integration with intelligent operation strategy," *IEEE Trans. Smart Grid,* vol. 5, no. 2, pp. 1129-1137, Mar. 2014.

[79] Y. Xu and C. Singh, "Adequacy and economy analysis of distribution systems integrated with electric energy storage and renewable energy resources," *IEEE Trans. Power Syst.,* vol. 27, no. 4, pp. 2332-2341, Nov. 2012.

[80] P. Wang, Z. Gao and L. Bertling, "Operational adequacy studies of power systems with wind farms and energy storages," *IEEE Trans. Power Syst.,* vol. 27, no. 4, pp. 2377-2384, Nov. 2012.

[81] S. Thapa and R. Karki, "Reliability benefit of energy storage in wind integrated power system operation," *IET Generation, Transmission and Distribution,* vol. 10, no. 3, pp. 807-814, Mar. 2016.

[82] R. Billinton and R. N. Allan, Reliability evaluation of power systems, New York, USA: Springer US, 1996.

[83] R. Billinton and W. Li, Reliability Assessment of Electrical Power Systems Using Monte Carlo Methods, New York, USA: Plenum, 1994.

[84] O. A. Ansari, N. Safari and C. Y. Chung, "Reliability assessment of microgrid with renewable generation and prioritized loads," in *2016 IEEE Green Energy and Systems Conference (IGESC)*, Long Beach, Nov. 2016.

[85] L. Wu, M. Shahidehpour and T. Li, "Stochastic security-constrained unit commitment," *IEEE Trans. Power Syst.,* vol. 22, no. 2, pp. 800-811, May 2007.

[86] R. N. Allan, R. Billinton, I. Sjarief, L. Goel and K. S. So, "A reliability test system for educational purposes - basic distribution system data and results," *IEEE Trans. Power Syst.,* vol. 6, no. 2, pp. 813-820, May 1991.

Appendix

Copyright Permission Letters

To Whom It May Concern:

I, Chi Yung Chung, hereby grant permission to Mr. Osama Aslam Ansari to reuse the following articles in his thesis titled "Compressed Air Energy Storage: Modelling and Applications for Sustainable Electric Power Systems".

- O. A. Ansari, J. P. Zhan and C. Y. Chung, "Optimal scheduling of compressed air energy storage considering turbomachinery characteristic curves," *IEEE Transactions on Sustainable Energy*, 2017, under review.

- O. A. Ansari, S. Bhattarai, R. Karki, and C. Y. Chung, "Reliability evaluation of bulk power system considering compressed air energy storage," in *2017 IEEE Electric Power and Energy Conference*, Saskatoon, Oct. 2017. (In press)

- O. A. Ansari, J. P. Zhan, and C. Y. Chung, "Stochastic planning of ESSs considering dynamic thermal rating," *Poster Presentation* in *2017 IEEE Power and Energy Society General Meeting,* Chicago, Jul. 2017.

I am aware that all University of Saskatchewan theses are also posted in the digital USask eCommons thesis repository, making the thesis openly available on the internet.

I am aware that Mr. Ansari has made additions to the work "Stochastic planning of ESSs considering dynamic thermal rating", partially re-worded the article, "Reliability evaluation of bulk power system considering compressed air energy storage".

Date:

Signature:

To Whom It May Concern:

I, Junpeng Zhan, hereby grant permission to Mr. Osama Aslam Ansari to reuse the following articles in his thesis titled "Compressed Air Energy Storage: Modelling and Applications for Sustainable Electric Power Systems".

- O. A. Ansari, J. P. Zhan and C. Y. Chung, "Optimal scheduling of compressed air energy storage considering turbomachinery characteristic curves," *IEEE Transactions on Sustainable Energy*, 2017, under review.

- O. A. Ansari, J. P. Zhan, and C. Y. Chung, "Stochastic planning of ESSs considering dynamic thermal rating," *Poster Presentation* in *2017 IEEE Power and Energy Society General Meeting,* Chicago, Jul. 2017.

I am aware that all University of Saskatchewan theses are also posted in the digital USask eCommons thesis repository, making the thesis openly available on the internet.

I am aware that Mr. Ansari has made additions to the work "Stochastic planning of ESSs considering dynamic thermal rating.

Date:

Signature:

To Whom It May Concern:

I, Rajesh Karki, hereby grant permission to Mr. Osama Aslam Ansari to reuse the following articles in his thesis titled "Compressed Air Energy Storage: Modelling and Applications for Sustainable Electric Power Systems".

- O. A. Ansari, S. Bhattarai, R. Karki, and C. Y. Chung, "Reliability evaluation of bulk power system considering compressed air energy storage," in *2017 IEEE Electric Power and Energy Conference*, Saskatoon, Oct. 2017. (In press)

I am aware that all University of Saskatchewan theses are also posted in the digital USask eCommons thesis repository, making the thesis openly available on the internet.

I am aware that Mr. Ansari has partially re-worded the article, "Reliability evaluation of bulk power system considering compressed air energy storage".

Date:

Signature:

To Whom It May Concern:

I, Safal Bhattari, hereby grant permission to Mr. Osama Aslam Ansari to reuse the following articles in his thesis titled “Compressed Air Energy Storage: Modelling and Applications for Sustainable Electric Power Systems”.

- O. A. Ansari, S. Bhattarai, R. Karki, and C. Y. Chung, “Reliability evaluation of bulk power system considering compressed air energy storage,” in *2017 IEEE Electric Power and Energy Conference*, Saskatoon, Oct. 2017. (In press)

I am aware that all University of Saskatchewan theses are also posted in the digital USask eCommons thesis repository, making the thesis openly available on the internet.

I am aware that Mr. Ansari has partially re-worded the article, “Reliability evaluation of bulk power system considering compressed air energy storage”.

Date:

Signature:

Copyright Permission for Figure 1.5

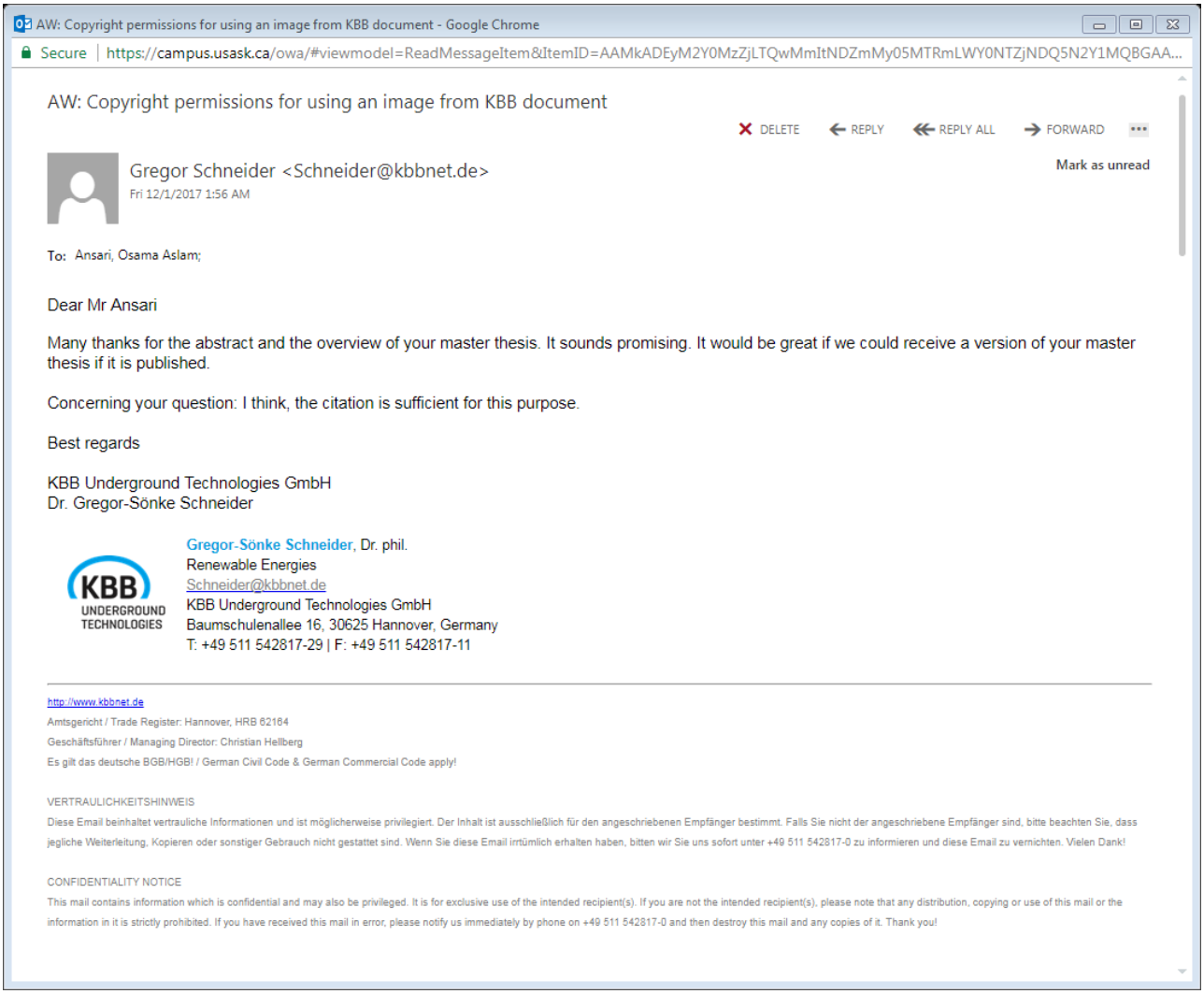

AW: Copyright permissions for using an image from KBB document - Google Chrome

Secure | https://campus.usask.ca/owa/#viewmodel=ReadMessageItem&ItemID=AAMkADEyM2Y0MzZjLTQwMmItNDZmMy05MTRmLWY0NTZjNDQ5N2Y1MQBGAA...

AW: Copyright permissions for using an image from KBB document

DELETE REPLY REPLY ALL FORWARD ...

Mark as unread

Gregor Schneider <Schneider@kbbnet.de>
Fri 12/1/2017 1:56 AM

To: Ansari, Osama Aslam;

Dear Mr Ansari

Many thanks for the abstract and the overview of your master thesis. It sounds promising. It would be great if we could receive a version of your master thesis if it is published.

Concerning your question: I think, the citation is sufficient for this purpose.

Best regards

KBB Underground Technologies GmbH
Dr. Gregor-Sönke Schneider

KBB UNDERGROUND TECHNOLOGIES

Gregor-Sönke Schneider, Dr. phil.
Renewable Energies
Schneider@kbbnet.de
KBB Underground Technologies GmbH
Baumschulenallee 16, 30625 Hannover, Germany
T: +49 511 542817-29 | F: +49 511 542817-11

http://www.kbbnet.de
Amtsgericht / Trade Register: Hannover, HRB 62164
Geschäftsführer / Managing Director: Christian Hellberg
Es gilt das deutsche BGB/HGB! / German Civil Code & German Commercial Code apply!

VERTRAULICHKEITSHINWEIS
Diese Email beinhaltet vertrauliche Informationen und ist möglicherweise privilegiert. Der Inhalt ist ausschließlich für den angeschriebenen Empfänger bestimmt. Falls Sie nicht der angeschriebene Empfänger sind, bitte beachten Sie, dass jegliche Weiterleitung, Kopieren oder sonstiger Gebrauch nicht gestattet sind. Wenn Sie diese Email irrtümlich erhalten haben, bitten wir Sie uns sofort unter +49 511 542817-0 zu informieren und diese Email zu vernichten. Vielen Dank!

CONFIDENTIALITY NOTICE
This mail contains information which is confidential and may also be privileged. It is for exclusive use of the intended recipient(s). If you are not the intended recipient(s), please note that any distribution, copying or use of this mail or the information in it is strictly prohibited. If you have received this mail in error, please notify us immediately by phone on +49 511 542817-0 and then destroy this mail and any copies of it. Thank you!

Copyright Permission for Figure 1.6

THE GEOLOGICAL SOCIETY OF AMERICA®

SCIENCE ▪ STEWARDSHIP ▪ SERVICE

3 November 2017

Osama A. Ansari
University of Saskatchewan

Dear Osama,
Permission is granted for your use of the following material in your thesis at the University of Saskatchewan.

Figure 9 from:

Grasby, S.E., and Chen, Z., 2005, Subglacial recharge into the Western Canada Sedimentary Basin—Impact of Pleistocene glaciation on basin hydrodynamics: Geological Society of America Bulletin, v. 117, p. 500–514, doi:https://doi.org/10.1130/B25571.1.

Best regards,

Jeanette Hammann
Director, GSA Publications
(303) 357-1048
jhammann@geosociety.org

3300 Penrose Place, P.O. Box 9140, Boulder, Colorado 80301–9140, USA

Tel +1.303.357.1000 ▪ Toll Free +1.800.472.1988 ▪ Fax +1.303.357.1070 ▪ www.geosociety.org